Electrostatic Layer-by-Layer Assembly of Ultrathin Films and Membranes

Containing Hexacyclen and p- Sulfonatocalix[n]arene Macrocycles

and Their Application for Highly Efficient Ion Separation

Inaugural - Dissertation

zur

Erlangung des Doktorgrades

der Mathematisch-Naturwissenschaftlichen Fakultät

der Universität zu köln

vorgelegt von

Ashraf M. EL-Hashani

aus Libyen

Köln 2007

Dedication

Dedicated to my parents, my wife, and my little daughters for their sense of humor, love, support and inspiration for all I have accomplished in my personal and professional pursuits.

ACKNOWLEDGMENTS

Abstract

New ultrathin films and membranes containing macrocyclic compounds are described, which were prepared upon electrostatic layer-by-layer (lbl) assembly. Five types of films were prepared:

(a) films of cationic macrocycles and anionic polyelectrolytes,
(b) films of cationic macrocycles and inorganic anions,
(c) films of anionic macrocycles and cationic polyelectrolytes,
(d) films of anionic macrocycles and inorganic cations, in some cases containing 18-crown-6 in additional, and
(e) films of anionic macrocycles and cationic macrocycles.

As cationic macrocycles, protonated 1,4,7,10,13,16-hexaazacyclooctadecane (**aza6**), and as anionic macrocycles, p-sulfonatocalix[n]arenes with n=6 (**calix6**) and n=8 (**calix8**) were used. As inorganic ions, hexacyanoferrate(II) anions (HCFII) and lanthanum(III) cations were used, while protonated polyvinylamine (PVA) and branched polyethylenimine (PEI) served as cationic polyelectrolytes, and polystyrene sulfonate (PSS) and polyvinylsulfate (PVS) as anionic polyelectrolytes. Film formation was characterized upon spectroscopic methods. Effects of pH, concentration of charged compounds and supporting electrolytes present in aqueous dipping solutions were investigated.

Ultrathin separation membranes were prepared upon alternating electrostatic adsorption of **aza6** and PVS on porous polyacrylonitrile/polyethylene terephthalate (PAN/PET) substrates. The rejection of divalent anions was only poor, but could be strongly enhanced after a treatment of the membrane with 0.1 M aqueous copper(II) acetate solution. Theoretical separation factors up to $\alpha(Cl^-/SO_4^{2-}) = 110$ and $\alpha(Cl^-/SO_3^{2-}) = 1420$ were found. Pressure-driven transport of ions, i.e., transport under nanofiltration conditions was also studied. The rejection of both Cl^- and SO_4^{2-} ions increased with increasing number of deposited bilayers and decreased with increasing operating pressure. At a pressure of 14 bar, the membrane consisting of sixty layer pairs exhibited a rejection of 56.5 % for sodium

chloride and about 98.6 % for sodium sulfate, i.e., a selectivity of 31 could be reached. The flux increased linearly with the operating pressure and decreased with increasing number of layer pairs.

Studying ion permeation across **calix8**/PVA membranes, it was found that rare earth metal chlorides $LnCl_3$ with Ln being La, Ce, Pr and Sm and related YCl_3 were strongly rejected. The theoretical separation factors $\alpha(NaCl/LaCl_3)$ and $\alpha(NaCl/YCl_3)$ were 138 and 160, for example. The transport of various neutral and charged aromatic compounds across **calix8**/PVA multilayer membranes was also investigated. The solutes were aniline (An), phenol (Ph), naphthaline (Np), alkali metal salts of benzene sulfonate (BS), naphthalene 2-sulfonate (NS) and benzene disulfonate (1,3-BDS). For the neutral compounds, a size-selective transport was found. For charged aromatic compounds, the transport was both size- and charge-selective. Size and charge-selectivity lead to a separation factor $\alpha(Ph/1,3\text{-}BDS)$ of 333.

Zusammenfassung

Neue ultradünne Filme und Membranen, die makrozyklische Verbindungen enthalten, wurden duch elektrostatische Schicht-für-Schicht Adsorption hergestellt. Fünf Typen von Filmen wurden untersucht:

(a) Filme aus kationischen Makrozyklen und anionischen Polyelektrolyten,
(b) Filme aus kationischen Makrozyklen und anorganischen Anionen,
(c) Filme aus anionischen Makrozyklen und kationischen Polyelektrolyten,
(d) Filme aus anionischen Makrozyklen und anorganischen Kationen, die in einigen Fällen 18-Krone-6 enthielten,
(e) Filme aus anionischen Makrozyklen und kationischen Makrozyklen.

Als kationischer Makrozyklus wurde protoniertes 1,4,7,10,13,16-Hexaazacyclooctadecan (**aza6**), und als anionische Makrozyklen p-Sulfonatocalix[n]arene mit n=6 (**calix6**) und n=8 (**calix8**) verwendet. Als anorganische Ionen wurden Hexacyanoferrat(II)-Anionen (HCFII) und Lanthan(III)-Kationen eingesetzt. Protoniertes Polyvinylamin (PVA) und Polyethylenimin (PEI) dienten als kationische Polyelektrolyte, und Polystyrolsulfonat (PSS) und Polyvinylsulfat (PVS) als anionische Polyelektrolyte. Die Filmbildung wurde durch spektroskopische Methoden verfolgt. Der Einfluss von pH, Konzentration der geladenen Komponenten und Gegenwart zusätzlicher Elektrolyte in den wässrigen Tauchlösungen wurde detailliert untersucht.

Ultradünne Trennmembranen wurden durch alternierende elektrostatische Adsorption von **aza6** und PVS auf porösen Polyacrylnitril/Polyäthylenterephthalat (PAN/PET)-Trägern hergestellt. Der Rückhalt zweiwertiger Anionen war nur schwach, konnte aber nach einer Behandlung der Membran mit 0.1 molarer wässriger Kupfer(II)azetatlösung stark erhöht werden. Theoretische Trennfaktoren bis zu $\alpha(Cl^-/SO_4^{2-})$ = 110 und $\alpha(Cl^-/SO_3^{2-})$ = 1420 wurden gefunden. Der druckgetriebene Ionentransport, d.h. der Transport unter Nanofiltrations-bedingungen wurde auch studiert. Der Rückhalt sowohl der Cl^-- als auch der SO_4^{2-}-Ionen nahm mit der Anzahl der adsorbierten Doppelschichten zu, während er mit

der Erhöhung des Drucks abnahm. Bei einem Druck von 14 bar zeigte eine Membran aus sechzig Schichtpaaren einen Rückhalt von 56.5 % für Natriumchlorid und ungefähr 98.6 % für Natriumsulfat, sodass eine Selektivität von 31 erreicht werden konnte. Der Fluss nahm linear mit dem Druck zu und nahm bei zunehmender Anzahl von adsorbierten Schichtpaaren ab.

Bei der Untersuchung der Ionenpermeation durch **calix8**/PVA Membranen wurde gefunden, dass Seltenerdmetallchloride $LnCl_3$ mit Ln = La, Ce, Pr und Sm und das verwandte YCl_3 stark zurückgehalten wurden. Die theoretischen Trennfaktoren $\alpha(NaCl/LaCl_3)$ und $\alpha(NaCl/YCl_3)$ lagen zum Beispiel bei 138 bzw. 160. Der Transport von verschiedenen neutralen und geladenen aromatischen Verbindungen durch die **calix8**/PVA Multischichtmembran wurde auch untersucht. Die Verbindungen waren Anilin, Phenol (Ph), Naphthalin (Np), Alkalimetallsalze des Benzolsulfonats (BS), Naphthalin-2-sulfonats (NS) und Benzol-1,3-disulfonats (1,3-BDS). Für die ungeladenen Verbindungen wurde ein größenselektiver Transport gefunden. Für die geladenen aromatischen Verbindungen war der Transport sowohl größen- als auch ladungsselektiv. Größen- und Ladungsselektivität führten zum Beispiel zu einem Trennfaktor $\alpha(Ph/1,3-BDS)$ von 333.

Table of Contents

Chapter Three – Results and Discussion   Page

Chapter Four – Experimental Details   Page

Chapter Five – Summary and Conclusion   Page

Chapter Six – References   Page

List of Symbols

α	Theoretical separation factor
γ	Activity coefficient
Λ	Conductivity
Λ_m	Molar conductivity
σ	Reflection coefficient
π	Osmotic pressure
$\Delta\pi$	Hydrodynamic pressure difference
μ	Chemical potential
μ^o	Standard chemical potential
A	Cross-section area of membrane
a	Activity
c_i	Initial concentration
c_f	Final concentration
c_m	Concentration of solute at membrane surface
c_p	Concentration of solute permeate
c_b	Bulk feed
d_{por}	Diameter of pores
d_{mem}	Membrane thickness
d	Pore diameter
D	Diffusion coefficient
f	Fractional resistance
F	Electrochemical potential
F_{ave}	Average driving force
F	Driving force
HPLC	High performance liquid chromatography
h	Hour
J	Flux
J_w	Water flux
J_s	Solute flux
J.c	Flow of solutes towards the membrane

$J.c_p$	Solute flow through the membrane
J_i	Flux of component
K	Permeability constant
L	Membrane thickness
Mem.	Membrane
M	Molecular weight
NF	Nanofiltration
n	Number of dipping cycles
p	Pressure
P	Permeation
P_R	Permeation rate
R	Retention coefficient or Rejection
R	Gas constant
RO	Reverse osmoses
S	Solubility
t	Time
T	Temperature
UV/Vis	Ultraviolet visible spectrophotometer
V	Volume
X_i	Mole fraction
ΔX	Gradient in potential
An	Aniline
BS	Sodium benzene sulfonate
1,3-BDS	Disodium benzene-1,3-disulfonate
18-crown-6	Crown ether
HCF(II)	Potasium hexacyanoferrate(II) trihydrate
NS	Sodium naphthalene-2-sulfonate
Np	Naphthalene
Ph	Phenol

PE$^+$	Cationic polyelectrolyte
PE$^-$	Anionic polyelectrolyte
PVA	Polyvinylamine
PVS	Polyvinylsulfate potassium salt
PAH	Polyallylamine hydrochloride
PSS	Sodium polystyrene sulfonate
PEI	Polyethylenimine branched
P4VP	Poly 4-vinylpyridin
PVSu	Polyvinylsulfonate sodium salt
PAA	Polyacrylic acid
CHI	Chitosan
PDADMA	polydimethyldiallylamoniumchloride
Aza6	1,4,7,10,13,16-Hexaazacyclo-octadecane
Calix4	Tetra-p-sulfonatocalix[4] arene
Calix6	Hexa-p-sulfonatocalix[6] arene
Calix8	Octa-p-sulfonatocalix[8] arene

1 Introduction

1.1 Electrostatic layer-by-layer assembly

Constructing films of defined composition and molecular organization has long been a priority in applied polymer science. In the past decades, versatile different methods for formation of homogeneous and ordered ultrathin films on solid supports were of interest. Among these techniques are Langmuir-Blodgett deposition [1-3], chemical deposition [4-8], thermal deposition, and spin coating [9]. Many of these fashions require a fairly well-controlled environment and a sophisticated segment of equipment and therefore involve high capital and operating costs. Furthermore, limitations exist in the range of materials that could be incorporated, particularly in the combination of a broad range of polyelectrolytes, macrocyclic, organic and inorganic compounds. Recently Decher et al. [10-13] reported a new method to build multilayered polyelectrolyte films, which led to an extraordinary growth in the field of thin films: when a charged surface is alternatingly exposed to polyelectrolytes of opposite charge, ultrathin composite films of few angstroms in thickness are obtained.
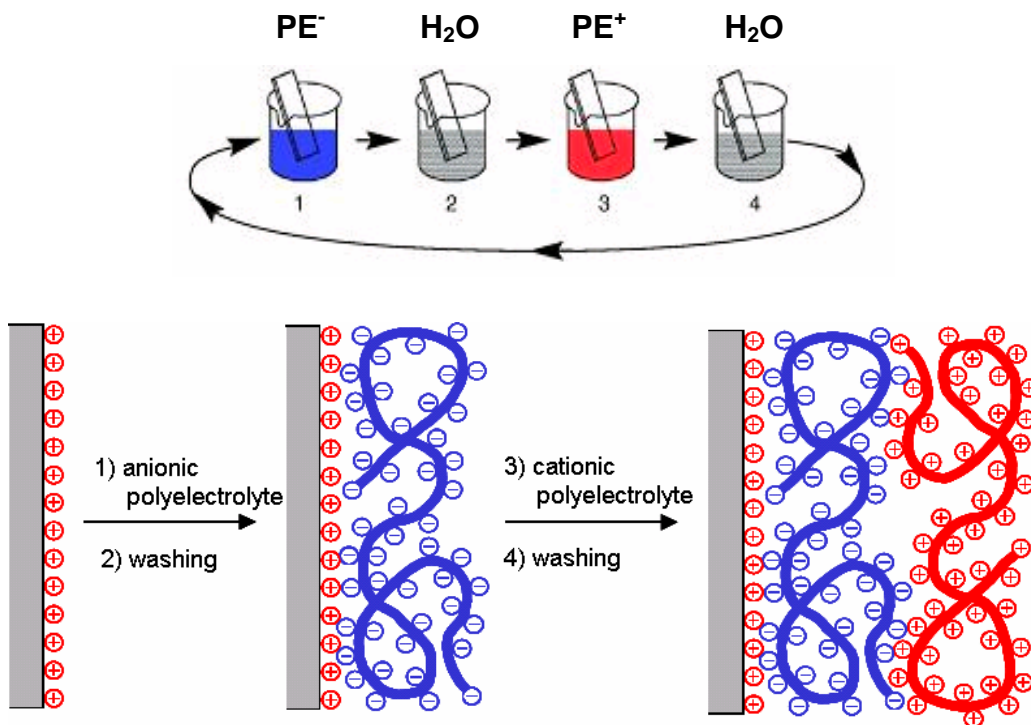
Fig. 1.1 Schematic representation of the alternating adsorption of polyanionic and polycationic molecules to build-up a polyelectrolyte multilayer thin film on a charged substrate (from ref. 10).

In fact, the process is a double adsorption cycle resulting in the formation of multilayers of cationic and anionic polyelectrolytes in alternating fashion. As illustrated schematically in Figure 1.1, a positively charged substrate is immersed into a solution of polyanions. Typically, a very thin monomolecular polyanion layer is produced on the surface, which induces a charge reversal leading to a negatively charged substrate. Surplus polymer molecules adhering are removed by simple washing. Upon subsequent dipping of the substrate into a solution of polycations, the polycations are adsorbed and a positively charged surface is recovered. By successive alternate deposition, it is then possible to construct multilayered polymer films. However, several studies indicate that monolayer polyion adsorption is a two step process: polyelectrolyte chains are anchored to the surface by some segments during a fast initial step, and then relax to a dense packing in a slower second step. Empirically, 10-20 min are often allowed for adsorption steps and the thickness of a monolayer deposited from an aqueous solution is about 1.2-1.4 nm [14-18].

The alternate layer-by-layer (lbl) assembly has been successfully extended to the preparation of functional thin films containing various macromolecules such as dyes [19-21], proteins [22,23], redox or conducting polymers [24], reactive polymers [25,26], macrocyclic compounds [27-29] and charged small molecules [30,31]. Numerous studies appeared, which were either concerned with fundamental aspects of film growth, structure, and morphology [32-48] or with the preparation and characterization of ultrathin films [49-53]. Furthermore, it has been demonstrated that multilayer thin films can exist in a variety of novel and unique structures, which make these composite films have even more broad applications in many areas such as integrated optics, electronics, sensors, anticorrosion and separation.

Under the normally chosen conditions, the lbl assembly of polyelectrolytes is nearly irreversible [14], so that the built-up films do not represent equilibrium structures. This adds to the versatility of the lbl method, but implies the need for careful adjustment of the various process parameters in order to control the deposition process. A particularity of lbl is the possibility to modify roughness and

thickness of the coatings for a given pair of polyelectrolytes by varying process parameters. In any case, molar mass of the polyelectrolyte, pH and ionic strength of the dipping solution may influence the growth of the film.

1.2 Ultrathin membranes via layer-by-layer assembly

Adsorption of multilayered polyelectrolyte films on porous supports provides a simple means to create charged ultrathin separation membranes. This technique is attractive because it affords control over the thickness, charge density, and composition of the active separation layer. In addition, variation of deposition conditions also allows optimization of membrane properties. The important step in the multilayer formation is the charge inversion following the polyelectrolyte adsorption to oppositely charged interface (Figure 1.2).
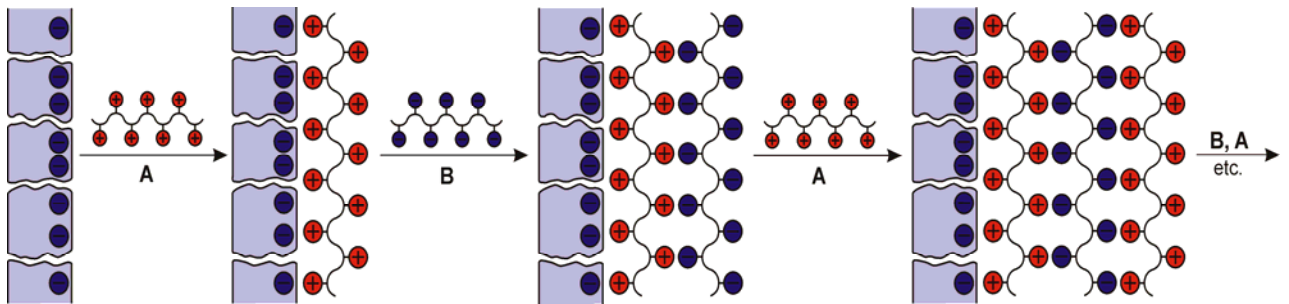
Fig. 1.2 Scheme of layer-by-layer assembly of polyelectrolytes on activated porous supporting membrane.

By repeating the adsorption steps several times, an ultrathin polyelectrolyte multilayer membrane is obtained. Some of the polymer-bound charges within the polyelectrolyte multilayer are not balanced by polymer repeat units of opposite charge, but by small exchangeable counterions. The excess polymer-bound charges act as ion-exchanger sites and are responsible for a high selectivity in ion transport.

In recent years, extensive studies have examined the ability of polyelectrolyte multilayers to act as selective separating membranes. The first studies on the transport behavior across polyelectrolyte multilayers were concerned with gas permeation. These composite membranes have shown a selectivity in the

transport of gases [54-56]. McCarthy et al. 1996 and Tieke et al. 1997 reported selectivities for oxygen and nitrogen using simple poly(allylamine hydrochloride) and poly(styrenesulfonate sodium salt) (PAH/PSS) polyelectrolyte multilayer membranes [54, 55], whereas hydrogen readily permeates through these films [54]. Sullivan and Bruening [56] found selectivities up to 6.9 for O_2/N_2 and 68 for CO_2/CH_4 permeation across imidized PAH/poly (amic acid) multilayer thin films.

Polyelectrolyte multilayers were also tested as pervaporation membranes. An initial study was reported by Tieke and co-workers [55]. Using PAH/PSS separating membranes on a poly(acrylonitrile) and poly(ethylene terephthalate) (PAN/PET) porous support, they tried to separate ethanol/water and benzene/cyclohexane. The separation was only modest, but after a careful adjustment of several parameters the ethanol/water separation could be considerably improved by the same authors [57-62].

In a recent study, by using multilayered polyelectrolyte membranes, the transport of ions under diffusion dialysis conditions was investigated by Krasemann and Tieke [58]. They demonstrated that the multi-bipolar structure of the polyelectrolyte membranes favors the separation of mono- and divalent ions by Donnan exclusion of the divalent ions. The permeation rate of sodium chloride across a PAH/PSS membrane is at least 15 times higher than for magnesium chloride. After adjusting the conditions of build-up of the membrane (pH and supporting electrolyte of dipping solution), the authors reported theoretical selectivities $\alpha(Na^+/Mg^{2+})$ up to 112.5 and $\alpha(Cl^-/SO_4^{2-})$ up to 45 [63]. Harris et al. [64] used an inorganic porous substrate (aluminum oxide with pore size of about 20 nm) coated with several PAH/PSS layers. They found high transport selectivities $\alpha(Cl^-/SO_4^{2-})$ and $\alpha(Cl^-/Fe(CN)_6^{3-})$ being 7 and 310, respectively. In further studies, it was demonstrated that the selectivity in the ion transport can be enhanced, if post deposition reactions are carried out [65]. Increasing the net fixed-charge density in the multilayer polyelectrolyte membrane [66, 67], or covalent cross-linking carried out in the membrane also increases the selectivity [68]. In a more recent study, Toutianoush and Tieke [69] investigated the ion transport across highly charged

PVA/PVS multilayered membranes. In agreement with the transport model based on Donnan exclusion/inclusion, it could be shown that the permeation rates of alkali and alkaline metal cations increase from Li^+ to K^+, and from Mg^{2+} to Ba^{2+}, that is in the direction of decreasing charge density of the naked ions. In the study of di- and multivalent Cu^{2+}, Ba^{2+}, La^{3+}, and hexacyanoferrate(II) ions across PVA/PVA, Toutianoush and Tieke [70], also reported that these ions are permanently fixed in the membrane either because of complex formation or replacement of ions with polymer-bound charged sites in the membrane.

Pressure-driven ion transport across the membrane is applied in technically important separation processes such as nanofiltration (NF) and reverse osmosis (RO). NF is becoming increasingly important for separation in areas such as water purification treatment and dye salt separation. These applications do not require the high NaCl rejection that is typical of RO membranes. NF occurs at significantly lower pressure and less energy is required. However, few studies were concerned with NF across polyelectrolyte multilayer membranes [71]. Jin et al. examined the ion transport and water flux under NF and RO conditions across PVA/PVS membranes [72]. The rejection of salts increases with increasing pressure applied, and a complete rejection was found for divalent salts such as $MgCl_2$ and $MgSO_4$, independently of feed concentration. Ion rejection of NaCl and Na_2SO_4 were 84 and 96% at 5 bar, and 93.5 and 98.5% at 40 bar, respectively. Stanton and others [73] reported that NF of mixed solutions of NaCl and Na_2SO_4 across a PSS/PAH membrane on porous alumina yields a rejection of Na_2SO_4 up to 95 %, a high selectivity (Cl^-/SO_4^{2-}) up to 80, and a water flux of about 1-2 m^3 m^{-2} day^{-1} at 4.8 bar. The authors point out that the membranes are potentially attractive for NF applications such as water and salt purification. The separation mechanism in NF can involve both electrical (Donnan) and steric (sieving) effects, and advantage of NF over RO is operation at moderate pressure with relatively high flux. The transport of neutral molecules eliminates Donnan effects and focuses exclusively on size-based selectivity. Bruening et al. demonstrated a selectivity up to about 150 in the transport of glucose/sucrose molecules. Furthermore, a size-based selectivity was found in the transport of various alcohol derivatives in both diffusion dialysis and nanofiltration across PSS/PAH, PSS/PDADMAC and PAA/PAH

multilayer polyelectrolyte membranes deposited on porous alumina [74, 75]. NF is an attractive technique for separation of fluoride from other monovalent anions using PSS/PDADMAC membranes on porous alumina supports, independently of pressure over a range of 3.6 to 6.0 bar. Fluoride was rejected by more than 70% [76]. Tieke et al. studied the pressure-driven transport of non-diluted and diluted artificial seawater at operating pressures between 10 and 40 bar across flat composite membranes containing 60 layer pairs of PVA/PVS. Flux and ion rejection of aqueous solutions of NaCl, Na_2SO_4, $MgCl_2$, and $MgSO_4$ were investigated. It was found that approximately 74% of sodium ions, 96% of calcium ions, and 98% of magnesium ions can be rejected from pure seawater in a single passage through the membrane at 40 bar [77].

Transport of organic compounds is of fundamental interest and importance for potential applications such as water purification, and separation of chemical compounds. Up to now, only a few studies were concerned with the permeation of organic compounds across polyelectrolyte multilayer films [78]. Jin et al. proved a size-selective transport of neutral and charged aromatic compounds across PSS/PDADMAC and PSS/PAH membranes, which is based on molecular sieving according to the different nanopore size of the polyelectrolyte complex membrane. For charged aromatic compounds, an additional charge-selective transport exists [79]. The selectivity in the ion transport can be enhanced, if a new type of skin separation layer is prepared consisting of cationic and/or anionic macrocycles and polyelectrolytes. These compounds exhibit highly selective interactions with inorganic and organic ions, as known from supramolecular chemistry.

1.3 Aim of the work

In all the previous studies, the preparation of ultrathin films and composite membranes based on lbl adsorption on solid substrates was based on linear or branched polyelectrolytes. However, the electrostatic lbl assembly also provides the possibility to incorporate di- or multivalent inorganic ions and macrocyclic compounds in the films, and increases the potential and applicability of the method even further, if appropriate counter partners are introduced. The crucial point of this work is the preparation of homogeneous and ultrathin separating membranes

with high constant flux and optimum separation capability. Due to specific interactions with certain molecules and ions, macrocyclic compounds represent important hosts in supramolecular chemistry. The host-guest complex formation behavior has prompted us to incorporate macrocyclic compounds in the membrane. Therefore, the principal purpose of this work was to introduce inorganic complex ions and macrocyclic charged compounds in the multilayered films and to use the films as sensors and selective composite membranes. To our knowledge, this is the first time that permselective multilayered membranes including macrocyclic compounds are reported.

In a first section of our work, we have chosen macrocyclic 1,4,7,10,13,16 hexaazaoctadecane (Hexacyclen = **aza6** = 18-azacrown) as cationic compound replacing a linear cationic polyelectrolyte in the membrane. Before studying the transport properties, we first investigated the preparation conditions (such as pH, presence of supporting electrolyte, and concentration of **aza6** in the dipping solution) of multilayer films on quartz substrates in detail. As anionic polyvalent counterion, we used poly(styrene sulfonate) (PSS), or poly(vinylsulfate) (PVS). Besides, also anionic macrocycles such as tetra-p-sulfonatocalix[4]arene (**calix4**), hexa-p-sulfonatocalix[6]arene **(calix6)**, or octa-p-sulfonatocalix[8]arene (**calix8**) were used as well as small inorganic tetravalent hexacyanoferrate(II), HCF(II). For all **aza6**/polyanion combinations, lbl films could be successfully prepared. The rather unexpected formation of lbl assemblies of the cationic macrocyclic **aza6** and the inorganic tetravalent HCF(II) reinforced us to also study analogous films with oppositely charged macrocycles and inorganic ions, i.e., anionic macrocyclic **calix6** or **calix8** and inorganic trivalent lanthanum cations, in presence and in absence of crown ether.

In a second section, we have investigated the ion transport across **aza6**/PVS membranes under diffusion dialysis and nanofiltration conditions, i.e., both a concentration gradient and a pressure difference across the membrane. The permeation measurements indicate that the **aza6** containing membranes are useful for separation of mono- and divalent anions, but high separation factors can only be obtained after a treatment of the membranes with an aqueous copper(II)

acetate solution resulting in a complex formation with **aza6**. The theoretical separation factors α(chloride/sulfate) and α(chloride/sulfite) are 110 and 1420, respectively. Under NF condition, the rejection of sulfate (98.6%) is higher than of chloride ions (56.5%) for 60 bilayers at 14 bar. Rejection decreases and flux increases with increasing Δp and rejection increases and flux decreases with the number of deposited layers.

In a third section, we utilized p-sulfonated calix[8]arenes as anionic part in bipolar **calix8**/PVA membranes and studied the permeability of a variety of mono-, di-, and trivalent metal ions. They exhibit a highly selective transport of inorganic metal chloride salts such as rare earth metal ions and yttrium ions. Since this effect cannot only originate from electrostatic forces we postulate an additional complex formation with the calixarene units. Due to the complex formation, the membrane is almost impermeable for rare earth metal ions. Very high separation factors α (NaCl/LnCl$_3$) up to 160 are observed. Furthermore, **calix8** contains a large hydrophobic cavity and it was found that the membranes also exhibit high selectivities for charged and uncharged aromatic compounds. The size of the aromatic units and the number of charged substituent groups were varied. For the neutral compounds, a size-selective transport was found and for the charged aromatic compounds, both a size- and charge-selective transport was observed.

2 Theoretical Aspects

2.1 Membranes

A membrane is a permeable or semi-permeable phase, consisting of polymers, semiconductor or metal oxides, which restricts the motion of certain species. Thus a membrane can be defined essentially as a barrier, which separates two phases and restricts the transport of various chemicals in a selective manner. A membrane can be homogenous or heterogeneous, symmetric or asymmetric in structure, solid or liquid, can carry positive or negative charges or can be neutral or bipolar. Transport through a membrane can be affected by convection or by diffusion of individual molecules, induced by an electric field or concentration, pressure differences or a temperature gradient. The performance of a membrane is defined in terms of two simple factors, flux and retention or selectivity. Flux or permeation rate is the flow rate of a fluid passing through the membrane per unit area and unit time. Selectivity is a measure of the relative transport rates of different components through the membrane. Retention is the fraction of solute in the feed retained by the membrane. A good membrane is characterized by a high selectivity or retention and a high flux or permeation capability [80].

2.1.1 Classification of membranes

The proper choice of a membrane should be determined by a specific application objective: particulate or dissolved solid removal, hardness reduction or ultra pure water production, removal of specific gases, molecules and ions. The end–user may also dictate the selection of membranes for industries such as potable water, effluent treatment, desalination or water supply for electronic or pharmaceutical manufacturing. The following section shows the types of membranes commonly used.

2.1.1.1 Microporous membranes

The membrane almost behaves like a fiber filter and separation occurs by a sieving mechanism determined by the pore diameter and particle size. Materials

such as ceramics, graphite, metal oxides, polymers etc. are used in making such membranes. The pores in the membrane may vary between 1.0 nm and 20 microns. Here the pore size (and pore size distribution) mainly determines, which particles or molecules are retained and which will pass through the membrane (Figure 2.1).
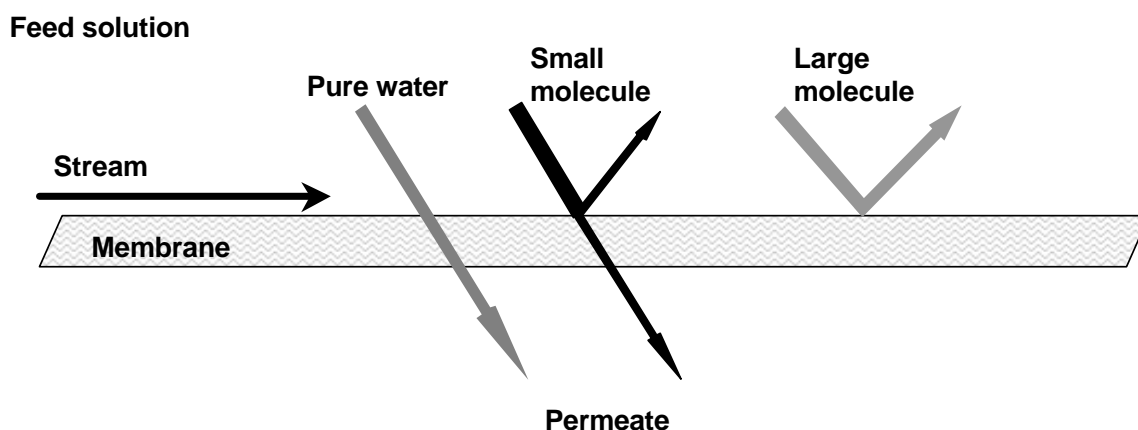
Fig. 2.1 Rejection model of membrane [81].

2.1.1.2 Homogeneous membranes

Homogeneous membranes are dense films, through which a mixture of molecules is transported by a pressure, concentration or electrical potential gradient. Using these membranes, chemical species of similar size and diffusivity can be separated efficiently when their concentrations differ significantly.

2.1.1.3 Asymmetric and composite membranes

An asymmetric membrane comprises a very thin (10 – 100 nm) skin layer on a highly porous (100 – 200 microns) thick substructure. Skin and substructure consist of the same material. The skin acts as the selective membrane. Its separation characteristics are determined by the nature of membrane material or pore size, and the mass transport rate is determined mainly by the skin thickness. The porous substructure acts as a support for the thin, fragile skin and has little effect on the separation characteristics. If skin and substructure are made of different materials, the membrane is denoted as ´composite membrane´.

2.1.2 Membrane separation processes

All membrane separation process have been developed for specific applications. The membrane has the ability to transport one component more readily than the other because of differences in physical and/or chemical properties between the membrane and the permeating component. Transport through the membrane takes place when a driving force acts on the individual components in the feed solution (Figure 2.1). The extent of the driving force F is determined by the gradient in potential across the membrane (ΔX) divided by the membrane thickness (L):

$$F = \frac{\Delta X}{L} \qquad\qquad\qquad (1)$$

Two main potential differences are important in membrane processes, the chemical potential difference $\Delta\mu$ and the electrical potential difference ΔF (the electrochemical potential is the sum of the chemical potential and the electrical potential). In passive transport, components or particles are transferred from a high potential to a low potential (eqn.1, Figure 2.2). The driving force is the gradient in potential ($\partial X/\partial L$). Instead of differentials it is often more useful to use differences ($\partial X/\partial xL \approx \Delta X/\Delta L$). The average driving force (F_{ave}) is equal to the difference in potential across the membrane divided by the membrane thickness:

$$F_{ave} = -\frac{\Delta X}{L} \qquad\qquad\qquad (2)$$

If no external forces are applied to the system, it will reach equilibrium when the potential difference has become zero. Equilibrium processes are not relevant and will therefore not be considered. When the driving force is kept constant, a constant flow will occur through the membrane after establishment of a steady state. There is a proportionality between the flux (J) and the driving force (F), i.e.
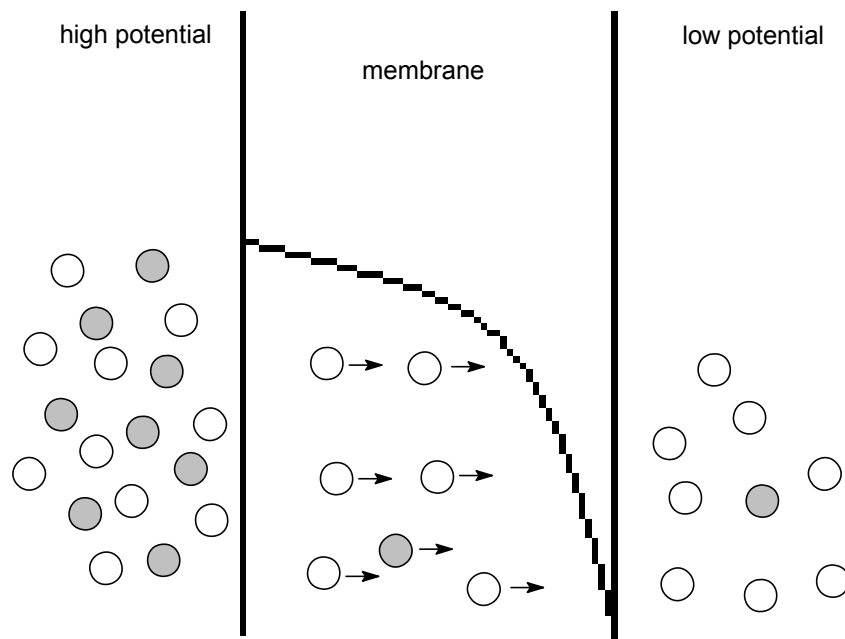
Fig. 2.2 Transport model of species across the membrane due to potential gradient.

Flux (J) = proportionality (D) x driving force (F)   (3)

J = - D ΔX/L

An example of such a linear relationship is Fick's law, which relates the mass flux to a concentration difference. The proportionality factor D is called the diffusion coefficient. D determines how fast the component is transported through the membrane, or measures the resistance exerted by the membrane as a diffusion medium, when a given force is acting on this component. The driving force ΔX/L, can be expressed as the gradient of X (potential) along a coordinate L perpendicular to the transport barrier.

2.1.2.1 Driving force F

As indicated above, the transport across a membrane takes place when a driving force is applied, i.e a chemical potential difference or an electrical potential difference acts on the individual components in the system. The potential difference arises as a result of differences in either pressure, concentration,

temperature or electrical potential. Membrane processes involving an electrical potential difference occur in electrodialysis and other related processes. The nature of these processes differs from that of other processes involving a pressure or concentration difference as the driving force.

In most of the membrane processes the driving force is a concentration c (or activity a) difference or a pressure p difference across the membrane. Parameters such as pressure, concentration and even temperature may be included in one parameter, the chemical potential μ.

$$\mu = f(T, p, a \text{ or } c) \tag{4}$$

Under isothermal conditions (constant T), pressure and concentration contribute to the chemical potential of component i according to

$$\mu_i = \mu_i^0 + RT\ln a_i + V_i p \tag{5}$$

where μ_i^0 is the chemical potential of 1 mol of pure substance at a pressure p and a temperature T. For pure components the activity is unity, i.e. a=1, but for liquid mixtures the activity is given by

$$a_i = \gamma_i x_i \; , \tag{6}$$

where x_i is the mole fraction and γ_i is the activity coefficient. For ideal mixtures the activity coefficient is unity, i.e. γ_i =1, so that the activity is equal to the mole fraction, i.e. $a_i = x_i$.

The chemical potential difference $\Delta\mu_i$ can be subdivided into a difference in composition and a difference in pressure according to

$$\Delta\mu_i = RT \; \Delta\ln a_i + V_i \Delta p \; . \tag{7}$$

An osmotic pressure arises when pure solvent permeates through a semipermeable membrane to dilute the electrolyte solutions. This situation is illustrated schematically in Figure 2.3.
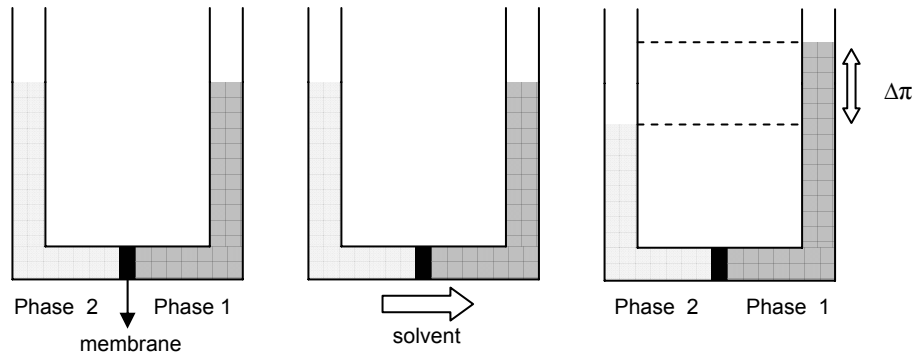
Fig.2.3 Schematic illustration of osmotic processes.

Here the membrane separates two liquid phases: a concentrated phase 1 and a dilute phase 2. At constant temperature, the chemical potential of the solvent in the concentrated phase (phase 1) is given by

$$\mu_{i,1} = \mu_{i,1}^0 + RT\ln a_{i,1} + V_i p_1, \tag{8}$$

while the chemical potential of the solvent in the dilute phase (phase 2) is given by

$$\mu_{i,2} = \mu_{i,2}^0 + RT\ln a_{i,2} + V_i p_2. \tag{9}$$

The solvent molecules in the dilute phase have a higher chemical potential than those in the concentrated phase ($a_{i,2}$ is largre than $a_{i,1}$). The chemical potential difference causes a flow of solvent molecules from the dilute phase to the concentrated phase as shown in Figure 2.3. This process continues until an osmotic equilibrium has been reached, i.e., until the chemical potentials of the solvent molecules in both phases are equal:

$$\mu_{i,1} = \mu_{i,2}. \tag{10}$$

Combination of eqn. 8, 9 and 10 results in

$$RT(\ln a_{i,1} - \ln a_{i,2}) = (p_1 - p_2)V_i = \Delta\pi\, V_i. \qquad (11)$$

The hydrodynamic pressure difference (p_1 – p_2) is called $\Delta\pi$. If only pure solvent is present on one side of the membrane, i.e., a_i=1, then eqn. 11 becomes

$$\pi = -\frac{RT}{V_i}\ln a_{i,2}. \qquad (12)$$

For very low solute concentrations $(\gamma_i \Rightarrow 1)$ eqn. 12 can be simplified further by applying Raoult's law:

$$\ln a_i = \ln\gamma_i x_i \approx \ln x_i \approx \ln(1 - x_j) = -x_j \qquad (13)$$

and

$$\pi = \frac{RTx_j}{V_i}. \qquad (14)$$

For a dilute solution, $x_j \approx n_j/n_i$ and

$$\pi\, n_i V_i = n_j RT$$

or

$$\pi\, V = n_j RT. \qquad (15)$$

Because $n_i V_i \approx V$ (for dilute solutions) and $n_j/V = c_j/M$, it follows that

$$\pi = c_j RT/M. \qquad (16)$$

This simple relationship between the osmotic pressure π and the solute concentration c_j is called the van't Hoff equation. It can be seen that the osmotic pressure is proportional to the concentration and inversely proportional to the molecular weight.

2.1.2.2 Transport through porous membranes

Porous membranes are used in microfiltration and ultrafiltration processes. These membranes consist of a polymeric matrix in which pores within the range of 2 nm to 10 micrometer are present. Ultrafiltration membranes generally have an asymmetric structure, where the porous top-layer mainly determines the resistance to transport. Particles are separated on the basis of their molecular size and shape with the use of pressure and specially designed semi-permeable membranes.
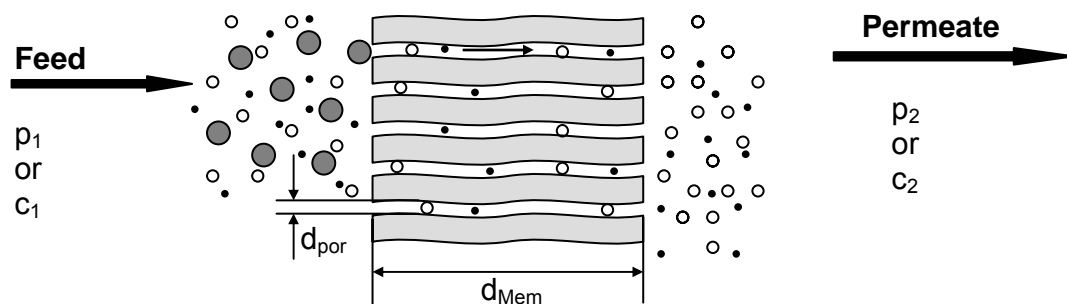
Fig. 2.4 Rejection model of porous membrane [81].

Low permeation rates may also be caused by a clustering of the penetrating molecules, i.e., the component diffuses not as a single molecule but in its dimeric or trimeric form. This implies that the size of the diffusing components increases and that the diffusion coefficient consequently decreases.

2.1.2.3 Transport through nonporous membranes

If the sizes of molecules have the same order of magnitude, porous membranes cannot achieve a separation. In this case, a nonporous membrane must be used. However, the term nonporous is rather ambiguous because pores are present on a molecular level in order to allow transport even in such a membrane. Basically, the transport of a liquid through a dense, nonporous membrane can be described in terms of a solution-diffusion mechanism, i.e.,

Permeability (P) = Solubility (S) x Diffusivity (D).   (17)

Solubility is a thermodynamic parameter and gives a measure of the amount of penetrant sorbed by the membrane under equilibrium conditions. The diffusivity is a kinetic parameter which indicates how fast a penetrant is transported through the membrane. Diffusivity is dependent on the geometry of the penetrant, for as the molecular size increases the diffusion coefficient decreases. However, the diffusion coefficient is concentration-dependent on the interacting system and even large molecules having the ability to swell the polymer can have large diffusion coefficients.

In order to describe transport through a porous or nonporous membrane two contributions must be taken into account, the diffusional flow (v) and the convective flow (u). The flux J of the component i through a membrane can be described as

$$J_i = c_i(v_i + u) \tag{18}$$

The contribution of convective flow is the main term in any description of transport through porous membranes. In nonporous membranes, however, the convective flow term can be neglected and only diffusional flow contributes to transport. From porous to nonporous membranes, an intermediate region exists where both contributions have to be taken into account. A solution-diffusion model will be used where each component dissolves into the membrane and diffuses through the membrane independently. The flux of a component through a membrane may be described in terms of the product of the concentration and the velocity, i.e., convective flow makes no contribution. Hence,

$$J_i = c_i \cdot v_i . \tag{19}$$

The mean velocity of a component i in the membrane is determined by the driving force X acting on the component and the fractional resistance f exerted by the membrane, i.e.,

$$v_i = \frac{X_i}{f_i} . \tag{20}$$

The driving force is given by the gradient $d\mu/dx$. The fractional coefficient can be related to the thermodynamic diffusion coefficient D_T. If ideal conditions are assumed, i.e., if the thermodynamic diffusion coefficient is equal to the observed diffusion coefficient,

$$J_i = \frac{D_i c_i}{RT} \frac{d\mu_i}{dx} \quad . \tag{21}$$

The chemical potential can be written as

$$\mu_i = \mu_i^0 + RT \ln a_i + v_i \cdot (p - p^0), \tag{22}$$

and substitution of eq. 22 into eq. 21 gives

$$J_i = \frac{D_i c_i}{RT} \left[RT \frac{d\ln a_i}{dx} + v_i \frac{dp}{dx} \right]. \tag{23}$$

2.1.2.4 Pressure-driven membrane processes

Pressure-driven membrane processes can be used to concentrate or purify a dilute (aqueous) solution. Particle or molecular size and chemical properties of the solute determine the structure, i.e., pore size and pore size distribution required for the membrane employed. Various processes can be distinguished related to the particle size of the solute and consequently to the membrane structure (Figure 2.5). These processes are microfiltration, ultrafiltration or hyperfiltration (nanofiltration NF and reverse osmoses RO see p. 20). As we go from microfiltration through ultrafiltration to hyperfiltration, the size (molecular weight) of the particles or molecules to be separated diminishes and consequently the pore sizes in the membrane must become smaller. This implies that the resistance of the membranes to mass transfer increases and hence the applied pressure has to be increased.
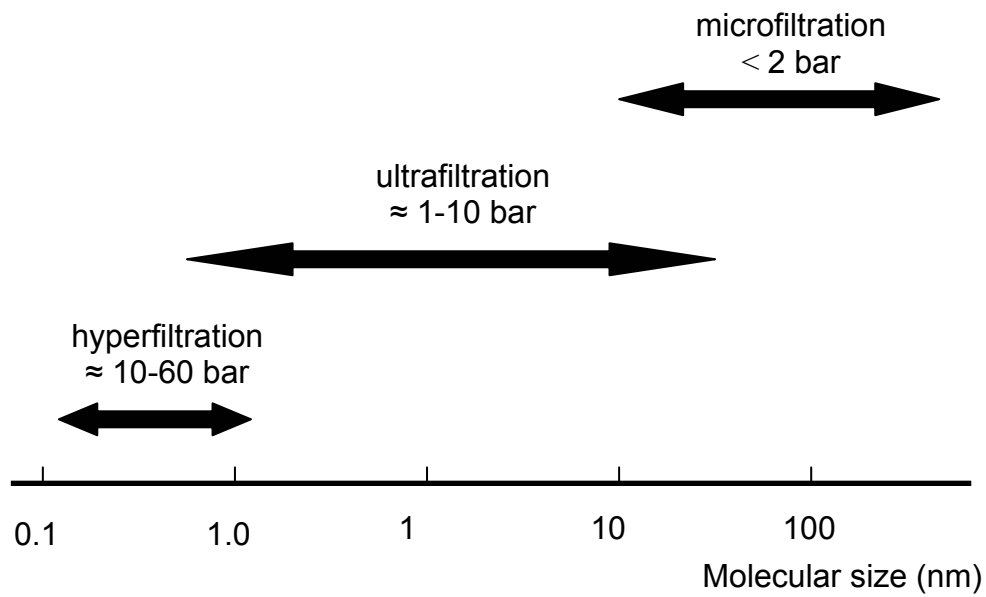
Fig.2.5 Application range of microfiltration, ultrafiltration and hyperfiltration [80].

The volume flow through these microfiltration membranes can be described by Darcy's law, the flux J through the membrane being directly proportional to the applied pressure:

$$J = K \ \Delta p , \tag{24}$$

where the permeability constant K contains structure factors such as the porosity ε and the pore size (pore size distribution). Hyperfiltration is normally used for aqueous solutions containing a low molecular weight solute, which is often a salt and very small amounts of organic solutes. The process involves the application of pressure to the liquid feed mixture as driving force, the total flux being given by the sum of the water flux J_w and the solute flux J_s. For highly selective membranes the solute flux can be neglected (even with less selective membranes the solvent flux is large compared to the solute flux):

$$J_{total} = J_W + J_S \approx J_W . \tag{25}$$

2.1.2.4.1 Nanofiltration separation processes

Nanofiltration is a form of filtration that uses membranes to separate different fluids or ions. NF is a membrane process whose nature lies between ultrafiltration and reverse osmosis (RO). NF is typically referred to as "loose" RO due to its larger membrane pore structure as compared to membranes used in RO, and allows more salt to pass through the membrane. Because it can operate at much lower pressure, and some of the inorganic salts can pass, NF is used in applications where high organic removal and moderate inorganic removals are desired. NF is capable of concentrating sugars, divalent salts, bacteria, proteins, particles, dyes and other constituents, which have a molecular weight greater than 1000 Dalton. Membranes used for NF consist of cellulosic acetate and aromatic polyamide type having characteristics as salt rejections from 95% for divalent salt to 40% for monovalent salts. An advantage of NF over RO is that NF can typically operate at higher recoveries, thereby conserving total water usage due to a lower concentrate stream flow rate.

The solutions containing the low molecular weight solutes have a much higher osmotic pressure than the macromolecular solutions used. In Figure 2.6, a membrane separating pure water from a salt solution is shown. The membrane is permeable to the solvent but not to the solute. In order to allow water to pass through the membrane, the applied pressure must be higher than the osmotic pressure. As can be seen in Figure 2.6, water flows from the dilute solution to the concentrated solution, if the applied pressure is smaller than the osmotic pressure. When the applied pressure is higher than the osmotic pressure, water flows from the concentrated solution to the dilute solution. The effective water flow can be represented by eqn. 24, if one assumes that no solute permeates through the membrane:
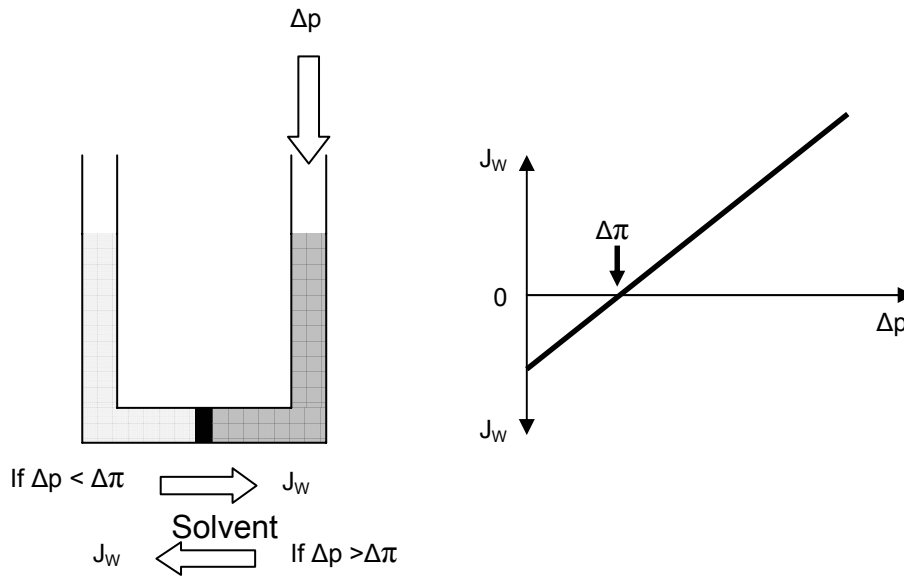
Fig.2.6 Schematic drawing of water flow (J_W) as a function of applied pressure.

$$J_W = A(\Delta p - \Delta \pi). \qquad (24)$$

In practice, the membrane may be a little permeable to low molecular solutes and hence the real osmotic pressure difference across the membrane is not $\Delta \pi$ but $\sigma \Delta \pi$, where σ is the reflection coefficient of the membrane towards that particular solute. When $R < 100\%$, then $\sigma < 1$ and flux J_W becomes

$$J_W = A(\Delta p - \sigma \, \Delta \pi). \qquad (25)$$

The selectivity of a membrane for a given solute is expressed by the retention coefficient or rejection coefficient R:

$$R = \frac{c_f - c_p}{c_f} = 1 - \frac{c_p}{c_f}. \qquad (26)$$

Consequently, as the pressure increases the selectivity also increases because the solute concentration in the permeate decreases.

2.1.2.5 Concentration difference as the driving force

Substances diffuse spontaneously from places with high chemical potential to those where the chemical potential is low (Figure 2.2). Processes which make use of a concentration difference as the driving force are gas separation, pervaporation, liquid membrane process and diffusion dialysis. A factor that enhances segmental mobility or chain mobility in general is the presence of low molecular penetrates. Increasing concentration of penetrates inside the polymeric membrane leads to an increase in the chain mobility and consequently to an increase in permeability (or diffusivity). The concentration of the penetrate inside the polymeric membrane is determined mainly by the affinity between the penetrate and the polymer.

2.1.2.5.1 Ion separation

If a concentration difference is applied across a homogeneous membrane, the process is called diffusion dialysis. Transport takes place by diffusion and separation is obtained through differences in diffusion rates because of differences in physical and chemical properties such as molecular weight, charge density and hydrophilicity. Kimura et al [82,83] reported that a bipolar membrane could be obtained from the successive coating of a porous support with a layer of a cationic and an anionic polyelectrolyte.
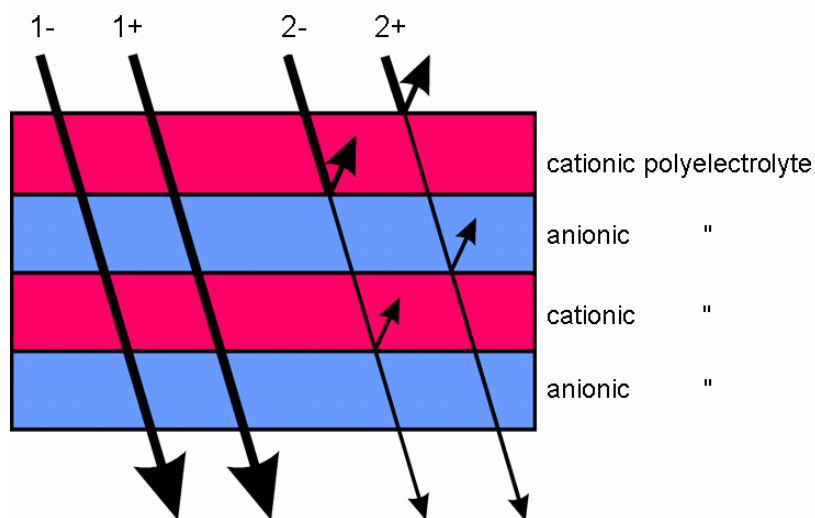
Fig. 2.7 Rejection model of a multibipolar polyelectrolyte membrane (from ref.[69]).

In Figure 2.7, the rejection model of a multi-bipolar polyelectrolyte multilayer membrane is shown. In the case of incomplete charge neutralization, individual layers generally represent barriers for ions of high charge density. Ions permeating through such a membrane receive strong repulsive forces from the equally charged parts (Donnan rejection) and attractive forces from the oppositely charged parts (Donnan attraction) of the membrane. For divalent permeating ions, the interactions are much stronger than for monovalent ones and thus, a high selectivity in ion transport occurs. The model implies that the ion separation becomes progressively more effective if the number of adsorbed polyelectrolyte layers is increased and that the separation achieved is independent of the surface charge of the membrane [63,84].

2.1.3 Transport resistance in membranes

In order to achieve a particular separation via a membrane process, the first step is to develop a suitable membrane. However, during an actual separation, the membrane performance can change very much with time, and often a typical flux-time behaviour may be observed: the flux through the membrane decreases over time. This phenomenon is mainly due to concentration polarization and fouling (Figure 2.9). All these factors induce additional resistances on the feed side to the transport across the membrane. The extent of these phenomena is strongly dependent on the membrane process and the feed solution employed.

2.1.3.1 Concentration polarization

For convenience, let us consider a solution consisting of a solvent and a solute. Since the membrane has the ability to transport one component more readily than the other separation is accomplished. When a driving force acts on the feed solution, the solute is retained by the membrane whereas the solvent passes the membrane. Thus the membrane has a certain retention for the solute, while the solvent can permeate. This implies that the concentration of the solute in the permeate c_p is lower than the concentration in the bulk c_b, which is in fact the basic concept of membrane separation. The retained solutes can accumulate at the membrane surface, where their concentration will gradually increase. Such a

concentration build-up will generate a diffusive flow back to the bulk of the feed, but after a given period of time, a steady-state condition will be established. The convective solute flow to the membrane surface will be balanced by the solute flux through the membrane plus the diffusive flow from the membrane surface to the bulk (only concentration polarization is considered). A concentration profile has now been established in the boundary layer (Figure 2.8).
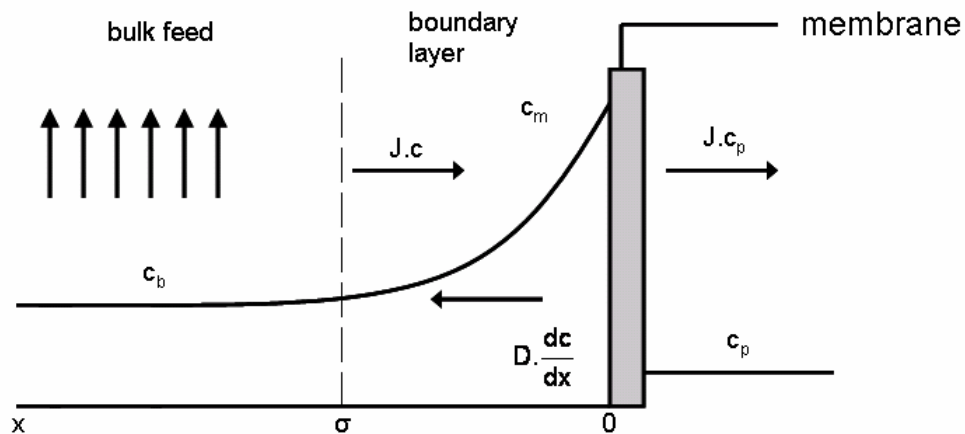
Fig.2.8 Scheme of concentration polarization[80].

However, near the membrane surface a boundary is formed where the concentration increases and reaches a maximum value at the membrane surface c_m. The convection flow of solutes towards the membrane may be written as $J \cdot c$. If the solute is not completely retained by the membrane, there will be a solute flow through the membrane equal to $J \cdot c_p$. The accumulation of the solute at the membrane surface leads to a diffusive back flow towards the bulk of the feed. Steady-state conditions are reached when the convective transport of solute to the membrane is equal to the sum of the permeate flow plus the diffusive back transport of the solute, i.e.,

$$J \cdot c = J \cdot c_p + D \frac{dc}{dx} \qquad\qquad (27)$$

The consequences of concentration polarization can be summarized as follows:

- Retention becomes lower, because of the increasing solute concentration at the membrane surface.
- Retention becomes higher in the case of mixtures of macromoleculer solutes, where concentration polarization can have a strong influence on the selectivity with respect to the lower molecular weight solute.
- Flux will be lowered.

2.1.3.2 Fouling

The flux decline is the result of membrane fouling, which may be defined as the (ir)reversible deposition of retained particles, suspensions, macromolecules, salts etc. Fouling occurs mainly in porous membranes, which are implicitly susceptible to fouling. For all polarization phenomena, the flux at a finite time is always lower than the original value. When steady-state conditions have been attained a further decrease in flux will not be observed, i.e., the flux will become constant as a function of time. Polarization phenomena are reversible processes, but in practice, a continuous decline in flux can often be observed (Figure 2.9).
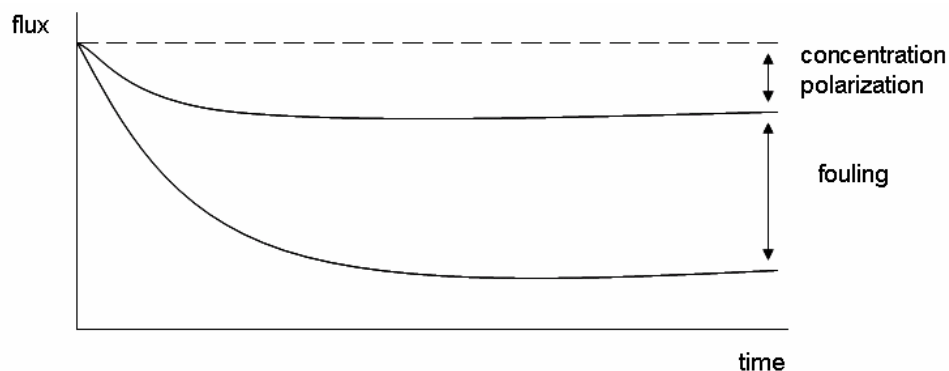
Figr.2.9. Flux as a function of time. Both concentration polarization and fouling can be distinguished.

Other than the driving force, the membrane itself is the main factor determining the selectivity and flux. In fact the composition of the membrane (its structure and material) determines the type of application, ranging from the separation of mono-, di-, and trivalent ions to the separation of organic molecules of an identical size or shape.

2.2 Layer-by-layer assembled membranes

For preparation of a good composite membrane using the layer-by-layer assembly method, suitable porous supports and polyelectrolytes have to be carefully chosen and suitable conditions for preparation of the composite membranes have to be optimized [85]. First step in the preparation of the composite membranes is the choice of a suitable supporting membrane. With one exception, only porous substructures were used. The advantage is that the transport across the composite membrane is only little affected by the substructure so that the separation achieved can be exclusively ascribed to the ultrathin polyelectrolyte multilayer adsorbed at the surface.

Second step in the preparation of the composite membrane is a selection of polyelectrolytes and adsorption of the separation layer. By using lbl alternating assembly of polyelectrolytes on charged porous substrate, a skin separation film is obtained with some advantageous properties: since each step adds about 0.5 nm to the total thickness of the film, an ultrathin, homogenous coating of precisely controlled thickness is obtained. In order to describe the influence of polyelectrolyte structure on separation behavior it is useful to briefly discuss the structure of the separating membrane.

(a)   (b)
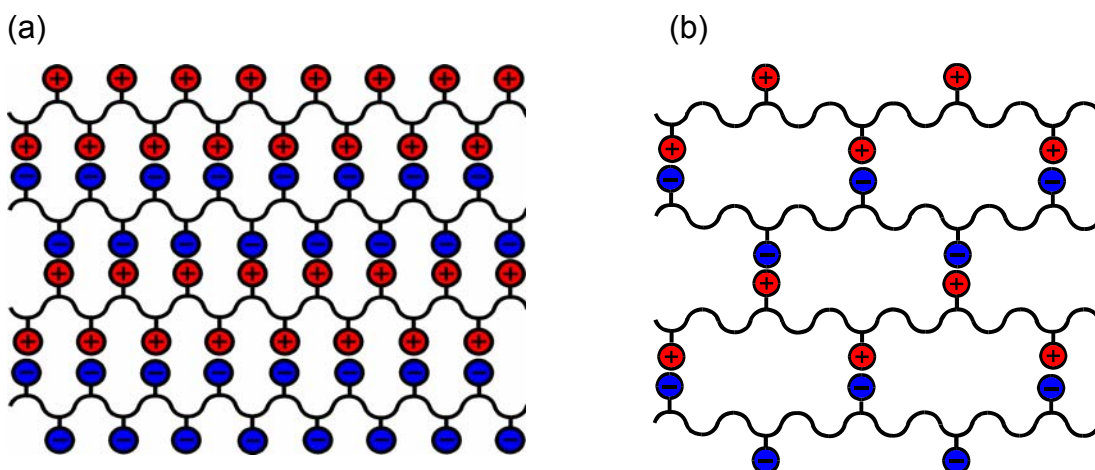
$$\text{Charge density } \rho_c = \left[\frac{\text{number of ion pairs per reapeat unit of polyion complex}}{\text{number of carbon atoms per repeat unit of polyion complex}} \right]$$

Figr.2.10 Simplified structure model of multilayered polyelectrolyte membrane and definition of charge density ρ ;(a) high charge desity, (b) low charge desity.

In Figure 2.10 a and b, a very idealized model of polyelectrolyte multilayer membrane is shown. According to this model, the membrane exhibits a physical network structure with pores of defined size in the angstrom range, which are denoted as nanopores. From this model one can derive that cross-linking density and mash size are controlled by the charge density ρ_c of polyelectrolyte used and by varying the conditions of the dipping solution. Using polyelectrolytes of high charge density, a network with small pores is formed (Figure 2.10 a), while with polyelectrolytes of low charge density a network with large or medium pore size can be expected (Figure 2.10 b), which should be very permeable to molecules and ions.
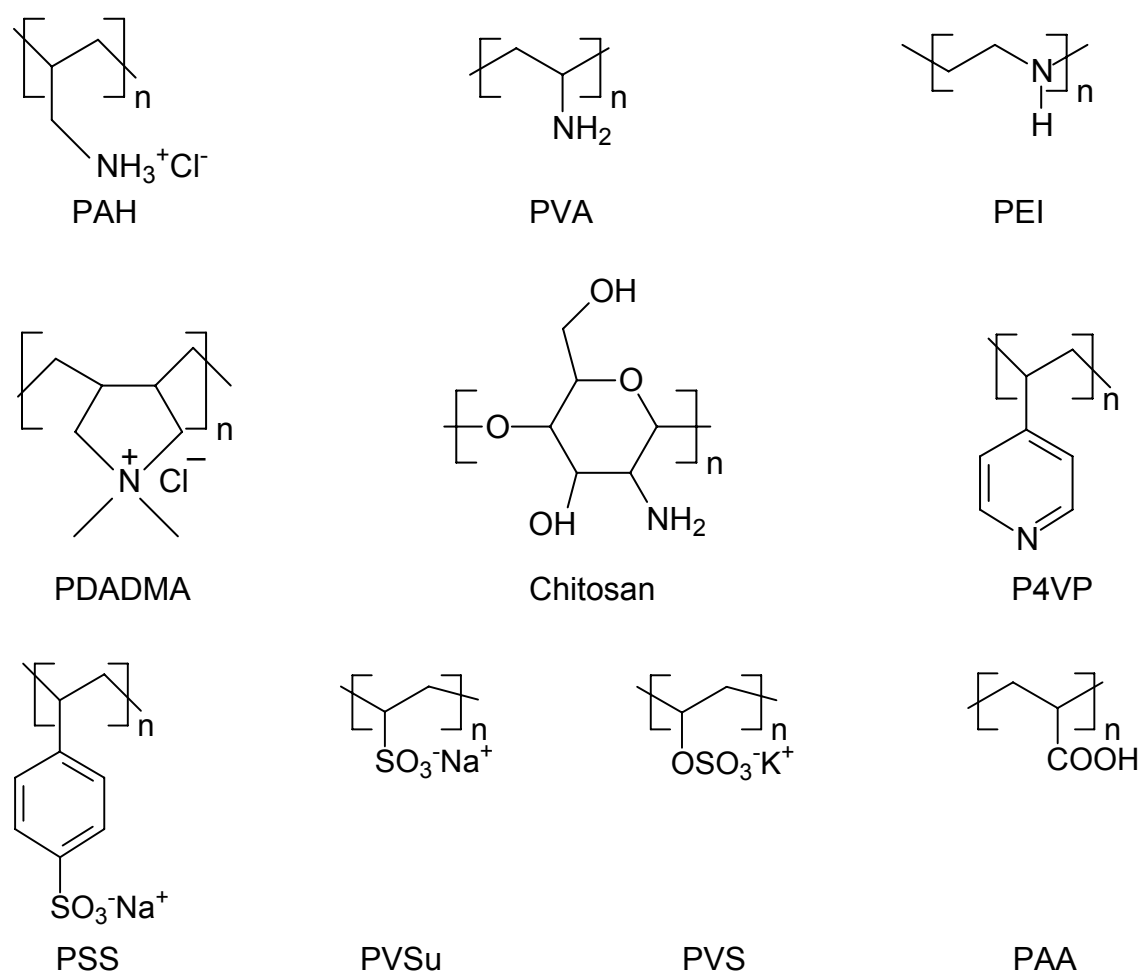
Fig.2.11 Structure of some polyelectrolyte compounds previously used for build up of multilayered membranes.

A wide variety of linear and branched polyionic compounds can be adsorbed, which allows to tailor appropriate membranes for various separation problems. In Figure 2.11, the various compounds previously used for preparation of the separation layer are complied. In recent years, a number of reviews on the transport properties of polyelectrolyte multilayer membranes already appeared [84-86].

In the third step, it was necessary to optimize the conditions for the polyelectrolyte adsorption. Usually the adsorption of individual polyelectrolyte layers is detected using UV/IR spectroscopy or X-ray reflectivity measurements [10-13, 49]. Several parameters were studied [55] such as kind of supporting membrane, pH of polyelectrolyte solution, molecular weight of polyelectrolyte, dipping time of substrate and supporting electrolyte added. The previous studies were quite helpful in defining optimum conditions for the preparation of the separating membranes. According to these studies it was also convenient to work with macrocyclic compounds, whose adsorption conditions onto porous supports are similar to polyelectrolytes.

2.2.1   Macrocyclic compounds

Beside polyelectrolytes, also small charged compounds such as bolaamphiphiles have been assembled as molecular layers in combination with oppositely-charged polyions. Macrocyclic compounds are known as building blocks from supramolecular chemistry, which often are able to act as host compounds for small molecules and ions. Incorporation of charged macrocycles in lbl- assemblies should therefore allow to improve the selectivity of the membranes for certain compounds. In the following, the use of polyazacrown ethers and p-sulfonatocalix[n]arenes as possible building blocks for lbl assembled membranes is discussed.

2.2.1.1 Azacrown ether as cationic macrocyclic compound

One system that has attracted interest with anion binding is the hexaaza macrocycle, 1, 4, 7, 10, 13, 16-hexaazacyclooctadecane ([18]aneN$_6$, **aza6**, L,

sometimes referred to as Hexacyclen or 18-azacrown-6 (Figure 2.12))[87]. Macrocyclic **aza6** has been shown to complex strongly and selectively a variety of inorganic anions [87-90].
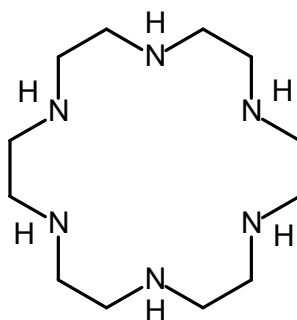
Fig.2.12 Structure of 1, 4, 7, 10, 13, 16-hexaazacyclooctadecane.

The important forms of **aza6** in aqueous solution at pH 6 are the tetra- and tri-protonated species. The ionic activity coefficients of H_3L^{3+}, H_4L^{4+}, and H_4LX^{3+} complexes are highly sensitive to ionic compounds such as inorganic phosphate, AMP, ADP, ATP, etc. [91,92]. The shape and size of the macrocyclic cavity are presumed to influence the bonding interactions within films and so to account for selectivity in the membrane [90-94]. Grechin et al. [95] reported that nitrogen atoms of nonsubstituted polyamines display electron-donor properties, which favour the formation of complexes with cations. Upon introduction of electron acceptor groups, these ligands become receptors of anions due to the local positive charge that appears at the nitrogen atoms. The **aza6** also forms much more stable and selective complexes with various transition-metal ions than do open chain analogues having the same donor arrangement. Thin layer chromatography (TLC) separation shows that the best separation of the **aza6** was achieved with citrate buffer solution at pH 6. It was larger than for relevant linear polyamines [96]. It has generally been assumed that electrostatic and ionic hydrogen bonding interactions provide the binding forces in anion complexes of protonated **aza6.** Mertesdorf et al. [97] prepared well-ordered monolayers of amphiphilic azacrowns films. The films exhibited distinct selectivity for nucleotides (ATP>ADP>AMP). Multilayers of one of these nucleotide-sensitive compounds, having a well-defined layer spacing, could be prepared on hydrophobized quartz via Langmuir-Blodgett deposition.

2.2.1.2 Calixarene as anionic macrocyclic compound

Calix[n]arenes are macrocyclic oligomers of phenol usually consisting of 4, 6, or 8 monomer units (n) and prepared by the base-catalyzed reaction of formaldehyde with a phenol derivative [98]. Calixarenes represent one of the most important macrocyclic host molecules in supramolecular chemistry [99, 100].
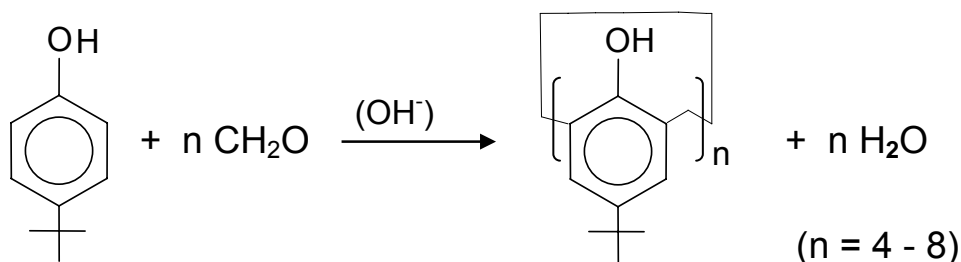
Like crown ethers [101] and cyclodextrins [102] they contain a large hydrophobic cavity, and but there are three major differences: 1) the internal cavity is lined by the π-electrons of the aromatic rings, in contrast to the pure σ-framework of cyclodextrins and crown ethers; and 2) only one rim is lined by hydroxyl groups, and 3) the rings are linked by methylene bridges, which results in a much greater rotational freedom of the individual rings. Thus calixarenes have a very different type of internal cavity, and a much greater range of possible conformers [103] (cavity size and shape) as compared with cyclodextrins. Their supramolecular host properties can therefore be expected to be distinctive. The molecular structures of three different p-sulfonatocalix[n]arenes with n= 4, 6, or 8 (**calix4**, **calix6**, or **calix8**) are shown in Figure 2.13.

Because of their basket shape they are suited for the complexation of small molecules and ions. Applications as extractors of metal ions [104, 105] as carriers in liquid membranes [106-108] and as sensors for heavy-metal ions [109] and volatile organic compounds were described [110]. Shinkai and co-workers [111, 112] reported that water-soluble hexasulfonated calix[6]arenes with various substituents could be associated with small organic molecules such as pyridine and 2-anilinonaphthalene [113,114].
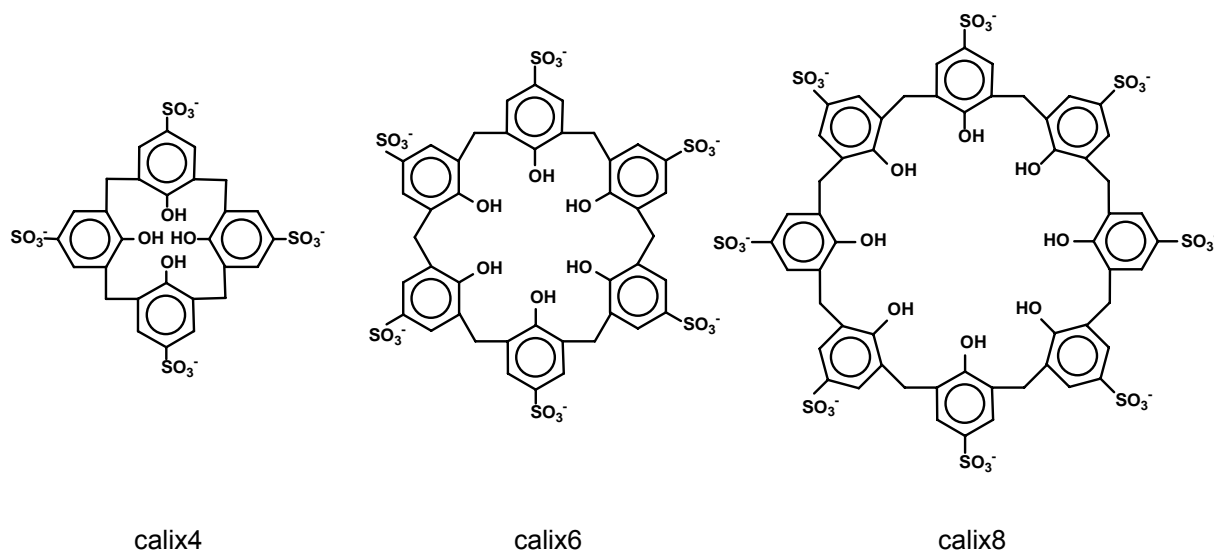
Fig.2.13 Structure of **calix4**, **calix6**, and **calix8**.

Although there is a growing interest in ultrathin, defect-free membranes exhibiting high flux and high separation capability, until now only a few attempts have been made to incorporate calixarene derivatives in membranes to improve their separation capability. Regen and others [115,116] prepared Langmuir and Langmuir-Blodgett films of well-ordered amphiphilic calixarene derivatives and used these films for gas permeation studies. The membranes exhibited high permeation selectivity for distinct gases such as helium. The selectivity was ascribed to a sieving effect originating from the regular pore structure in the films. In other work [117,118], the selective binding of metal ions from the aqueous subphase to monolayers of calixarenes floating on the water surface was studied. However, only a few studies were concerned with electrostatically adsorbed multilayer films containing calixarene derivatives.

Swanson and co-workers [110] described multilayer films of polyelectrolyte/calixarene, which were used as chemically selective layers for organic-vapor detection. Yang and Cao reported on photosensitive multilayer films of diazoresins and calixarenes [119]. However, the use of self-assembled calixarene-containing multilayer films as ion-selective membranes has not been reported previously. In the course of our study on self assembled films for ion-sieving and sieving of molecules, we became interested in calixarenes because of

their basket-shape and stereochemical conformations of these molecules [120], which might enable selective transport due to complexation or sieving of distinct ions or molecules. Stimulated by the studies of Atwood et al. [121] Arimori [122] and Raston and co-workers[123,124], who demonstrated the formation of supramolecular assemblies containing p-sulfonato-calix[n]arenes and specific metal ions, our work has been focused on the investigation of the inclusion complexes in the membrane of two families of host molecules, namely **aza6** and calixarene. These hosts are large macrocycles with well-defined internal cavities capable of including smaller guest molecules.

2.2.2   Deposition conditions

Under the normally chosen conditions, the lbl assembly of polyelectrolytes is nearly irreversible [14], so that the built-up films do not represent equilibrium structures. This adds to the versatility of the lbl method, but implies the need for careful adjustment of the various processing parameters in order to control the deposition process. A particularity of lbl assembly is the possibility to modify roughness and thickness of the coatings for a given pair of polyelectrolytes by varying process parameters. In any case, the molar mass of the polyelectrolyte, pH and ionic strength of the dipping solution may influence the growth of the film.

2.2.2.1   Concentration effects

The influence of polyelectrolyte concentration on the adsorption step is generally weak if a critical threshold value is exceeded [14, 15]. There is a lower limit for the polymer concentration to allow lbl assembly, which seems to be around 10^{-7} molL^{-1} for polyelectrolyte solutions under salt free conditions, somewhat depending on the nature of the substrate [125]. In case that a very low polyelectrolyte concentration shall be applied, successful deposition under the given condition should be verified first. In most studies reported so far, polyelectrolyte concentrations have been set to about 10^{-2} mol L^{-1} [125-127].

2.2.2.2 Salt effects

Preparing different ultrathin films from the same polymer via changing ionic strength contributes much to the versatility of the lbl assembly. In general, addition of salt to the adsorbate polyelectrolyte solution increases the thickness and density of individual adsorbed layers [12-15, 38], but this effect is not obligatory because the surface roughness may increase [13, 14, 128]. While a small amount of salt can speed up the adsorption process somewhat, adsorption is slowed down at high ionic strengths [129]. Nevertheless, it should be kept in mind that very high ionic strength can induce desorption of the polymers, in particular when using low molar mass or weak polyelectrolytes [128-131]. These effects were explained by partial binding of the low molar mass ions to the polyions, and screening of the binding sites. The addition of electrolytes (salt) allows one to control the growth step (i.e., the increase of the thickness of bilayers from 0.5 to 5-8 nm) [32]. The process of film growth was checked by ultraviolet and infrared spectroscopy and by the method of X-ray and neutron reflectometry. Several previous investigations have shown that there is a critical minimum charge density effect on the growth of multilayered films [129-131]. Caruso and co-workers have suggested that, below the critical charge density, addition of the next layer leads to almost complete removal of the previously deposited layer and thus multilayers cannot grow. Above the critical charge density, the rate of film growth was influenced by the structure of the adsorbing polyelectrolytes: thicker and rougher film are produced with increasing salt concentration in the aqueous dipping solution [47].

2.2.2.3 pH effects

The effect of pH on lbl assembly is pronounced, but complex [36]. On the one hand, increasing amounts of acid, base, or buffer to establish a given pH will raise the ionic strength. This should lead to thicker adsorbed layers (Figure 2.14). On the other hand, many of the charged groups used, such as protonated amines or carboxylates, are prone to the protonation-deprotonation equilibrium. However, Rubner et al. [42,132], found that the adjusted pH modifies the degree of ionization of weak polyelectrolytes in solution and in a multilayer film. In all cases, the bilayer thickness exhibited a dramatic change from molecularly thin bilayers to much

thicker bilayers when the degree of ionization of the weak polyelectrolytes changed. In addition, it was found that the degree of ionization of weak polyelectrolytes in multilayer films is also influenced strongly by the type of complementary polyelectrolyte used in the assembly process.
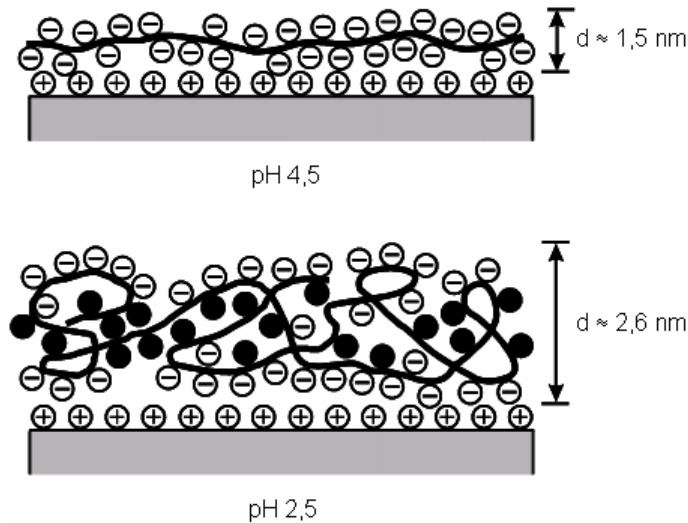
Fig.2.14 Structure of weak polyelectrolyte on substrate at different pH.

An introduction of small molecules such as tannic acid (TA) and dyes into LbL self assembly were investigated by Lvov and others [133, 134]. They found that the dissolution of the film may occur, if pH is changed and extreme pH values may completely prevent film growth by favoring desorption. The rates and the extent of swelling were also found to be depending on pH conditions under which the layers were fabricated [135]. In fact, most studies on pH effects reported an optimum pH range. Using lbl assembly, Voegel et al. [136] have reported that the construction of poly L-lysine (PLL) and hyaluronic acid (HA) films take place in over two build-up regimes. The first one is characterized by the formation of isolated islands that grow both by addition of new polyelectrolytes on their top and by mutual coalescence of the islands. The second regime sets in once a continuous film is formed. After the deposition of the eighth layer pair an exponential increase was observed. This exponential growth is explained by the diffusion of free PLL chains into the interior of the film when the film is in contact with a PLL solution, and by the diffusion out of the film of a fraction of the free chain and their interaction with HA chains at the outer limit of the multilayer when the film is further brought in

contact with a HA solution. In our group, Toutianoush and others [137] found by means of ultraviolet (UV) studies that dipping solutions of pH 6.8, without a supporting electrolyte, are most suited for preparation of lbl assemblies of p-sulfonato-calix[n]arenes with n= 4, 6, 8, and polyvinylamine. It was suggested that successful deposition requires appropriate matching of the charge density and conformation of polyelectrolyte molecules, rather than a minimum charge density. It should be also noted that nonlinear growth of multilayers may be observed when a poor match between the two oppositely charged polyelectrolytes occurs [4, 138].

Mendelsohn and others [139] found that a substantial and irreversible transformation of morphology of weak polyelectrolyte films based on poly(acrylic acid) and poly(allylamine) took place after immersion into an acidic solution. The resulting microporous structures are up to three times the thickness of the original films, reduce relative density, and are stable against further rearrangement under applied conditions. In addition, the microporous films undergo a secondary reorganization in neutral water, leading to a morphology with more discrete through pores. A mechanism is proposed for these transformations based on interchain ionic bond breakage and reformation in this highly protonating environment leading to an insoluble precipitate on the substrate, which undergoes decomposition.

3 Results and Discussion

3.1 Preparation and characterization of multilayer films

In the present part of the work, we wish to elucidate the factors, which influence the absorption increment of electrostatic multilayer films containing macrocyclic compounds. The prime variables, which determine the homogeneity and stability of multilayer films are the pH, concentration, and ionic strength of aqueous dipping solutions of polyelectrolytes [128-141]. In the following, we discuss the effects of these parameters on the build-up of films of **aza6** and PSS on quartz substrates.

3.1.1 Multilayer films of aza6 and PSS

The layer-by-layer assembly of **aza6** and PSS on quartz substrates was investigated.
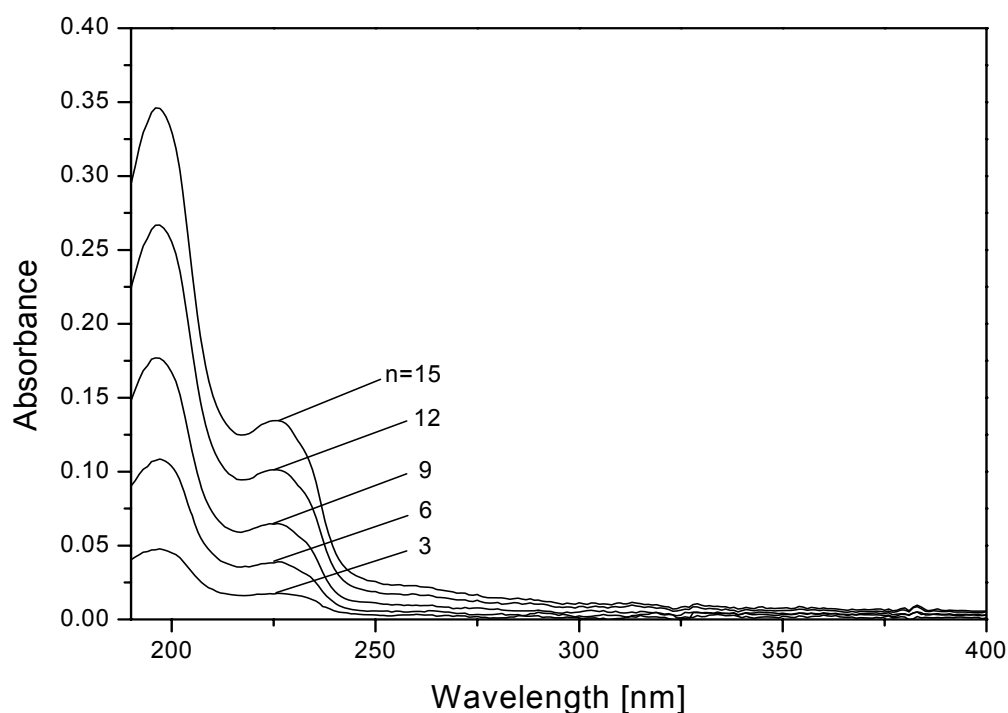
Fig. 3.1 UV-vis spectra of **aza6**/PSS multilayered films on quartz substrate with different number n of deposited bilayers at pH 6.0.

Since **aza6** does not contain a UV chromophor, the build-up of the multilayer was analyzed after deposition of different numbers of bilayers (i.e. **aza6**/PSS pairs) instead of individual layers. The UV/VIS spectrum of PSS in aqueous solution has a maximum absorption peak at 226 nm. This peak was used to trail the amount of deposited bilayers by UV/VIS spectroscopy. In Figure 3.1, a collection of spectra is shown taken after deposition of each of three bilayers. The absorption increases with the number of bilayers indicating successful film growth for both **aza6** and PSS. The quantity of the increase of absorbance with the number of dipping cycles (a ´dipping cycle´ indicates the successive unique immersion of the substrate into the two solutions of a negatively and positively charged compound, each dipping followed by a careful rinsing of the coated substrate with water) is strongly dependent on the layer structure. In order to determine the best deposition conditions, the effect of changing the pH was investigated first.

3.1.1.1 Effects of pH on film formation

The pH of the dipping solutions was varied and the maximum UV absorption of samples, which were subjected to different numbers n of dipping cycles, was determined. In Figure 3.2, the plot indicates a nearly linear film growth at values 6.0 and 1.7, while at pH 5.0, 3.7, 2.7, and 0.9 a superlinear growth was found. The superlinear growth was most pronounced for the multilayer prepared at pH 3.7. If 12 dipping cycles were applied, the sample exhibits the high absorbance of 0.8. Presumably the linear growth can be related to the presence of a flat smooth film with regularly packed layers, while a nonlinear increase is caused by somewhat irregular deposition. Molecular aggregation of the macrocyclic compounds may create a rougher surface with space in between, in which the counter polyion can interpenetrate. Consequently, more molecules can be adsorbed in the next layer, resulting in a superlinear growth of the multilayers [134, 140]. Superlinear growth may also be the result of migration of weakly bound compounds from the core of the multilayer to the surface [46, 141]. In the subsequent dipping step, the mobile compound reacts with an oppositely charged compound at the surface and the film thickness increases. The same will also apply to the small and only little charged

aza6 macrocycles, which can easily depart to the surface where they are captured by the oppositely charged PSS chains.
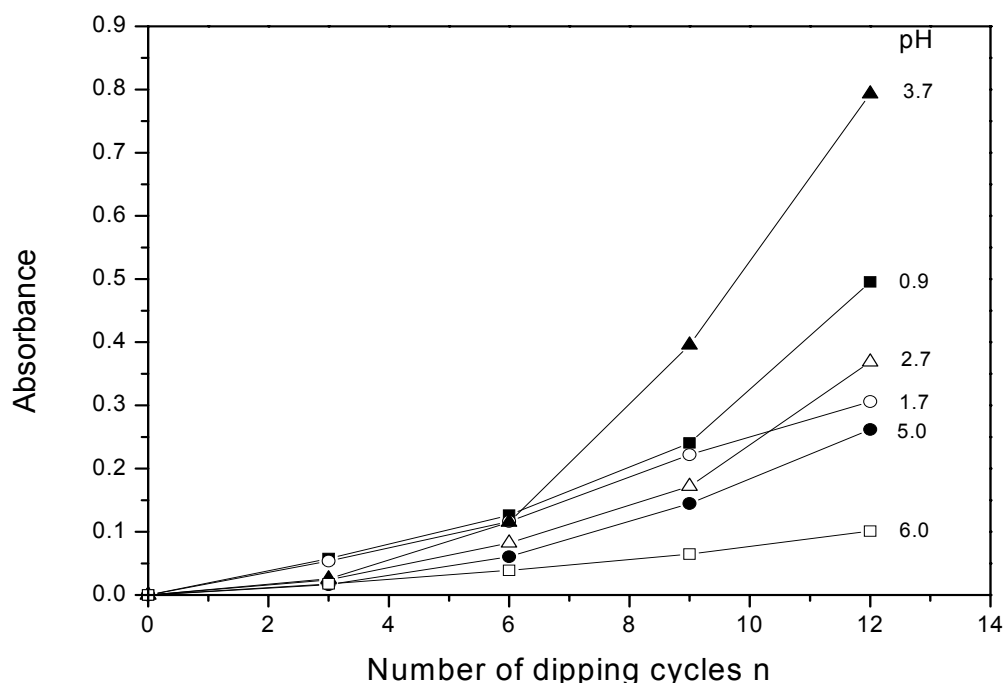
Fig. 3.2 Maximum absorbance of **aza6**/PSS multilayer assemblies prepared at different pH on quartz as a function of the number of dipping cycles.

Upon alternating lbl adsorption **aza6**/PSS complexes are formed, which give rise to a superlinear growth depending on the pH, because the protonation constants for **aza6**·H$^+$ to **aza6**·6H$^+$ are 10.2, 9.2, 8.7, 4.1, ~ 2 and ~ 1, respectively [94, 142]. The protonation equilibria can be represented as:

$$\textbf{aza6} \xrightleftharpoons[\textbf{pK}_a\ \textbf{10.2}]{\textbf{H}^+} \textbf{aza6·H}^+ \xrightleftharpoons[\textbf{pK}_a\ \textbf{9.2}]{\textbf{H}^+} \textbf{aza6·2H}^+ \xrightleftharpoons[\textbf{pK}_a\ \textbf{8.7}]{\textbf{H}^+} \textbf{aza6·3H}^+ \xrightleftharpoons[\textbf{pK}_a\ \textbf{4.1}]{\textbf{H}^+} \textbf{aza6·4H}^+ \xrightleftharpoons[\textbf{pK}_a\ \textbf{2.0}]{\textbf{H}^+}$$

$$\textbf{aza6·5H}^+ \xrightleftharpoons[\textbf{pK}_a\ \textbf{1.0}]{\textbf{H}^+} \textbf{aza6·6H}^+.$$
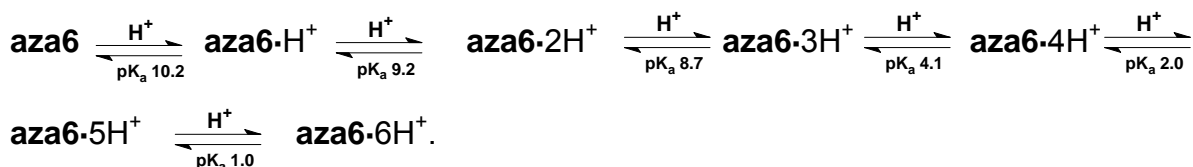
Thus one can expect that layer-by-layer adsorption proceeds progressively easier and more polycations will be deposited, if the pH value is lowered. This means that a high protonation favours a high charge density and the compound is more easily adsorbed. However, this was only true, if linear or branched weak polyelectrolytes

were used, but in case of charged macrocyclic compounds the situation was inverse, i.e., more protonation, less adsorption. The reason is that in macrocycles the charges are concentrated in a small space, which may effect the conformation of molecules and cause that the macrocycles repel each other during deposition and form poorly packed layers. In Figure 3.3, the absorbance of multilayers subjected to different numbers n of dipping cycles is plotted versus the pH of the dipping solution. From this plot, two effects are obvious. First, there is evidence that the multilayer structure of the first layers differs from that of the subsequent layers. G. Ladam et al. [41] described three different regions in a multilayer system.
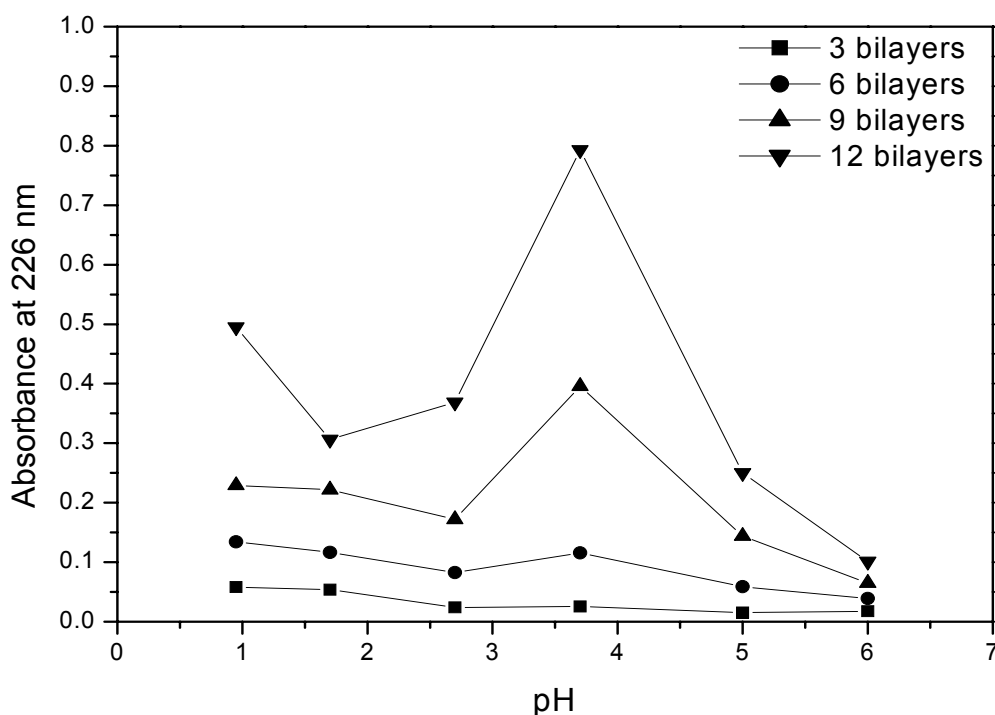
Fig. 3.3 Plot of the maximum UV absorption at 226 nm of **aza6**/PSS films with different number of bilayers as a function of the pH value of dipping solution.

The precursor zone of about the first six layers is affected by substrate properties, while in a core zone and outer zone the growth is dependent on the conformation and charge density of the polyion. Second, a clear peak of the absorption occurs for multilayers deposited at pH 3.7 as soon as more than 6 bilayers are deposited. At this pH, the majority of **aza6** macrocycles is present in the **aza6**$\cdot$4H$^+$ state and it

can be expected that the adsorption of the macrocyclic polycations proceeds with irregular deposition, creating a rougher surface with holes and cavities, in which the next PSS polyanion can penetrate. Thus the surface becomes rougher, and more material can be deposited in the next step resulting in a nonlinear growth of the multilayers [141]. However, Toutianoush and others [137] have shown for multilayers of PVA and p-sulfonato-calix[4]arenes that four-fold ionized rings still have a high tendency to desorb from their position in the multilayer. Thus one can expect a similar behaviour from the four-fold protonated **aza6** rings. This means that at pH 3.7 the deposition is indeed improved, but desorption still takes place, which results in the observed exponential layer growth. At pH 1.7 and 2.7, **aza6**·$6H^+$ and **aza6**·$5H^+$ states are increasingly formed, and the highly protonated macrocycles are more fixed in the multilayer repelling each other. In this case the appearance of inhomogenities can be attributed to an electrostatic repulsion of the protonated ammonium head groups. At pH 0.9, the protonation of PSS sets in. Thicker and less homogeneous PSS layers are adsorbed, which again favours a superlinear growth as indicated in Figure 3.3.

However, protonation not only affects the interaction among the head groups but also influences the conformation of the macrocycles, which in turn affects the packing of the **aza6** molecules in the layer.
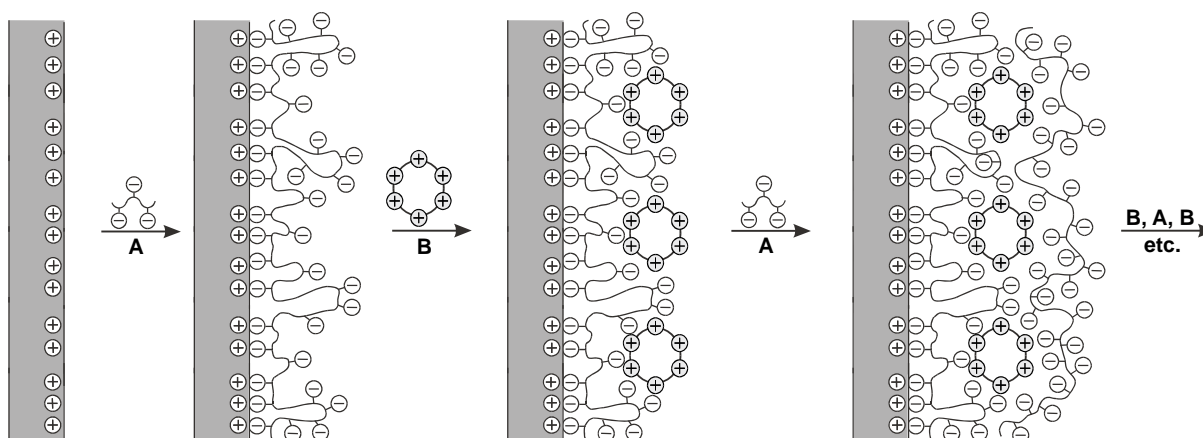
Fig. 3.4 Scheme of alternate electrostatic lbl assembly of **aza6**/PSS multilayer films on a charged substrate. The actual orientation of the macrocyclic rings is still unknown.

Thus a complex interplay between intra- and intermolecular electrostatic interactions exists, which is reflected in aspects of irregular growth behavior of

layers for which it is difficult to find a simple interpretation. In this section it has been shown that the formation and the stability of the multilayer structures of **aza6** and PSS depend on the charge density and spatial orientation of macrocyclic molecules. For weak polyelectrolytes, which have a pH dependent charge, the pH is an important variable. A scheme describing the alternate adsorption of **aza6** and PSS is shown in Figure 3.4.

3.1.1.2 Effects of concentration on film formation

The influence of the concentration of aqueous dipping solutions of **aza6** and PSS on the build-up of multilayer films was studied.
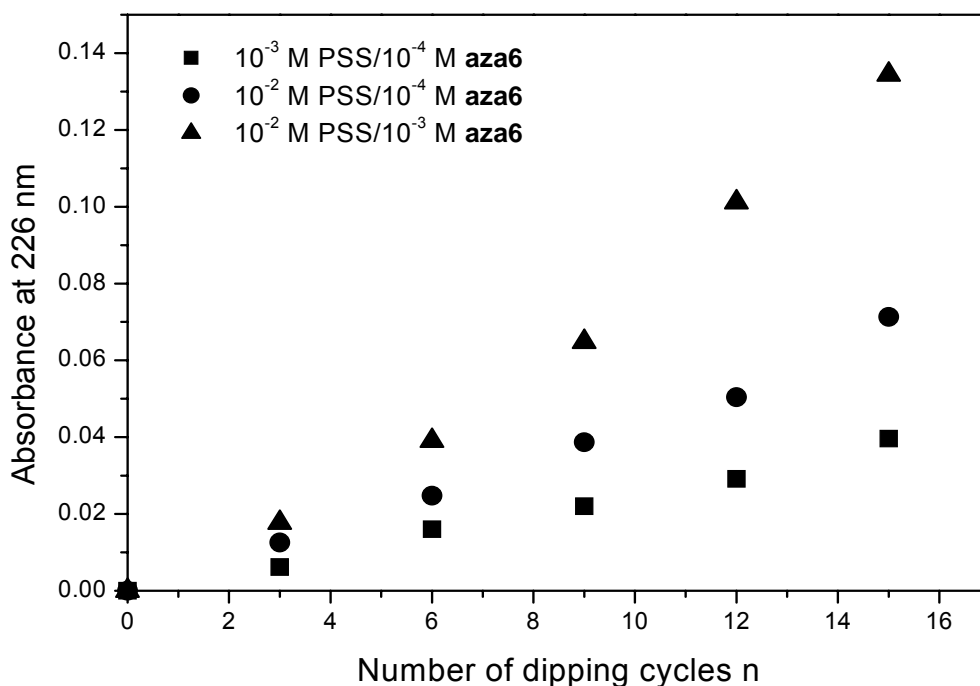
Fig. 3.5 Maximum absorbance of **aza6**/PSS multilayer assemblies prepared at different concentrations on quartz as a function of the number of dipping cycles.

The experiments were carried out at pH 6.0, which is the optimum pH value for a linear growth of the multilayers. It was found that a variation of the concentration does not influence the linearity of the film growth, but the amount of adsorbed

material is affected as shown in Figure 3.5. The maximum absorbance at 226 nm of **aza6**/PSS multilayers prepared from aqueous dipping solutions of different concentration is plotted versus the number of dipping cycles. For 12 bilayers, an increase in the PSS concentration from 10^{-3} to 10^{-2} mol L^{-1} leads to an increase of the absorbance at 226 nm by 40% (from 0.03 to 0.05). This is due to adsorption of more PSS chains per unit area of the substrate. An increase of the **aza6** concentration from 10^{-4} to 10^{-3} mol L^{-1} has an even stronger effect on the PSS adsorption, which increases by 50% for the same number of bilayers (from 0.05 to 0.10). At the higher concentration, more macrocycles are adsorbed and a higher positive charge density is provided at the surface so that more PSS chains are adsorbed and so on.

3.1.1.3 Effects of salt addition on film formation

Besides the effects of pH and concentration, the influence of an additional supporting electrolyte in the dipping solution on the multilayer growth was studied. Multilayers were build up at the optimum pH values of 6.0 and 1.7, and a concentration of 10^{-3} and 10^{-2} mol L^{-1} of **aza6** and PSS, respectively. Our study shows that the ionic strength of the polyelectrolyte solutions strongly influences the amount of charged macrocyclic molecules deposited during multilayer formation. We first consider a multilayer formed by alternating exposure of polyelectrolyte (PSS) and **aza6** in 1.0 molar aqueous NaCl. The maximum UV absorption of samples, which were subjected to different number n of dipping cycles with and without addition of salt to the aqueous dipping solutions are shown in Figures 3.6 a and b. The plots indicate a nearly linear film growth at pH values 6.0 and 1.7 without any supporting electrolyte added, while the addition of 1.0 mol L^{-1} NaCl to the dipping solution causes that a plateau of maximum absorbance is reached after deposition of 6 bilayers at pH 6.0 and 3 bilayers at pH 1.7. The absorbance of the first 6 bilayers prepared at pH 6.0 and a content of 1.0 mol L^{-1} NaCl of the dipping solution is about 60% stronger than for the same multilayer films prepared in absence of salt. However, for the film prepared from the salt containing solution, the absorption increment decreases with increasing number of deposited layers indicating that less material is adsorbed per dipping step.
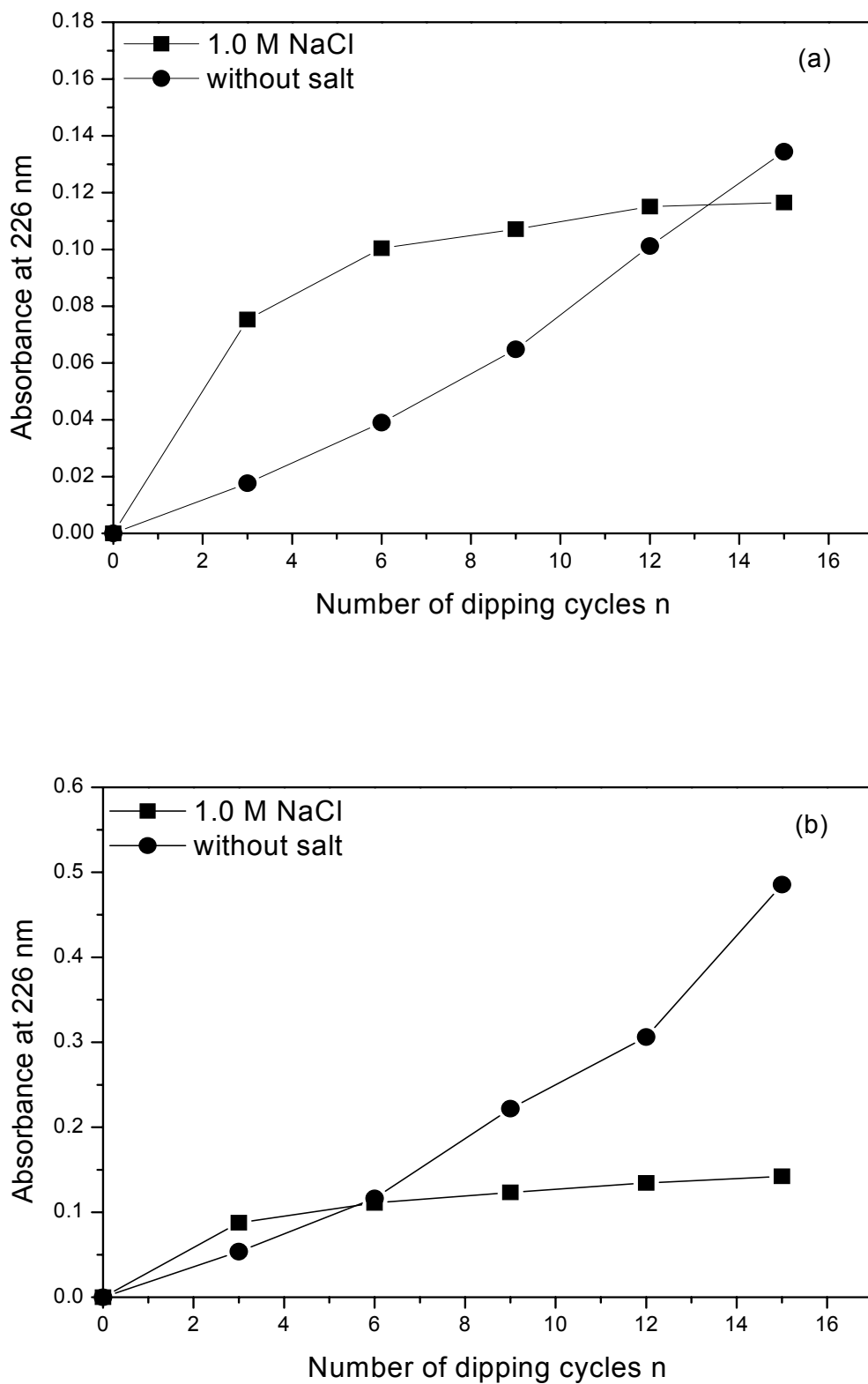
Fig. 3.6 Maximum absorbance of **aza6**/PSS multilayer assemblies prepared with and without salt on quartz as a function of the number of dipping cycles at pH 6.0 (a) and pH 1.7 (b).

Therefore the absorption of a 15 bilayers film prepared in presence of salt is about 13% lower than for the film prepared in absence of salt. The same situation was observed for a dipping solution with 1.0 mol L^{-1} NaCl at pH 1.7, but the plateau already occurs after 3 bilayers. The absorption reached after deposition of 15 bilayers is about 39% larger than for the films prepared in absence of salt. We believe that the increase of the growth step is explained by the fact that the addition of salt leads to the formation of dense coils of PSS chains which in turn are adsorbed without unfolding and therefore provide the formation of thicker layers during deposition. In some cases, the addition of salt to the dipping solutions not only increases the thickness of the saturated adsorption layer and thus the thickness of individual layers, but also enhances the surface roughness and, for more than 3 to 6 cycles, causes a complete flinching of the growth process [15]. The layer-by-layer procedure, which is based on electrostatic attraction of oppositely charged polyelectrolytes, may reverse when using high salt content. It is imaginable that the polymer, especially at high salt concentration, can extract **aza6** macrocycles from the surface because an equilibrium should exist between **aza6** that is adsorbed at the surface and **aza6** in solution [128]:

Polymer-**aza6** $_{adsorbed}$ + Polymer $_{solution}$ → **aza6**-Polymer complex $_{solution}$ + Polymer $_{adsorbed}$ (1)

The presence of salt in the polyelectrolyte solution probably influences **aza6** extraction from the surface during multilayer deposition. Due to electrostatic screening between macrocycles and polyelectrolytes, desorption may occur. So it seemed useful to prepare the membranes on porous substrate under conditions of pH = 6.0, a concentration of **aza6** of 10^{-3} molL^{-1} and polyelectrolytes of 10^{-2} monomolL^{-1}, and without any supporting electrolyte added.

3.1.2 Multilayer films of p- sulfonato-calix[8]arene and polyvinylamine

Since it was already proven in our lab [137] that anionic p-sulfonato-calix[n]arenes with n = 4, 6, 8 are suited for preparation of multilayer films, the layer-by-layer deposition of **calix8**/PVA on quartz substrates was studied using UV spectroscopy. Because of the phenolic chromophor, **calix8** exhibits a strong UV

absorption with maxima at 211 and 285 nm. As shown in Figure 3.7, the UV absorption increases linearly with the number of deposited **calix8**/PVA layer pairs. This is a clear indication that the same amount of chromophor is adsorbed in each dipping cycle. The UV spectroscopic study was quite helpful in order to optimize the multilayer build-up. The conditions were found to be optimum, if the pH of the dipping solutions was 6.8, and no supporting electrolyte was added. The same preparation conditions were also applied for the coating of the porous supporting membranes.
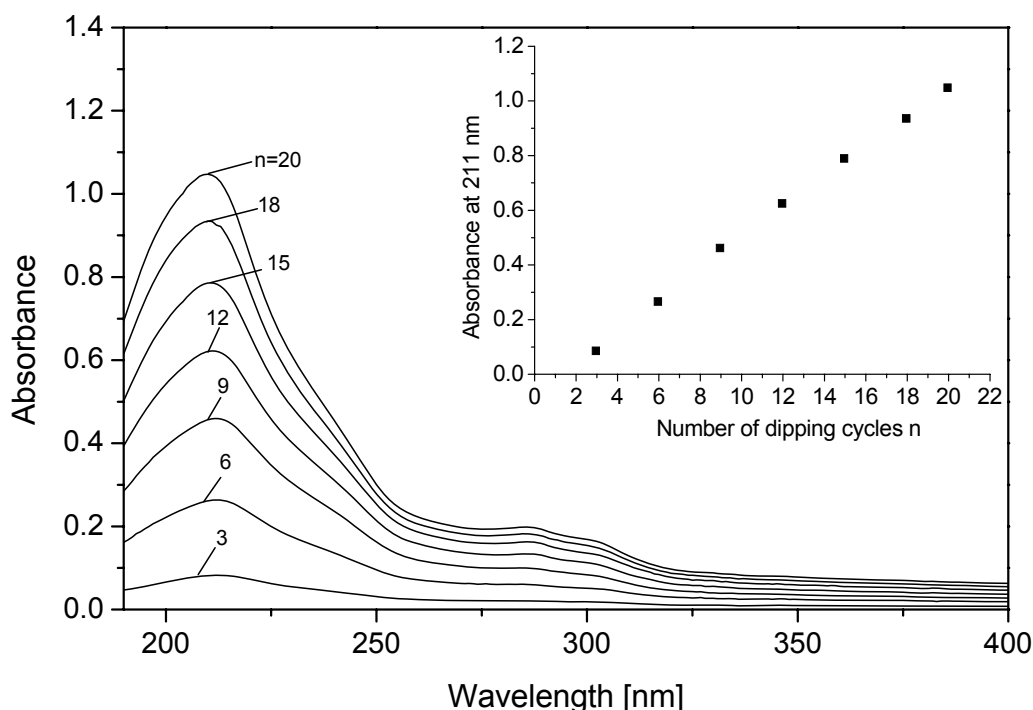
Fig. 3.7 UV-vis spectra of **calix8**/PVA multilayered films on quartz substrate with different number of deposited bilayers at pH 6.8.

3.1.3 Multilayers of aza6 and calix8 or calix6

It was also tried to build up multilayers entirely consisting of cationic and anionic macrocyclic compounds on solid supports. As a first example, the alternating layer-by-layer assembly of positively charged **aza6** and negatively charged **calix8** was studied.
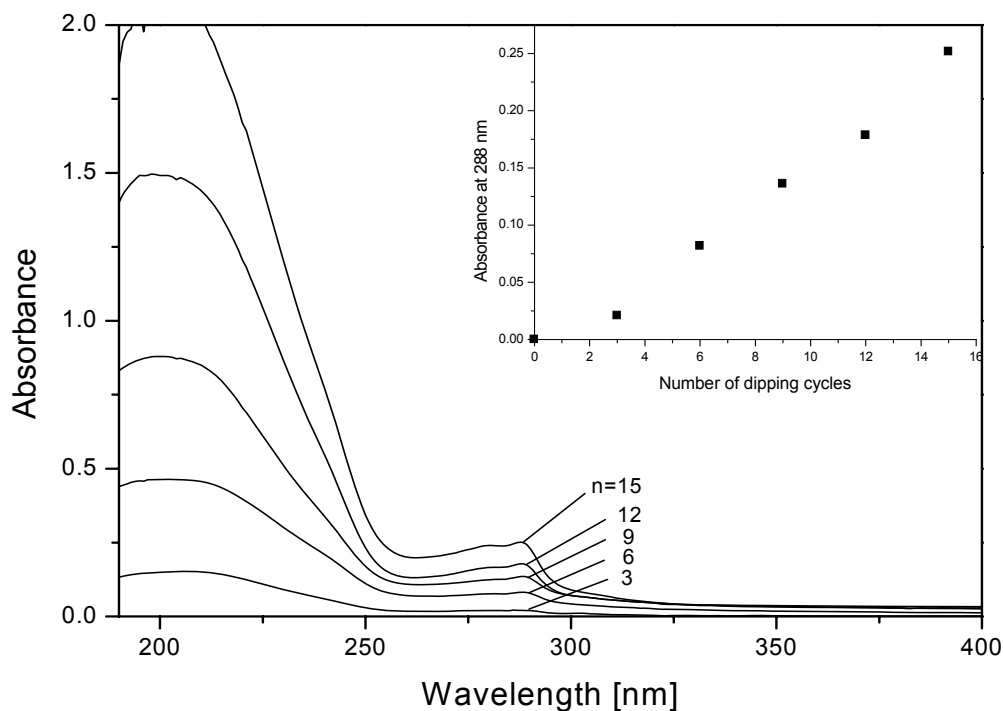
Fig. 3.8 UV-vis spectra of **aza6/calix8** multilayered films on quartz substrate at pH 1.7. The inset shows the increase of the maximum absorption at 288 nm as a function of the number n of deposited bilayers.

For multilayer fabrication, a quartz substrate precoated with three layer pairs of PVA/PVS was alternately dipped into aqueous solutions of the cationic and anionic macrocycles. The pH value of the dipping solution was 1.7, the concentration of the macrocycles was 10^{-3} mol L^{-1}. As indicated in Figure 3.8, the absorbance of the calixarene chromophor with shoulder at 288 nm increases linearly with the number of dipping cycles. This means, the same amount of **calix8** (and probably **aza6** as well) was adsorbed per dipping cycles. We also succeeded in the preparation of multilayers containing **aza6** and **calix6** macrocycles. The layer-by-layer assembly was carried out at pH 6 of the dipping solution. As can be seen in Figure 3.9, the growth proceeds linearly, but the absorbance increment is approximately six times lower than for the **aza6**/**calix8** multilayers shown in Figure 3.8.
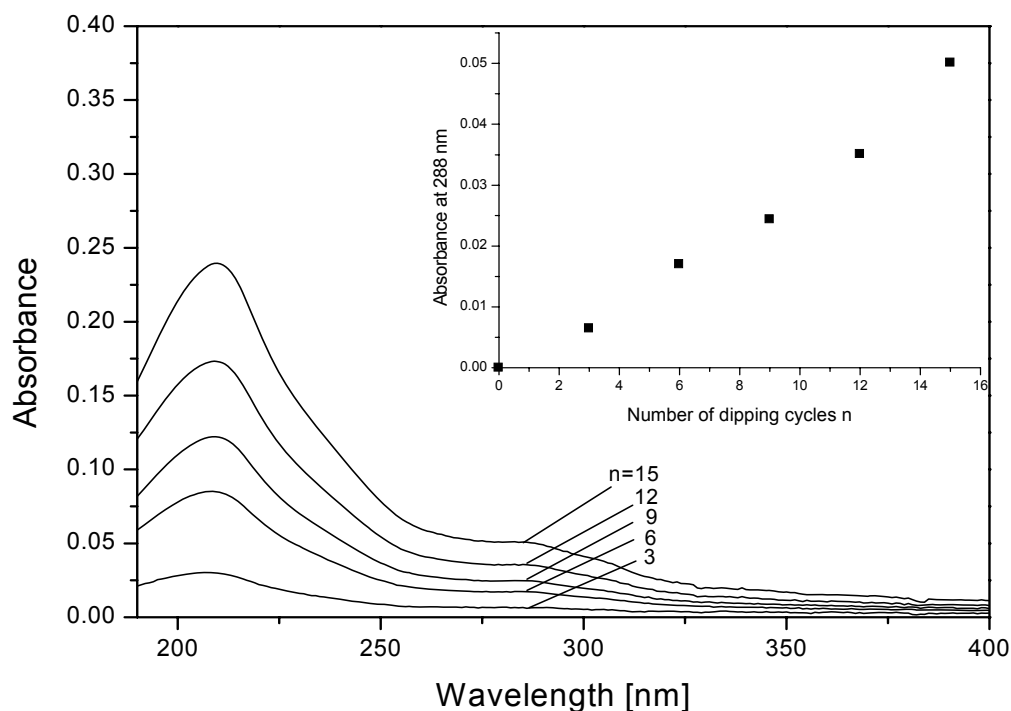
Fig. 3.9 UV-vis spectra of **aza6**/**calix6** multilayered films on quartz substrate at pH 6.0. The inset shows the increase of the maximum absorption at 288 nm as a function of the number n of deposited bilayers.

The **calix6** rings contain two ionic groups less than **calix8**, and at pH 6, the **aza6** macrocycles are less protonated than at pH 1.7. Consequently, both the cationic and anionic macrocycles are less charged and the adsorption of these rings provides a lower charge density at the interface so that in the next layer less macrocycles are adsorbed again.

A relevant scheme indicating the alternate adsorption of the two oppositely charged macrocycles in their fully ionized states is shown in Figure 3.10. Note that the actual orientation of the macrocycles has not been determined yet.
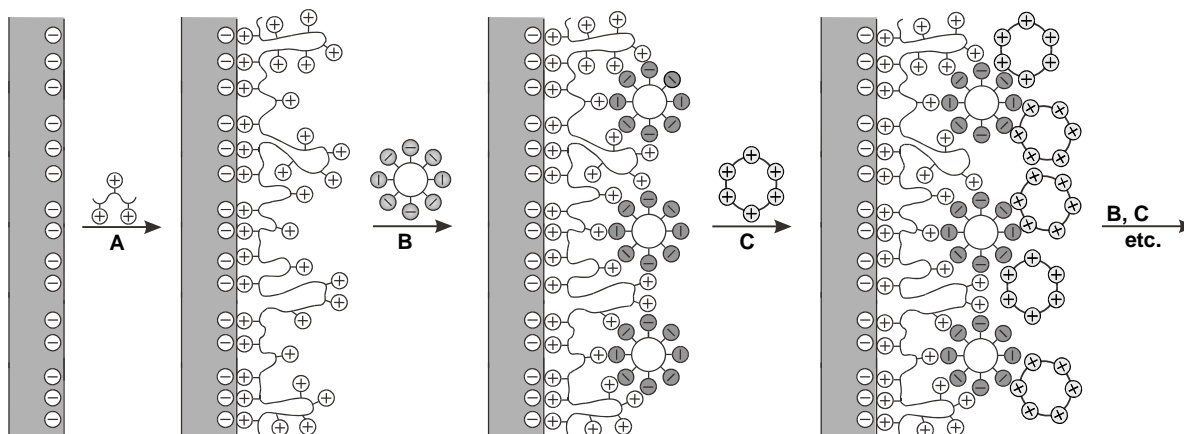
Fig. 3.10 Scheme of alternate electrostatic lbl assembly of **aza6/calix8** multilayer films on a charged substrate. The actual orientation of the macrocyclic rings is still unknown.

3.1.4 Multilayers of aza6 and hexacyanoferrate(II)

From **aza6** macrocycles it is known that they are capable of forming complexes with organic and inorganic anions [89, 94, 142-145].
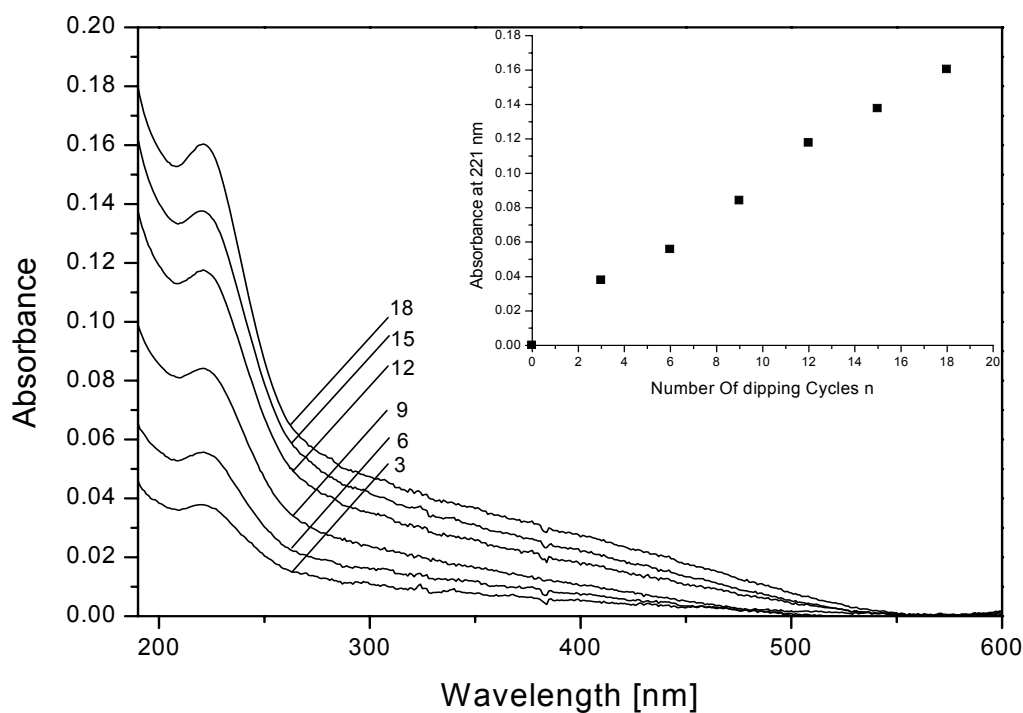
Fig. 3.11 UV-vis spectra of **aza6**/HCF(II) multilayered films on quartz substrate at pH 2.0. The inset shows the increase of the maximum absorption at 221 nm as a function of the number n of deposited bilayers.

Thus it was tried to prepare multilayers of positively charged **aza6** and negatively charged hexacyanoferrate (II) counterions. HCF(II) ions were chosen because of their intense UV-absorption and the high charge number of four. The pH of the dipping solutions was 2 in order to obtain a high degree of protonation of the macrocycles. In Figure 3.11, UV spectra monitored after adsorption of 3 to 18 **aza6**/HCF(II) bilayers are shown. As indicated in the inset, the maximum absorbance at 221 nm originating from the HCF(II) anions increases linearly with the number of dipping cycles.
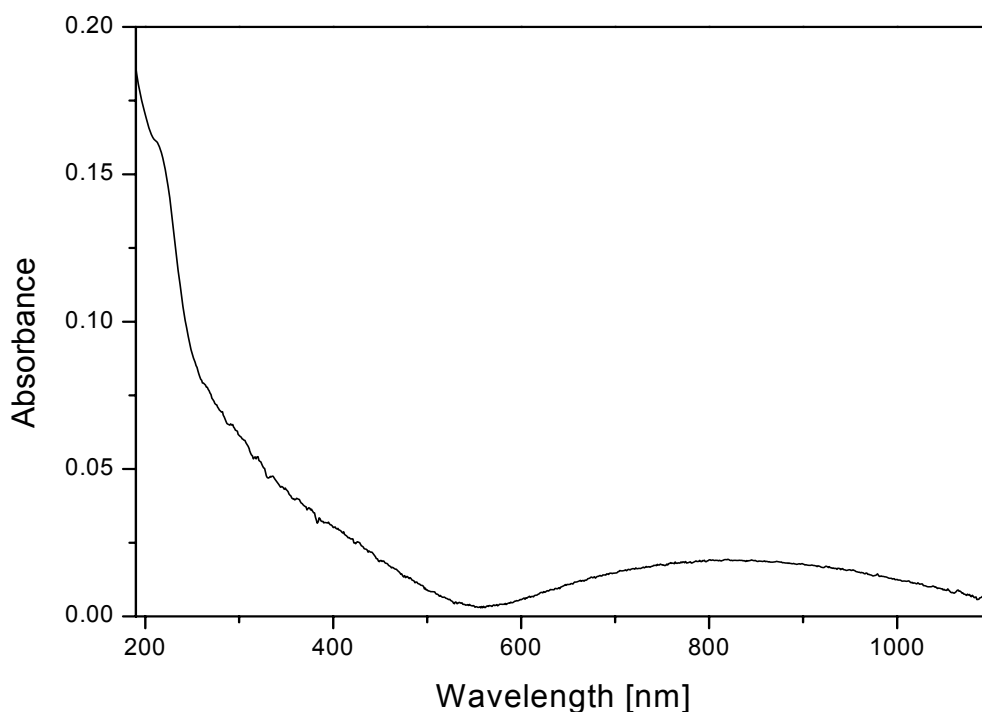
Fig. 3.12 UV-vis spectrum of **aza6**/HCF(II) films on quartz substrate (12 bilayers) after dipping into aqueous ferric chloride solution (10^{-2} mol L^{-1}) for 30 min.

This means in each dipping cycle the same amount of HCF(II) is added to the substrate. The **aza6**/HCF(II) multilayers are very sensitive to Fe(III) ions. Dipping a multilayer (18 bilayers) into a 10 mmol L^{-1} aqueous solution of ferric chloride results in a rapid blue coloration due to formation of Prussian Blue (PB, iron(III) hexacyanoferrate(II)) particles at the substrate. In Figure 3.12, a visible spectrum of the sample after dipping into ferric chloride solution for 30 min is shown. The

broad charge transfer peak of PB with maximum at 800 nm [146] is clearly detectable. Hence, the **aza6**/HCF(II) multilayers are useful for sensing Fe(III) ions present in solution.

3.1.5 Multilayers of p-sulfonatocalix[n]arenes and lanthanum(III) cations

Similar to the formation of multilayer films of cationic macrocycles and inorganic anions, a multilayer formation of anionic macrocycles and inorganic cations is imaginable. From recent publications it is known that p-sulfonatocalix[n]arenes with n being 4 or 6 are able to form complex salts with rare earth metal ions such as La(III) and Ce(III) [147,148]. In the complex salts, hydrogen-bonded arrays of the two compounds exist exhibiting the shape of bi-layers, capsules, spheres or tubules [121].
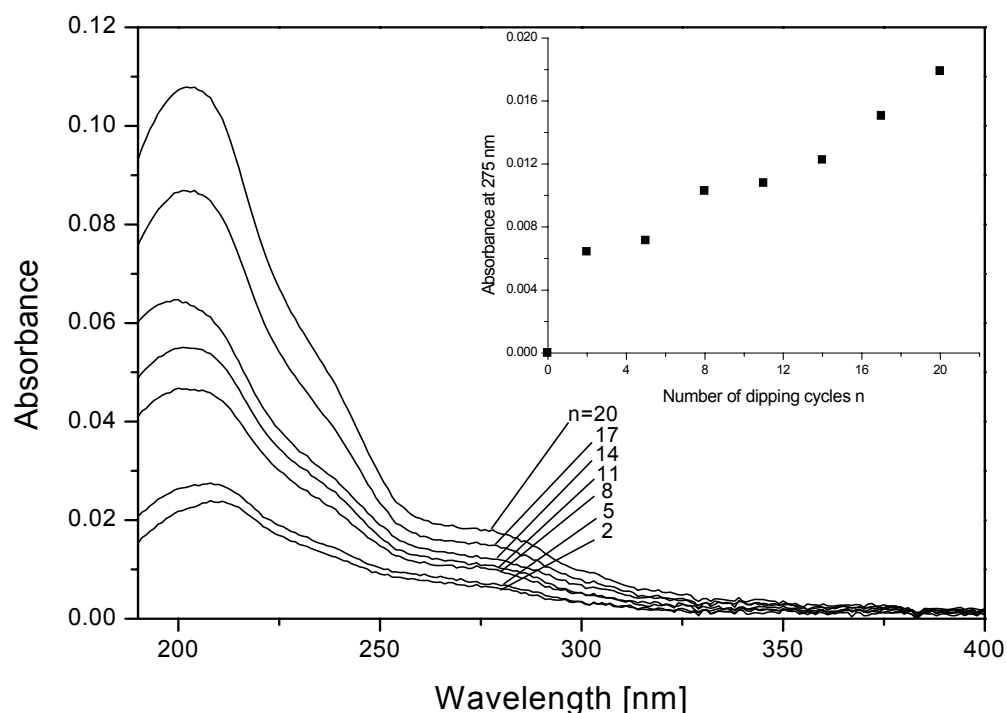
Fig. 3.13 UV-vis spectra of La(III)/**calix8** multilayered films on quartz substrate at pH 7.0. The inset shows the increase of the maximum absorption at 275 nm as a function of the number n of dipping cycles.

Therefore it was interesting to find out whether similar structures can be built up on solid substrates upon a simple layer-by-layer adsorption experiment. As a first example, it was tried to prepare multilayered films of La(III) cations and **calix8** anions. The experiment was carried out at pH 7.0, the concentration of the compounds in the aqueous dipping solution was 10^{-2} mol L^{-1}. In Figure 3.13, the UV spectra of substrates coated with a different number of bilayers are shown. The optical absorption with shoulder at 275 nm and maximum at 204 nm originates from the p-sulfonato-substituted calixarene chromophor. As recognizable from the inset, the film growth monitored at 275 nm is fairly linear, despite of the jump between zero and two bilayers. The jump is due to the fact that the substrate precoating with three polyelectrolyte layer pairs provides a higher charge density than the subsequent lanthanum or calixarene layers. Attempts to prepare multilayers from dipping solutions of only 10^{-3} mol L^{-1} were not successful. A decrease of the pH from 7 to 3 caused a large scatter of the absorbance values due to a less regular film growth. Polyelectrolyte layer pairs provide a higher charge density than the subsequent lanthanum or calixarene layers. It was also tried to prepare multilayers from La(III) and **calix6** or **calix4**. Using **calix6**, the experiments were as successful as with **calix8**. However, with **calix4**, the absorbance for a 12 bilayers sample was ten times lower than for **calix8**. Due to the small ring size, the mobility of the **calix4** rings is higher and desorption is favoured. Thus only few **calix4** macrocycles remain on the substrate.

3.1.6 Multilayers of p-sulfonatocalix[8]arenes, lanthanum(III) cations and 18-crown-6

Since crown ethers are known as good complexants for rare earth metal ions [121,149, 150], it was also tried to prepare multilayers of La(III) cations and calixarene anions in presence of crown ethers in the La(III) containing dipping solution. As crown ether, 18-crown-6 was used; the rare earth metal salt was lanthanum(III) chloride. The ratio of crown ether to lanthanum was 1:1. We hoped that the crown ethers act as hosts for the lanthanum ions in the aqueous phase forming a positively charged La(III)-crown ether complex, which is adsorbed in the subsequent layer-by-layer deposition.
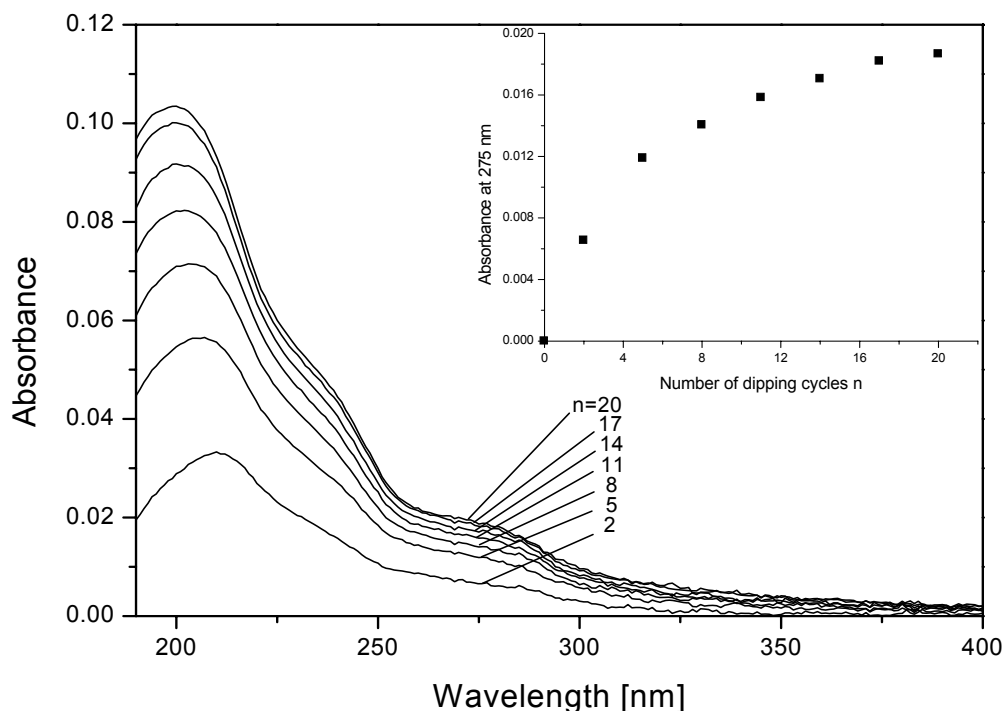
Fig. 3.14 UV-vis spectra of La(III)/18-crown-6/**calix8** multilayered films on quartz substrate at pH 7.0. The inset shows the increase of the maximum absorption at 275 nm as a function of the number n of dipping cycles.

Our optimism was supported by recent publications, in which the formation of crystalline complex salts of La^{3+}, 18-crown-6 and **calix4** was described [121, 149, 150], X-ray structure studies revealed a complex "ferris wheel" structure of inorganic cations, crown ether and calixarene compounds, which was hold together by a variety of cohesive forces including hydrogen bonding, electrostatic, π-stacking, coordinative and van der Waals-interactions [149]. As the UV spectra in Figure 3.14 indicate, the absorption at 275 nm increases with the number of dipping cycles applied. Surprisingly, for the first ten bilayers the absorption increment is about 20 percent larger than for the films prepared in absence of 18-crown-6. However, with increasing number of deposited layers, the films become more and more hydrophobic. Water is increasingly dripped off from the film surface. Consequently, less material is adsorbed per dipping step and the absorption increment decreases.
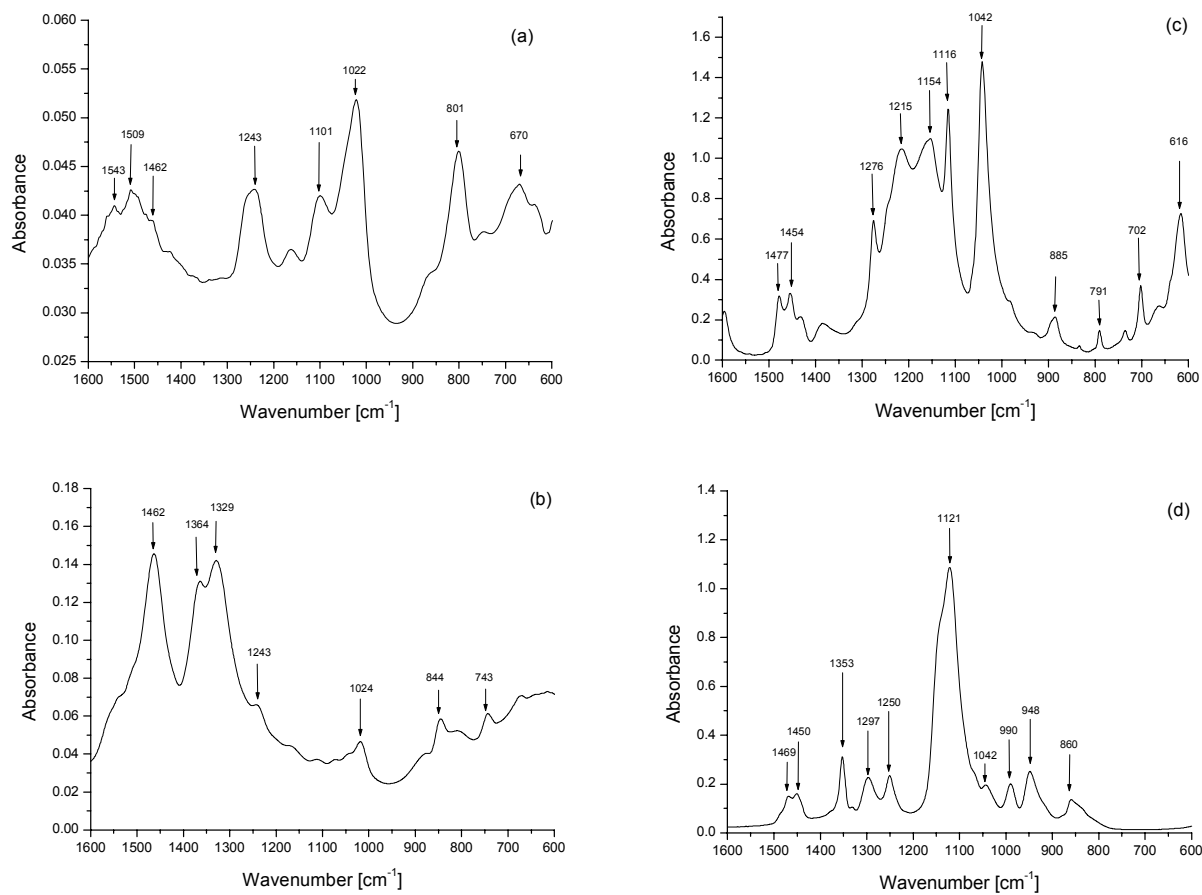
Fig. 3.15 ATR-IR-spectra of multilayered films of (a) La(III)/**calix8** and (b) La(III)/18-crown-6/**calix8** on zinc selenide, and IR-spectra of KBr dispersions of (c) **calix8** and (d) 18-crown-6.

In order to clearly prove the presence of 18-crown-6 in the multilayer films, ATR-IR spectra were recorded. In Figure 3.15, IR spectra of 20 double layers **calix8**/La(III) (sample 1) and **calix8**/La(III)/18-crown-6 (sample 2), both deposited on zinc selenide crystals, are compared. The spectra clearly differ in the fingerprint region from 1500 to 1250 cm^{-1}. Sample 2 exhibits strong absorption peaks with maxima at 1462, 1364 and 1329 cm^{-1} (Figure 3.15b), which are missing for sample 1 (Figure 3.15a). The peak at 1462 cm^{-1} can be assigned to the CH$_2$ deformation mode of **calix8** [151], while the peaks at 1364 and 1329 cm^{-1} can be ascribed to the asymmetric C-O-C vibration of the ether units [152] in 18-crown-6. For comparison, the bulk spectra of **calix8** and 18-crown-6 dispersed in potassium bromide are also shown (Figure 3.15 c and d). The crown ether compound exhibits strong vibrational modes at 1469, 1450 and 1353 cm^{-1}, which correspond to the

modes in the multilayer spectra. **Calix8** exhibits two peaks of the CH_2 deformation mode at 1477 and 1454 cm^{-1}, and no peak in the 1353 cm^{-1} region. Thus it can be concluded that 18-crown-6 is present in the lbl assembled films, the crown ether acting as ligand for the lanthanum ions. A proposed structure of the multilayer assembly is indicated in Figure 3.16. Further structure studies are necessary to fully analyze the mutual organization of the different compounds in the multilayer film.
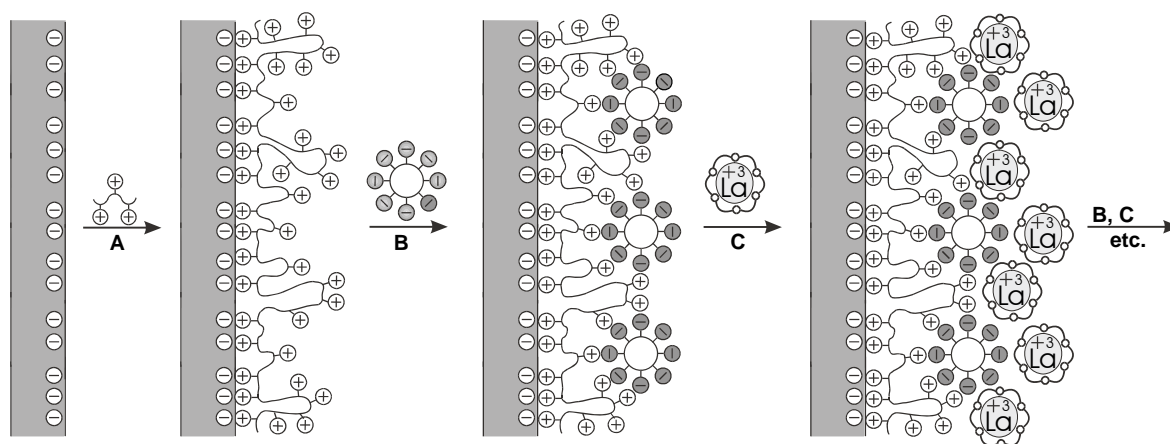
Fig. 3.16 Scheme of alternate electrostatic lbl assembly of La(III)/18-crown-6/**calix8** multilayer films on a charged substrate precoated with a polycation layer. The actual orientation of the macrocyclic rings is still unknown.

3.2 Materials transport across the membranes

3.2.1. Ion permeation measurements

In section 3.1.1.1, we already demonstrated that the layer-by-layer assembly of **aza6** and polystyrenesulfonate is strongly depending on the pH of the dipping solutions. A linear film growth was only observed at pH values 1.7 and 6.0, whereas at pH values between 3 and 4, a strongly superlinear growth was found. The origin is that the protonation of **aza6** is highly pH-dependent. At high pH values (pH > 10), **aza6** is only mono-protonated, while at low pH (pH < 1), the azacrown compound is present in the six fold protonated state [145]. At intermediate pH, **aza6** attains a partially protonated state [145]. In order to guarantee a steady and reproducible formation of the membranes, the lbl

assembly was therefore carried out in the linear growth regime using dipping solutions of pH 6.0. The preparation method of the membranes is schematically outlined in Figure 3.4 (Scheme 1). As the polymeric substrate, a porous PAN/PET membrane was used [85, 153].

3.2.2. Ion permeation through the aza6/PVS membrane

To investigate the separation of ions under dialysis condition, ion permeation measurements were performed using a U-shaped two chamber apparatus described in the experimental part in chapter 4.2.4.1 [63, 85]. In Figure 3.17a, the permeation rates P_R of sodium chloride, sodium sulfate and sodium sulfite through the **aza6**/PVS membrane (60 layer pairs) are plotted. The permeation rate of sodium chloride is rather high: $18.9 \cdot 10^{-6}$ cm·s^{-1}, much higher than across an all-polyelectrolyte PEI/PVS control membrane (PEI: branched polyethyleneimine, a long chain analogue of **aza6**), for which only $11.1 \cdot 10^{-6}$ cm·s^{-1} were found.
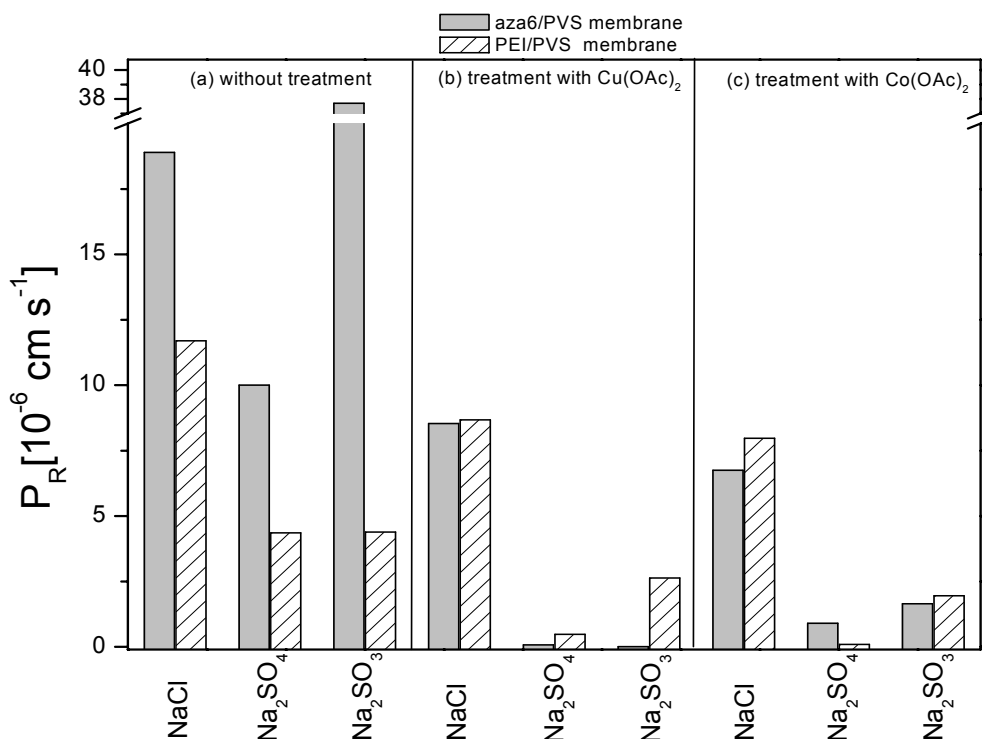
**Fig. 3.17** Permeation rates P_R of 0.1 M aqueous solutions of sodium chloride, sodium sulfate and sodium sulfite across **aza6**/PVS membrane and PEI/PVS control membrane before (a) and after treatment with copper (II) acetate (b) or cobalt (II) acetate (c).

The high P_R value of NaCl points to the presence of relatively large pores in the **aza6**/PVS membrane, which indeed favour a high flux, but prevent a good separation. In fact, for **aza6**/PVS membranes, the separation factor α (chloride/sulfate) is only 2, while for PEI/PVS membranes it is 2.7 (Table 3.1). The selectivity can be ascribed to Donnan rejection of the ions by the equally charged parts of the membrane [63]. Since the divalent sulfate ions exhibit a higher charge density than the monovalent chloride ions, they are more strongly rejected and therefore the P_R value is lower. Compared with PAH/PSS membranes, which under optimal conditions exhibit $\alpha(Cl^-/SO_4^{2-})$-values up to 45.0 [63], the separation of the **aza6**/PVS membrane is extremely low. It is also striking that the permeation rate of sulfite ions is as high as for sodium chloride. If the permeation of sodium chloride solution is repeated after sulfite permeation, a value of $68.9 \cdot 10^6$ cm s^{-1} is found. This indicates that the membrane structure has changed irreversibly. The origin is that the 0.1 molL^{-1} sodium sulfite solution exhibits a pH value of 9.2, which is high enough to cause a partial dissociation of the **aza6**/PVS polyion complex. We analyzed the dry residue of the permeate solution using infrared spectroscopy and found a clear indication for **aza6**. Therefore we can assume that **aza6** is partially leached out after complex dissociation, holes are formed and the ion selectivity gets completely lost.

3.2.2.1 Complex formation with copper(II) acetate

Previous work has shown that **aza6** acts as a receptor for metal cations and various anions [89, 94, 142-144, 154-156]. Thus it seemed worth-while to treat **aza6**/PVS membranes with aqueous solutions of various transition metal salts.
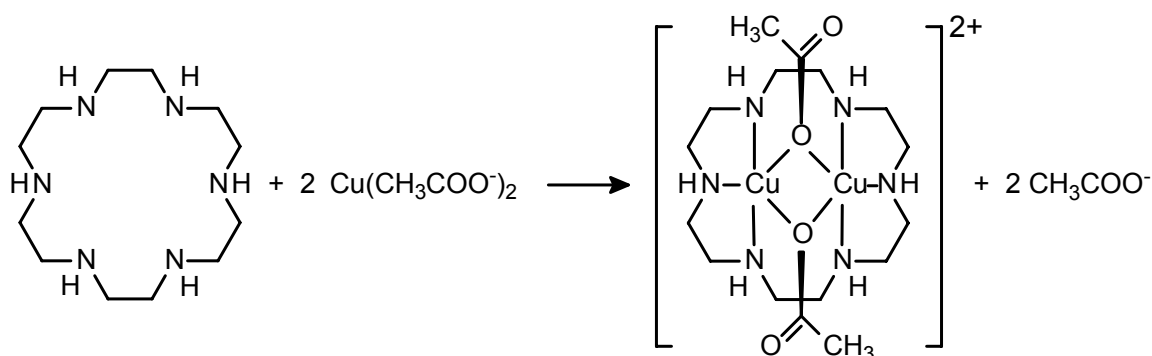
Fig. 3.18 Scheme of complex formation between **aza6** and copper(II) acetate (from ref. 157).

It was hoped that the treatment induces a complex formation of the transition metal salts and **aza6**, which alters and perhaps enhances the ion transport selectivity of the membrane. According to recent work, **aza6** is able to form binuclear copper complexes after treatment with copper(II) acetate (Figure 3.18) [157,158], while a treatment with cobalt(II) and nickel(II) salts leads to mononuclear metal complexes [154]. We began our studies with **aza6**/PVS films on quartz substrates and immersed the films in 0.1 molL^{-1} aqueous copper(II) acetate solution for 60 min. Subsequently the films were washed twice in Milli Q water for 10 min and UV/visible spectra were monitored. Two series of films were studied, which both differed in the number of adsorbed bilayers, while the pH of the dipping solutions was always 6, or they differed in the pH of the dipping solutions, and the number of deposited bilayers was always 12. As shown in Figure 3.19, the originally colorless films turned into blue upon immersion in the copper salt solution.
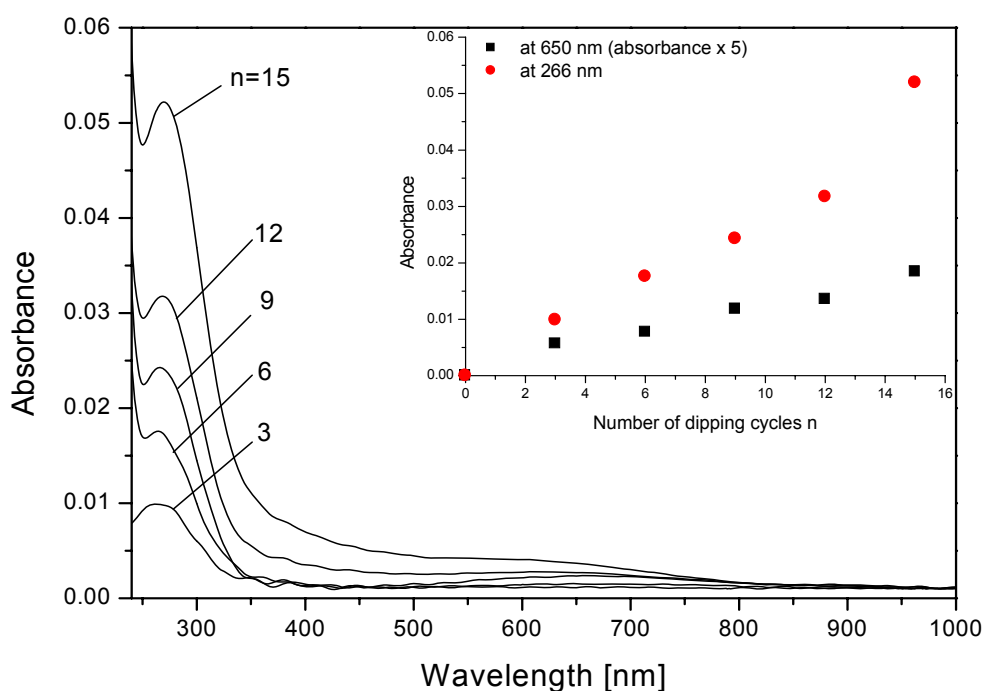
Fig. 3.19 UV-visible absorption spectra of **aza6**/PVS multilayer assemblies of different thickness on quartz, monitored after additional immersion in 0.1 molL^{-1} aqueous copper(II) acetate solution. In the inset, the maximum absorbances at 266 and 650 nm are plotted versus the number n of dipping cycles.

The films exhibit a very broad d-d absorption band at 650 nm and a band in the UV region at 266 nm originating from ligand-to-metal charge transfer transitions [159]. The inset of Figure 3.19 shows that the absorbance increases nearly linearly with the number of deposited layers. This means that equal amounts of copper ions are taken up by each layer of the film.
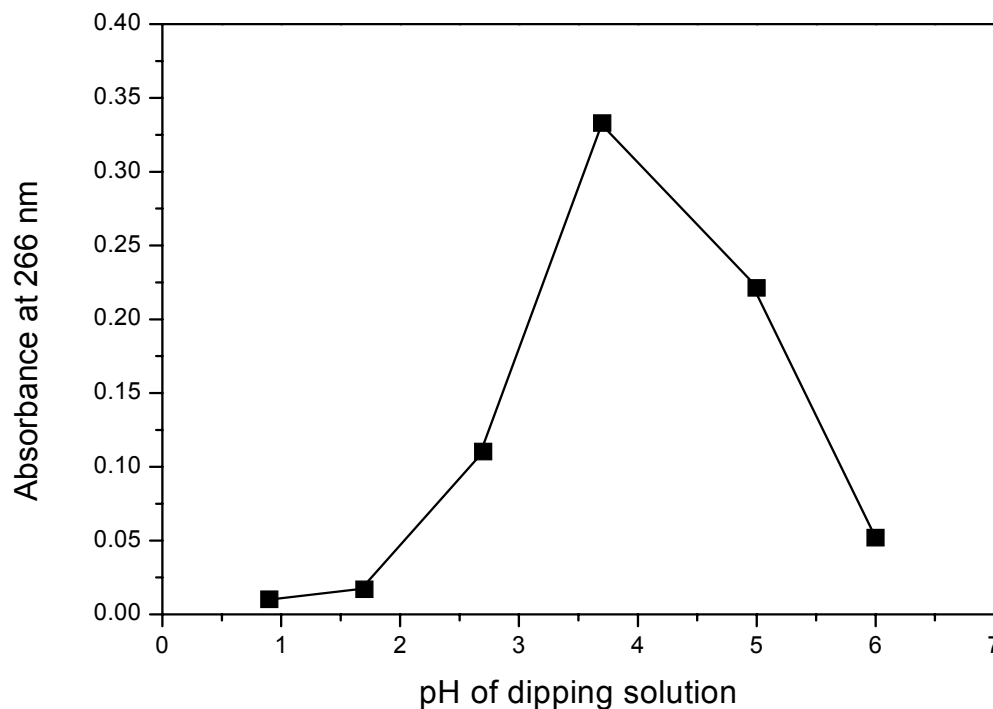
Fig. 3.20 Plot of the maximum absorbance at 266 nm versus the pH of the dipping solution used for lbl assembly. Samples: **aza6**/PVS multilayered films on quartz (12 dipping cycles) after additional immersion in 0.1 molL^{-1} aqueous copper(II) acetate solution.

In Figure 3.20, the maximum absorbance at 266 nm obtained after treatment with copper acetate is plotted versus the pH value of the dipping solutions, from which the **aza6**/PVS films were adsorbed. One recognizes a strong peak at pH 3.7, which indicates that membranes prepared at this pH are able to take up the largest amount of copper ions. Since at pH 3.7 the film growth is extremely superlinear, it can be inferred that the total film thickness is larger, and therefore more copper ions are taken up.

In order to clarify whether the complex formation is also accompanied with an uptake of acetate ions, ATR-IR spectra of **aza6**/PVS films were monitored. For this purpose, the films deposited on zinc selenide substrates were monitored. In Figure 3.21, the IR spectra of 15 bilayers are shown before and after treatment with aqueous copper(II) acetate solution. The spectra are rather similar except for two bands occurring at 1540 and 669 cm^{-1} subsequent to the acetate treatment. The 1540 cm^{-1} mode is typical for the asymmetric C-O stretching mode of the carboxylate group [159], and therefore is a strong indication for the presence of acetate ions in the film, very likely coordinated with the copper-**aza6** complex.
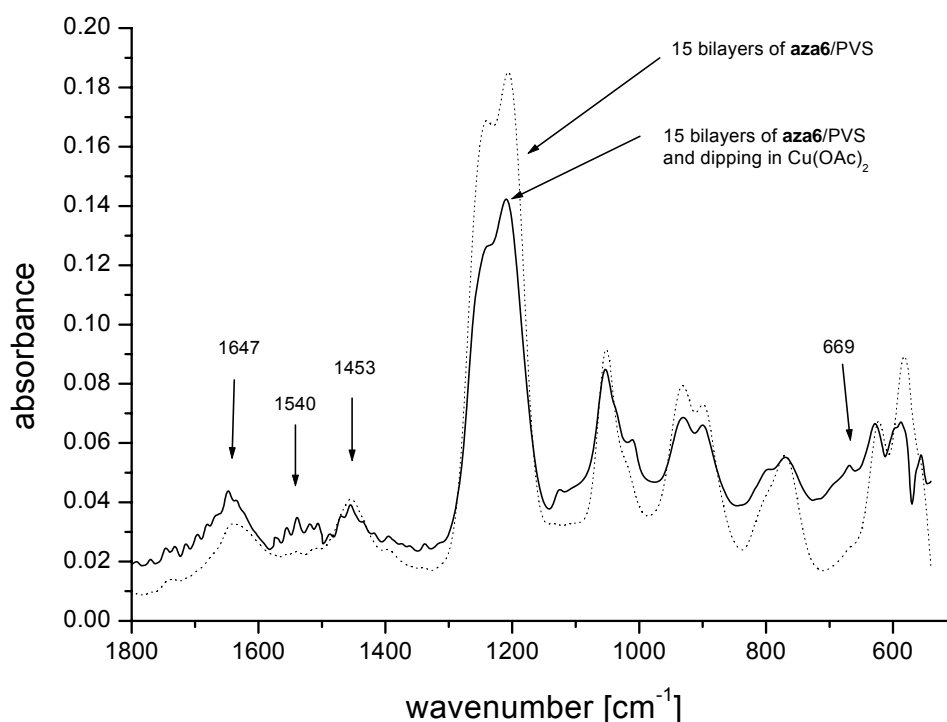
Fig. 3.21 ATR-IR spectra of **aza6**/PVS multilayered films on ZnSe (15 dipping cycles) before and after treatment with 0.1 molL^{-1} aqueous copper(II) acetate solution.

3.2.2.2 Ion permeation after treatment with copper(II) acetate

In further experiments the influence of a treatment with copper(II) acetate on the ion permeation across the **aza6**/PVS membranes was studied. For these experiments, porous PAN/PET supporting membranes were coated with up to 60 layer pairs **aza6**/PVS. The pH of the dipping solutions was always 6.0 in order to guarantee a regular (i.e., homogeneous and linear) film growth. Then the membranes were treated with a 0.1 molL^{-1} aqueous copper(II) acetate solution for

one hour. The membranes turned blue and even after subsequent extensive washing with pure water they did not lose the blue coloration (Figure 3.22). After the copper salt treatment, the permeation of various aqueous salt solutions was investigated. In Figure 3.23, the P_R values of numerous sodium salts with different anions, and chloride salts with different metal cations are represented.

20bilayers   **40bilayers**   **60bilayers**

Fig. 3.22 View of the bluish coloured **aza6**/PVS membranes (20, 40 and 60 bilayers) after treatment with 0.1 molL^{-1} aqueous copper(II) acetate solution and careful washing with water.

3.2.2.3 Selectivity in anion transport

Let us first discuss the permeation of various sodium salts with different anions. It is striking that the salts with divalent anions (except for carbonate) exhibit significantly lower permeation rates than the salts with monovalent anions (Figure 3.23a). This can be ascribed to a stronger electrostatic repulsion of these anions from the negatively charged parts of the membrane [63]. The permeation rates decrease in the series thiosulfate > sulfate > sulfite, because the sulfate and especially the sulfite ions are smaller than the thiosulfate ions, and their charge density is therefore higher so that they are more strongly rejected. The different permeation rates of the monovalent anions are more difficult to explain because two opposing effects may occur. From chloride to iodide, the size of the anions increases and the charge density decreases, and therefore the P_R value should actually increase.
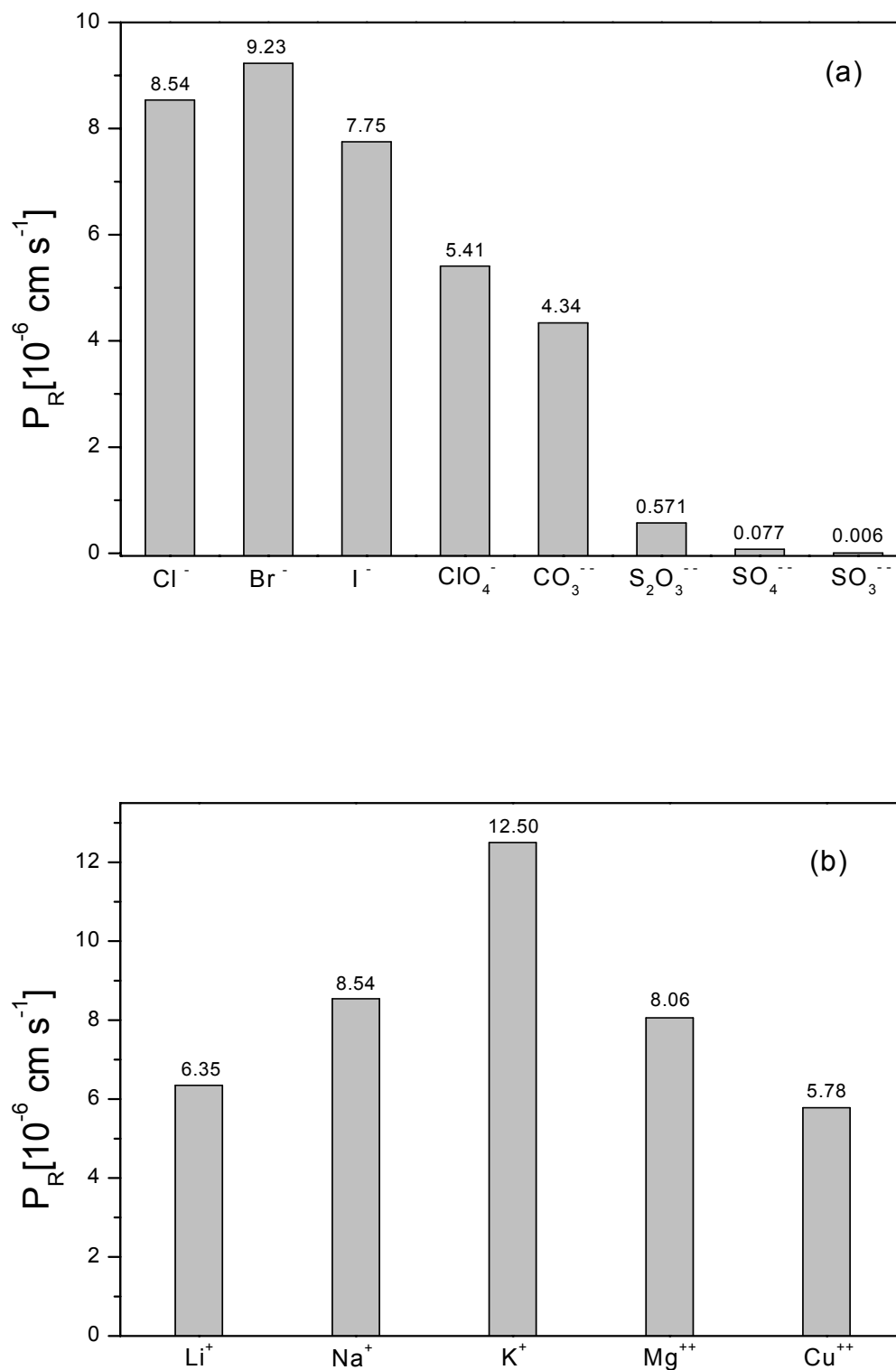
Fig. 3.23 Permeation rates P_R of various sodium salts with different anions (a) and various metal chlorides with different cations (b) across **aza6**/PVS membranes (60 bilayers) after immersion in $0.1 \, molL^{-1}$ aqueous copper(II) acetate solution.

However, the size of the iodide ion (diameter: 0.44 nm [160]) is so large that it might approach the size of the nanopores in the membrane [79]. Thus the membrane acts as a size-selective filter diminishing the transport rate of the iodide ions. For perchlorate ions, the size-based selectivity is even more pronounced. The high permeability of the carbonate ions finds its explanation in the high pH value of the unbuffered solution, which causes a partial dissociation of the **aza6**/PVS ion pairs in the membrane. As a result, holes and defects are formed, so that the flux is increased, but the selectivity of the membrane is decreased. Due to the large difference in the permeation rates of mono- and divalent anions, the theoretical separation factors are unusually high, as for example α(chloride/sulfate) = 110 and α'(chloride/sulfite) = 1420 (see also Table 3.1). Up to now, there is no all-polyelectrolyte multilayer membrane, which exhibits such high α values.

Table 3.1 Separation factors α(chloride/sulfate) and α'(chloride/sulfite) of **aza6**/PVS membranes (60 bilayers on PAN/PET) before and after treatment with 0.1 $molL^{-1}$ aqueous copper(II) acetate, cobalt(II) acetate and nickel(II) acetate.

Membrane	Treatment with	α	α'
Aza6/PVS	none	2	-- --*
PEI/PVS	none	2.7	2.7
Aza6/PVS	Cu(II)acetate	**110**	**1420**
PEI/PVS	Cu(II)acetate	18	3.3
Aza6/PVS	Co(II)acetate	17	10
PEI/PVS	Co(II)acetate	80.5	4.1
Aza6/PVS	Ni(II)acetate	6.3	-- --*
PEI/PVS	Ni(II)acetate	-- --**	-- --**

 *) membrane partially dissolved
**) not determined

For comparison, a PEI/PVS control membrane prepared under the same conditions as the **aza6**/PVS membrane exhibits α-values of 18 and 3.3, respectively (see Figure 3.17b and Table 3.1). For this membrane, the blue coloration is much weaker indicating that the complex formation is much less pronounced. Compared with the cyclic structure of **aza6**, the random conformation of the PEI chains is probably less suitable for the complex formation.

3.2.2.4 Influence of membrane thickness on anion transport

It was also interesting to study the influence of the number of deposited bilayers on the ion permeation behaviour of the copper(II) treated membranes. In Figure 3.24, the P_R values of the three sodium salts (chloride, sulfate, sulfite) are plotted versus the number of dipping cycles applied. The different permeation rates at zero deposited layers are caused by the precoating of the bare substrate with two layer pairs of PVA/PVS. The precoating was necessary to provide a surface of high and homogeneous charge density for the subsequent adsorption of the first layer of **aza6**.
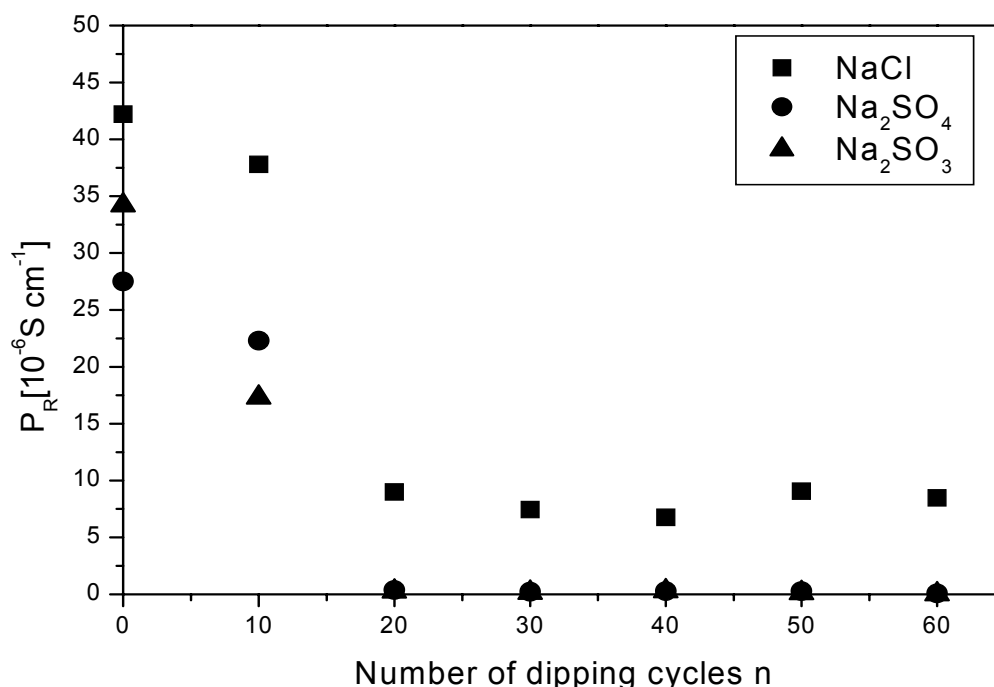
Fig. 3.24 Plot of P_R values of sodium chloride, sodium sulfate and sodium sulfite versus the number of dipping cycles of **aza**6/PVS on PAN/PET supporting membrane.

After 10 dipping cycles, the permeation behaviour did not change significantly. Still the pores of the substrate are only partly covered with the **aza6**/PVS membrane. However, after twenty dipping cycles, mono- and divalent ions exhibit significantly different permeation rates. Now the membrane is free of macroscopic defects, the ion permeation becomes highly selective. Further adsorption of layer pairs only slightly improves the selectivity. In principle, the experiment demonstrates that the adsorption of twenty layer pairs is sufficient to obtain an ion selective membrane (but the probability to obtain a defect-free membrane is clearly higher, if more than twenty layer pairs are adsorbed).

3.2.2.5 Selectivity in cation transport

Let us now discuss the transport of various metal chloride salts shown in Figure 3.23b. The P_R values of the 1,1- and 2,1-electrolyte salts are not very different. In the series of the alkali metal ions, the P_R value weakly increases in the series $Li^+ <$ $Na^+ < K^+$. Since the charge density of the ions decreases from lithium to potassium, the electrostatic repulsion of the K^+ ion is lowest and therefore the permeation rate is highest. Surprisingly, the permeation rate of Mg^{2+} is as high as Na^+, although the charge density of the magnesium ion is much higher. In conclusion, the measurements of the P_R values indicate that the electrostatic repulsive forces on the metal cations are much weaker than on the anions, and no real discrimination is found for the transport of the mono- and divalent cations.

3.2.2.6 Ion permeation after complex formation with Co(OAc)$_2$ and Ni(OAc)$_2$

Besides copper acetate, also other transition metal salts such as cobalt(II) and nickel(II) acetate were studied on a possible complex formation with **aza6**. After treating the **aza6**/PVS membrane with cobalt(II) acetate, it attained a pink color indicating the incorporation of cobalt(II) ions. Again permeation rates of sodium chloride, sulfate and sulfite were measured. If one compares Figure 3.17(a and c), one recognizes that after a cobalt treatment the P_R values of the three salts are lower than before, and that the decrease is especially strong for the salts with the divalent anions. However, the changes are less strong than after the copper acetate treatment (Figure 3.17b). The separation factors α(chloride/sulfate) and

α(chloride/sulfite) are 17 and 10, respectively (see also Table 3.1). A comparable treatment of the PEI/PVS control membrane also led to a decrease of the P_R values, the separation factors were 85.5 and 4.1, respectively (Table 3.1). After a treatment of the **aza6**/PVS membrane with nickel(II) acetate, the separation factor α(chloride/sulfate) was 6.3, while permeation of the aqueous sodium sulfite solution led to gradual decomposition of the membrane due to its high pH value. The gradual decomposition was indicated by the exponential increase of the conductivity in the permeate chamber as a function of time (Figure 3.25). In case of a stable membrane, a linear increase would have been observed. In Figure 3.25, the exponential and linear increase for the permeation of sodium sulfite across an **aza6**/PVS membrane treated with either nickel(II) or copper(II) acetate is demonstrated.
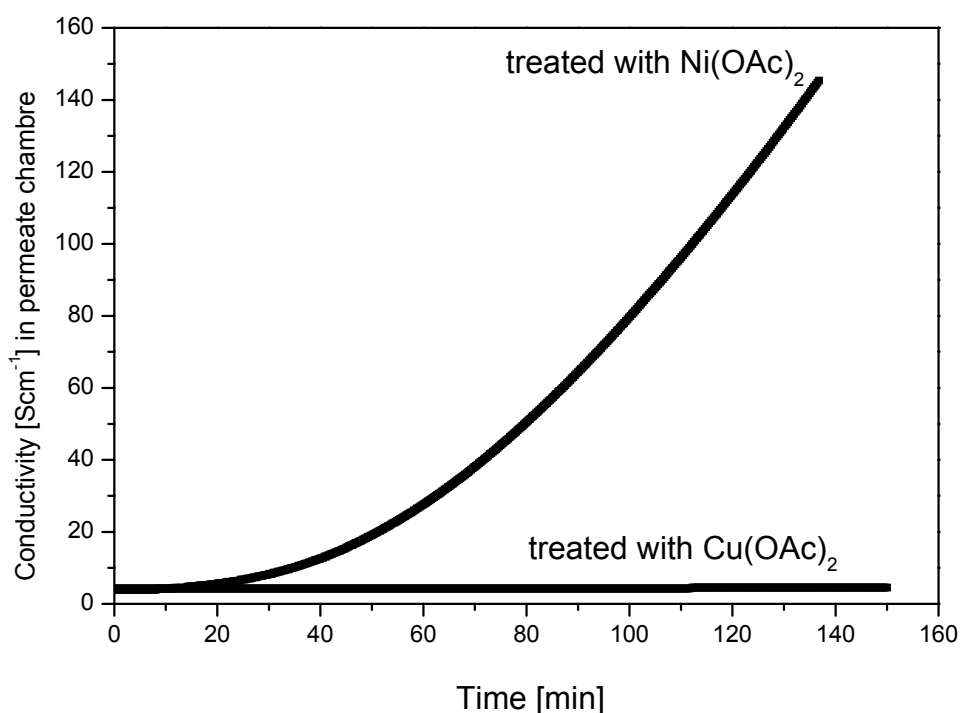
Fig. 3.25 Plot of conductivity in permeate solution versus time during the permeation of sodium sulfite (feed: 0.1 molL^{-1} aqueous solution) across the **aza6**/PVS membrane (60 bilayers) after its additional treatment with nickel(II) acetate or copper(II) acetate.

Our study shows that cobalt and nickel acetate affect the P_R values much less than copper(II) acetate does. There is only little dependence of $Co(OAc)_2$ and $Ni(OAc)_2$ complexation on the transport behaviour of the multilayer membranes. The reason is that the metal-ligand interaction is weaker, and only mononuclear complexes are formed with **aza6**.

3.2.2.7 Model for enhancement of anion transport

In the following, a possible origin of the enhanced anion separation of the **aza6**/PVS membrane after treatment with copper(II) acetate is discussed. Since the membranes were prepared at a moderate pH of 6.0, it can be inferred that the **aza6** macrocycles are adsorbed mainly in the triply protonated state. The positive charges are neutralized by the negative charges of PVS. An idealized picture of the resulting layered structure of the membrane is depicted in Figure 3.26 (left side). Treatment with $Cu(OAc)_2$ proceeds under complex formation with **aza6**, i.e., two copper and two acetate ions are coordinated with one **aza6** macrocycle, respectively, as indicated in the subsequent equation:

$$[\textbf{aza6} \cdot 3\,H]^{3+} \cdot 3\,PVS^- + 2\,Cu(OAc)_2 \;\rightarrow\; [\textbf{aza6} \cdot 2\,CuOAc]^{2+} \cdot 2\,PVS^- + 2\,HOAc + H^+ + PVS^-$$

Upon the reaction, three protons are set free from the macrocycles and the positively charged, divalent complex is formed.
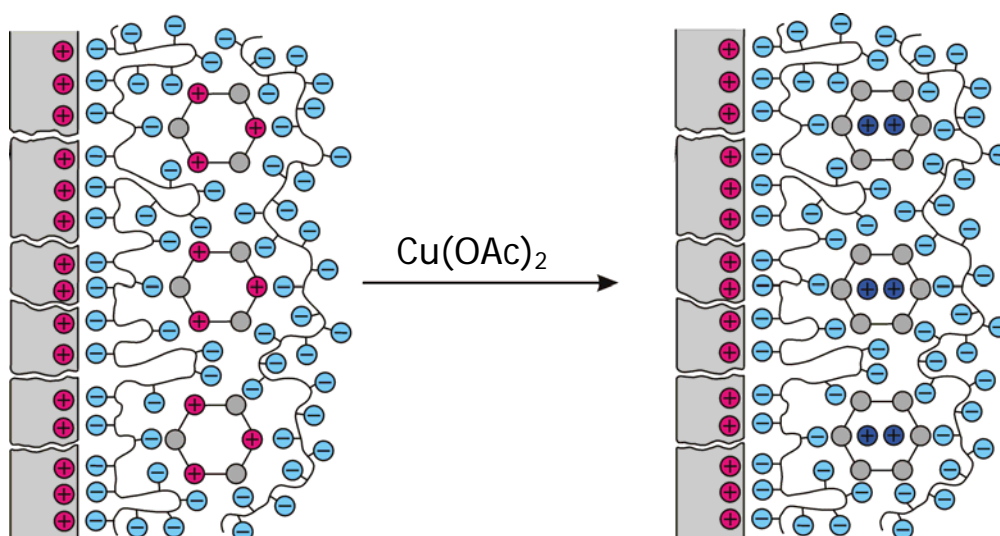
Fig. 3.26 Scheme of complex formation between triply protonated **aza6** and copper(II) acetate in the lbl-assembled **aza6**/PVS membrane.

While the protons are released from the membrane (either as HOAc or H^+), the surplus sulfate groups of PVS continue to be fixed in the membrane and induce a negative excess charge in the membrane (Figure 3.26, right side). The excess charge is responsible for the rejection of the divalent anions. In fact, this reaction resembles previous methods to create excess charges in multilayered polyelectrolyte membranes in order to enhance the ion separation [68].

3.2.3 Salt transport under nanofiltration conditions

The salt transport across the **aza6**/PVS membranes was also studied under nanofiltration (NF) conditions. While diffusion dialysis utilizes a concentration gradient for the solute transport across a membrane, NF is a pressure-driven separation process. Development of stable NF membranes with constant flux and selectivity, as well as resistance to fouling, could further expand the utility of a macrocycle-based multilayer membrane. Nanofiltration is considered to be useful for the separation of ionic compounds from solutions containing mixtures of electrolyte solutes. In order to show a high salt rejection along with high flux, the multilayered membrane must be thick enough to completely cover the pores of the underlying substrate. In order to find the optimum thickness, a series of **aza6**/PVS membranes with different number of deposited layers were prepared. Permeate flux and ion rejection of different kinds of ions were investigated at different operating pressure Δp.

For this purpose, nanofiltration experiments were conducted in a home made apparatus shown schematically in the experimental section 4.2.4.3a, Figure (4.5). The operating pressure Δp represents the difference between applied pressure p and the osmotic pressure π of the feed solution. In Figure 3.27 (a and b), the percentages of chloride and sulfate ions rejected by different numbers of deposited bilayers are plotted versus the operating pressure. As expected, the rejection of both Cl^- and SO_4^{2-} ions increases with increasing the number of deposited bilayers.
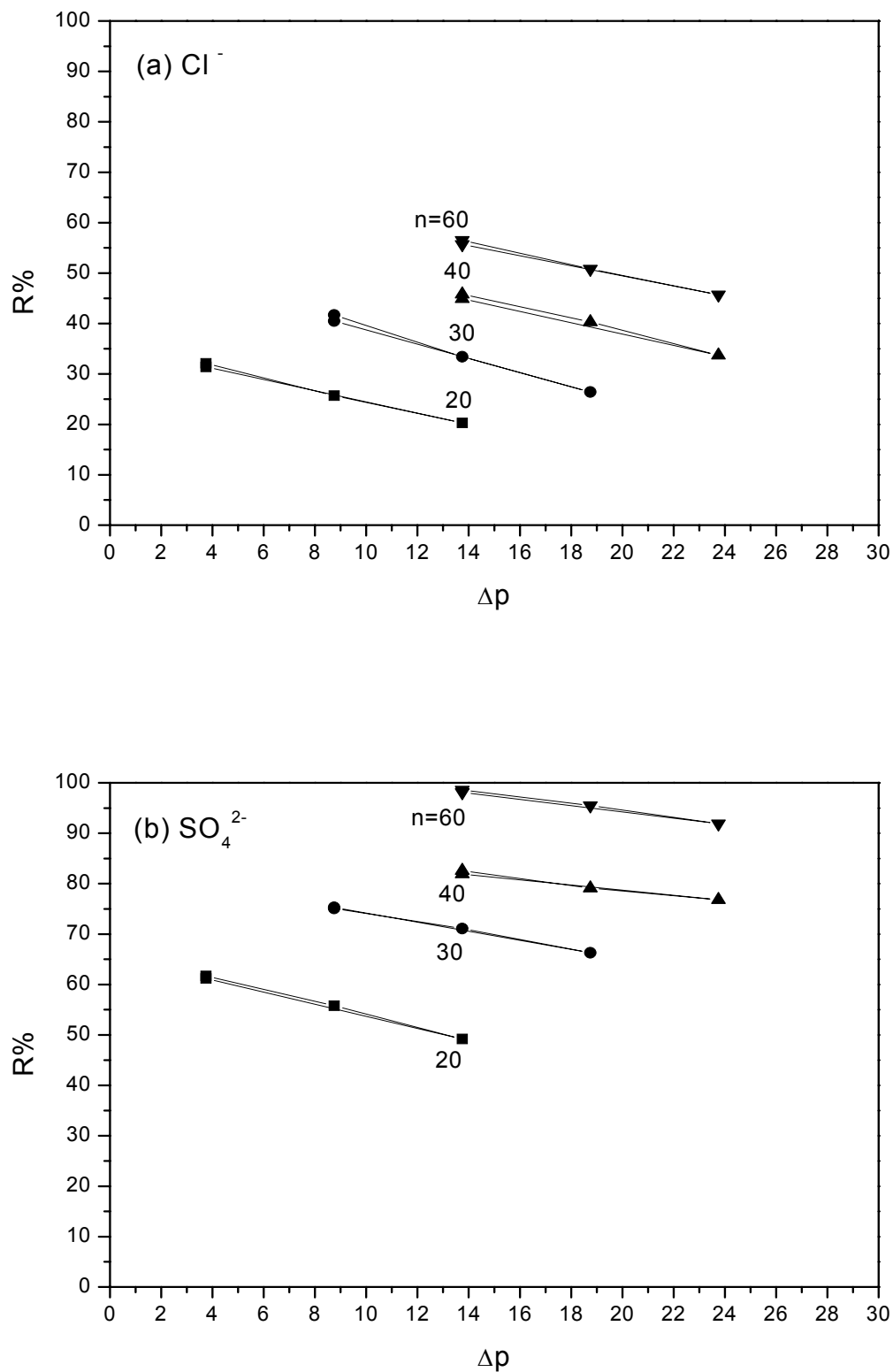
Fig. 3.27 Plot of rejection of (a) sodium chloride and (b) sodium sulfate salt (conc.: 10 mmolL^{-1}) as a function of the operating pressure Δp for membranes with different number n of bilayers deposited.

However, it is unusual that the rejection decreases with increasing operating pressure. A possible origin is a structural rearrangement, which leads to an increase of the pore size in the separating layers. The effect of a treatment with $Cu(OAc)_2$ on the nanofiltration performance of the membranes was also investigated. For the porous substrate coated with only 20 layer pairs of **aza6**/PVS, the rejection of chloride ions increases from 13.3% to 20.3% upon a treatment with $Cu(OAc)_2$, the operating pressure being 14 bar. Similar results were obtained for the rejection of sulfate ions, which changed from 30.6% to 49.2% upon treatment with copper acetate (Table 3.2).

Table. 3.2 Rejection, flux, and selectivity of mixed 10 mmolL^{-1} solution of NaCl and NaSO$_4$ through membranes with different numbers of **aza6**/PVS bilayers under nanofiltration conditions.

Number of bilayers	Δp [bar]	Flux J [l / m^2 h]	R %		Selectivity Cl$^-$ / SO$_4^{2-}$
			Cl$^-$ (NaCl)	SO$_4^{2-}$ (Na$_2$SO$_4$)	
20*	4.35	9.3	25.6	40.1	1.24
	8.95	19.02	19.4	34.8	1.23
	13.95	26.09	13.1	30.6	1.25
20	3.95	5.11	32.1	61.7	1.77
	8.95	10.598	25.7	55.8	1.68
	13.95	17.56	20.3	49.2	1.57
30	9.35	0.311	41.7	75.1	2.34
	14.55	0.567	33.4	71.1	2.30
	18.75	0.753	26.4	66.3	2.18
40	13.95	0.415	45.8	82.6	3.12
	19.15	0.705	40.3	79.1	2.86
	24.55	0.978	33.7	76.8	2.86
60	13.95	0.362	56.5	98.6	31.07
	19.75	0.627	50.8	95.5	10.93
	24.55	0.846	45.7	91.9	6.70

* Without $Cu(OAc)_2$ treatment

The difference in rejection originates from the complexation of **aza6** with $Cu(OAc)_2$. As shown in Table 3.2 and in Figure 3.27 (a and b), the rejection of chloride and sulfate ions increases with increasing number of deposited bilayers. In Table 3.2, the results of nanofiltration experiments are compiled. The rejection of Cl^- decreases and the rejection of SO_4^{2-} increases compared with single-salt experiments [73]. This occurs because the concentration of Na^+ in the mixed feed solutions is higher than that of Cl^-, and thus the diffusive flux of Na^+ is higher than that of Cl^-. The difference in diffusive fluxes results in a diffusion potential that enhances the Cl^- transport.

In a solution containing Na_2SO_4, a diffusion potential enhancing the SO_4^{2-} flux also develops because the diffusivity of Na^+ in the membrane is much larger than that of SO_4^{2-}. The presence of Cl^- in the mixed-salt solutions reduces the diffusion potential of sulfate, and thus SO_4^{2-} rejection is increased in mixed solutions. All copper(II) treated membranes, for which the SO_4^{2-} rejection is up to 98.6%, showed a Cl^- rejection lower than 56.5%. Based on the 56.5% rejection of Cl^- ions and 98.6% rejection of SO_4^{2-} ions found for a membrane of sixty layer pairs at 14 bar, a selectivity of 31 can be calculated.

In Figure 3.28, the permeation flux is plotted versus Δp for **aza6**/PVS membranes with different number n of bilayers deposited. The flux increases linearly with the operating pressure. For porous supports coated with only 20 layer pairs, the permeation flux increases from 9.3 L m^{-2} h^{-1} at about 4.0 bar to 26.09 L m^{-2} h^{-1} at about 14.0 bar. Treatment of membranes of same number of bilayers with $Cu(OAc)_2$ causes that the entire permeation flux becomes lower, the values being 5.11 and 17.56 L m^{-2} h^{-1} at 4.0 and 14.0 bar, respectively. Similar results were found for the copper treated membranes coated with 30, 40, and 60 layer pairs; at an operating pressure of approximately 14 bar the permeation flux decreases from 0.567 to 0.415 and 0.362 L m^{-2} h^{-1}, respectively.
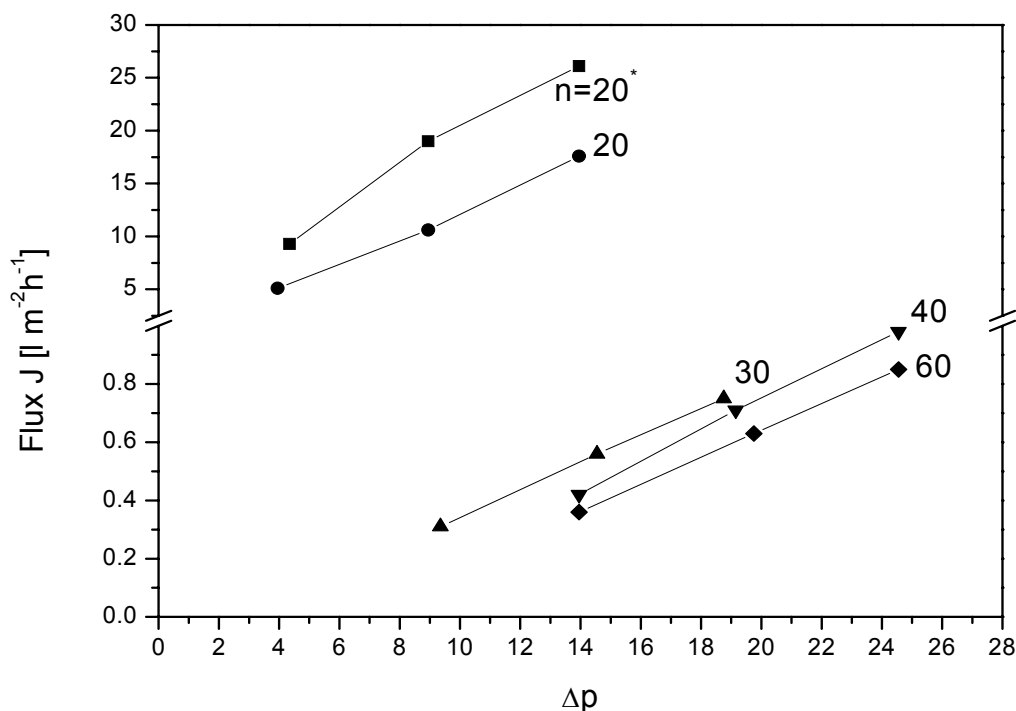
Fig. 3.28 Plot of permeation flux of mixed 10 mmolL^{-1} solutions of sodium chloride and sulfate as a function of the operating pressure Δp for **aza6**/PVS membranes treated with Cu(OAc)$_2$ prior to the permeation experiment for different number n of bilayers. The asterisk indicates that this membrane was not treated.

In Figure 3.29, the permeation flux and the rejection of aqueous NaCl and NaSO$_4$ solutions at about 14.0 bar are plotted as a function of the number of deposited bilayers. As expected, the flux decreases with increasing number of layer pairs, while the rejection increases.

The flux of the bare substrate is 3318 L m^{-2} h^{-1}, while after coating the substrate with 20 layer pairs the flux is reduced to 17.56 L m^{-2} h^{-1}, which means a reduction by a factor of about 189. If the substrate is coated with 60 layer pairs, the flux is even further reduced by a factor of 9.2·10^3. It can also be seen that the rejections of chloride and sulfate are 20.3% and 49.2%, respectively, after coating with only 20 layer pairs. If 60 bilayers are deposited, the rejection increases to 56.5% for chloride and to 98.6% for sulfate. The selectivities of Cl$^-$/SO$_4^{2-}$ also changed from

1.6 to 31, if the thickness of the membrane was changed from 20 to 60 bilayers, respectively.
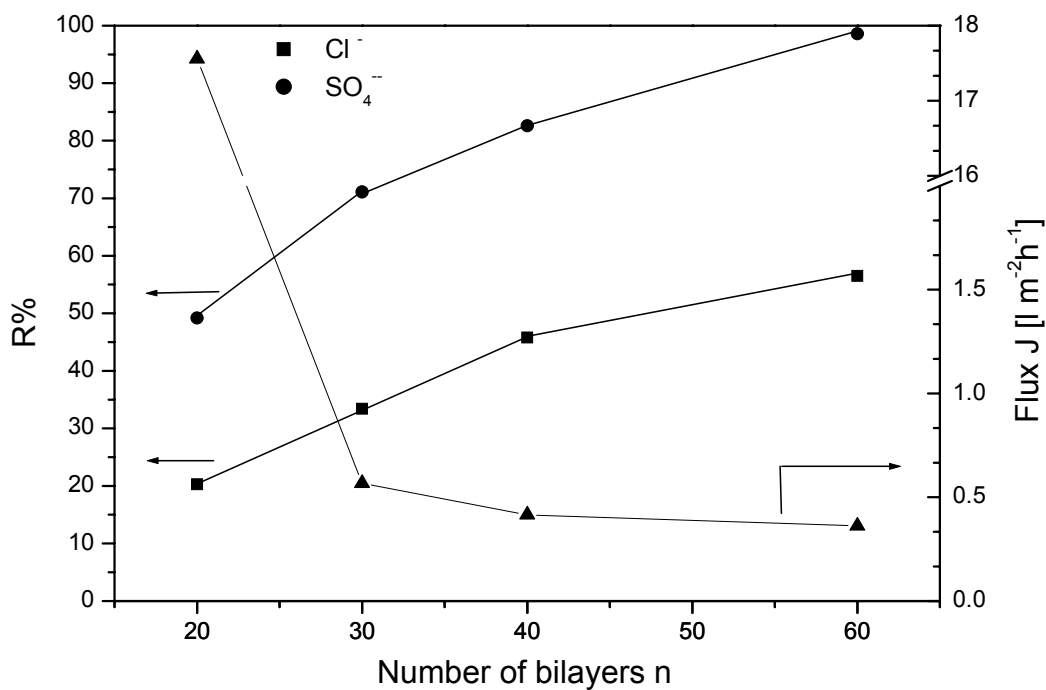
Fig. 3.29 Plot of permeation flux and rejection R as a function of the number n of dipping cycles. The operating pressure was 14 bar.

3.2.4 Ion permeation through membranes containing p-sulfonato-calix[n]-arenes

It was already previously shown in our group that p-sulfonated-calix[n]arenes with n being 4, 6, and 8 can be incorporated into ultrathin membranes using the alternating layer-by-layer assembly method. The first studies on ion separation were reported using multilayer membranes of p-sulfonato-calix[n]arenes with different ring size and cationic polyelectrolytes such as PAH, PVA, and PDADMAC [137].
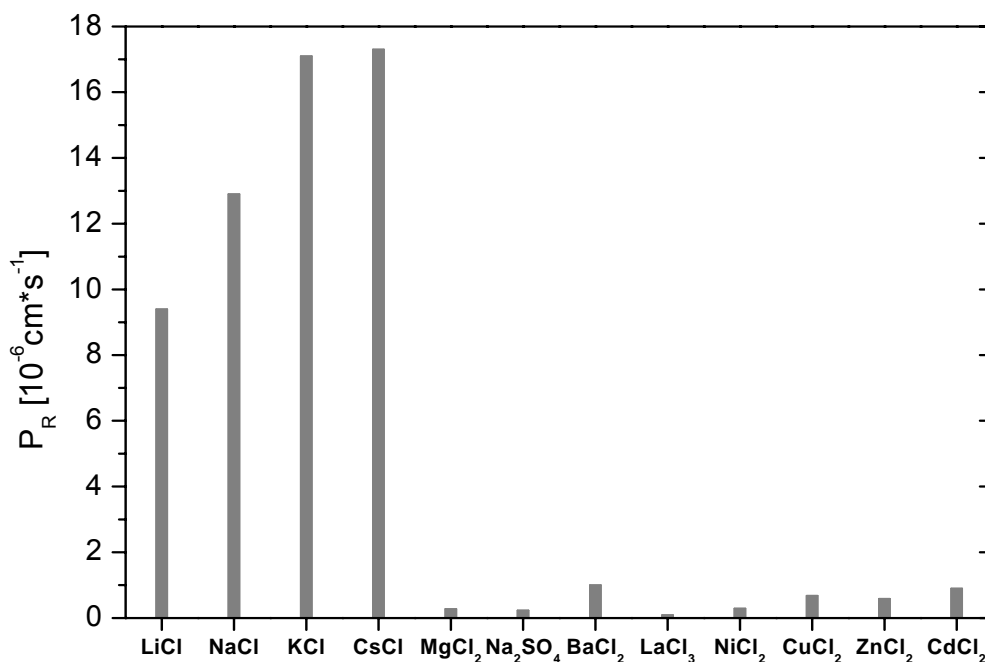
Fig. 3.30 Permeation rates of various electrolytes salts across a **calix8**/PVA membrane at 60 dipping cycles [from ref. 137].

In Figure 3.30, the P_R values of a variety of metal chlorides are plotted, an extremely low transport rate for lanthanum ions was found. This was especially true, if the membrane contained 60 bilayers of octa-p-sulfonato-calix[8]arene **(calix8),** whereas alkali metal ions could easily pass the membrane. Since **calix8** is known to specifically interact with rare earth metal ions under formation of complexes [146, 147, 161], it was of interest to investigate the transport of a variety of lanthanide ions and related yttrium ions across the membrane in more detail and to compare the results with metal ions of lower charge density.

3.2.4.1 Ion permeation through p-sulfonato-calix[8]arene and PVA

A high number of layers was deposited in order to avoid holes and defects in the films, which could severely decrease the reproducibility of the permeation measurements. The ion transport was followed by measuring the increase of conductivity $\Delta\Lambda/\Delta t$ in the permeate chamber. Typical Λ versus t- curves for permeation of NaCl and LaCl$_3$ are shown in Figure 3.31. For both electrolytes, a

linear increase of the conductivity was observed, but the slope $\Delta\Lambda/\Delta t$ for the sodium-containing solution was much higher than for the solution containing the lanthanum salt. From the slopes $\Delta\Lambda/\Delta t$, the permeation rates P_R were calculated.
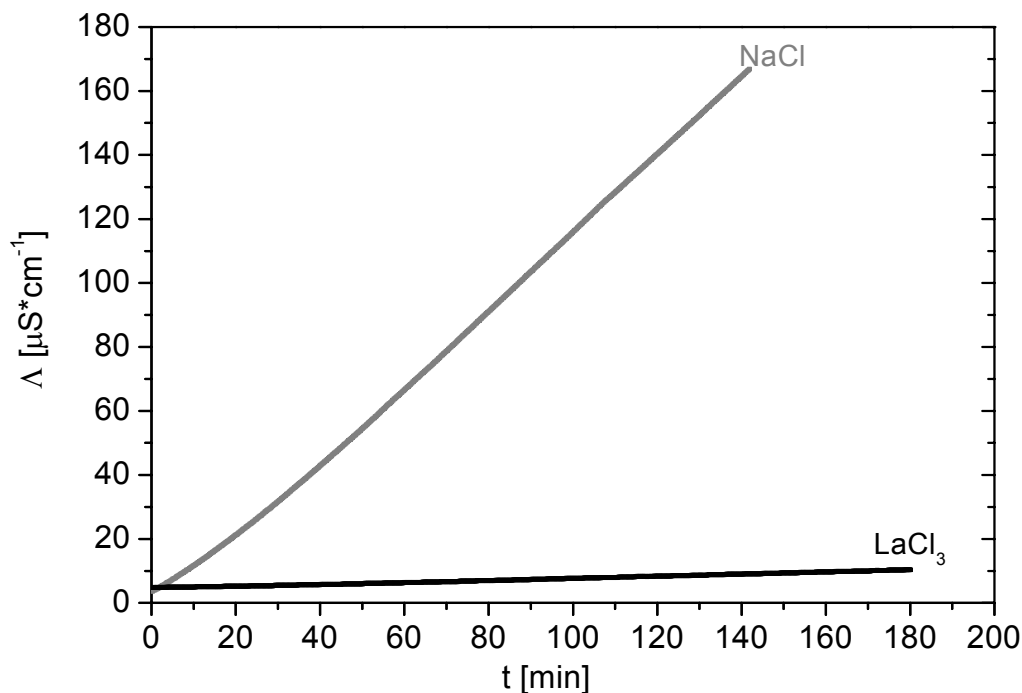
Fig. 3.31 Plot of conductivity Λ vs. time for permeation of aqueous 0.1 molL^{-1} NaCl and LaCl$_3$ solution across a **calix8**/PVA membrane (60 layer pairs).

In Figure 3.32, the P_R values of a variety of metal chlorides are listed in the series of increasing atomic number of the cation. The corresponding P_R values and theoretical separation factors α are compiled in Table 3.3. Besides a number of trivalent rare earth metal chlorides and the related yttrium(III) chloride, the chloride salts of sodium, magnesium, and zinc were also studied, for comparison. It can be seen that sodium chloride exhibits a high permeation rate, whereas the other metal chlorides exhibit rather low P_R values. Compared with magnesium and zinc the permeation rates of the lanthanide salts and yttrium chloride are especially low. Since the anions are identical for all electrolyte salts, the differences can only be related to the cations and their different interactions with the membrane. Several kinds of interaction are imaginable such as electrostatic interaction with the polymer-bound charged groups in the membrane, complex formation with the

p-sulfonato-calixarene moieties or electrostatic repulsion by the amino groups of the cationic polyelectrolyte.
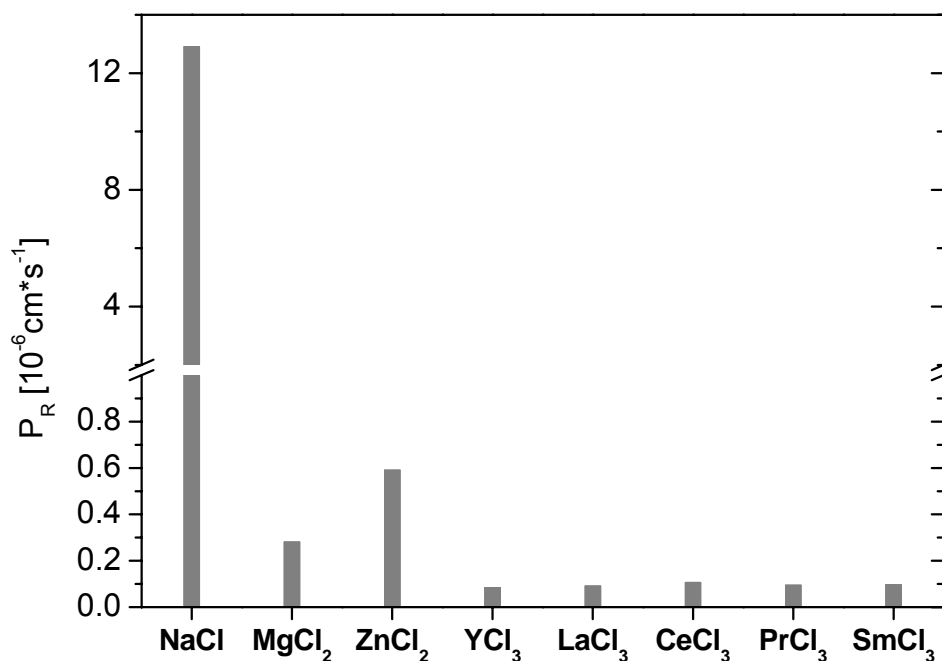
Fig. 3.32 Permeation rates of various electrolytes salts across a **calix8**/PVA membrane (60 layer pairs).

Since the **calix8**/PVA membranes are formed upon the same mechanism of electrostatic layer-by-layer adsorption as the all-polyelectrolyte multilayer membranes, the same kind of electrostatic interactions of the permeating ions with the membrane-bound charged groups can also be expected. This means the previously described model in section 2.1.2.5.1 [62-65, 162] of ion transport through polyelectrolyte multilayer films can be applied to the **calix8**/PVA membranes. According to the rejection model [63] of the multibipolar polyelectrolyte membrane, the permeating ions receive strong rejective forces from the equally charged parts of the membrane, which are stronger for the divalent ions than for the monovalent ions because of their higher charge density. This behaviour is also found for the **calix8**/PVA membranes, as the different P_R values of NaCl and $MgCl_2$ indicate. The theoretical separation factor

$\alpha(NaCl/MgCl_2)$ is 43, while for the PVA/PVS membrane prepared under salt-free or salt–containing conditions it was 9 or 51, respectively [69].

Table 3.3 Permeation rates P_R and separation factor α of tri- and divalent metal salts across **calix8**/PVA-membranes (60 layer pairs). Membranes were prepared from aqueous dipping solutions of pH 6.8, no salt added.

Electrolyte	P_R [10^{-6} cm/s]	α (NaCl/XCl$_3$)
NaCl	12.5 ± 1.0	160 ± 6
YCl$_3$	0.080 ± 0.005	
NaCl	12.5 ± 1.1	138 ± 8
LaCl$_3$	0.09 ± 0.01	
NaCl	13.0 ± 1.1	128 ± 12
CeCl$_3$	0.101 ± 0.009	
NaCl	12.8 ± 0.9	130 ± 10
PrCl$_3$	0.091 ± 0.008	
NaCl	12.7 ± 0.8	130 ± 9
SmCl$_3$	0.093 ± 0.008	
Electrolyte	**P_R [10^{-6} cm/s]**	**α (NaCl/XCl$_2$)**
NaCl	12.9 ± 1.0	43 ± 6
MgCl$_2$	0.28 ± 0.04	
NaCl	12.9 ± 1.0	20 ± 2
ZnCl$_2$	0.59 ± 0.04	

The rare earth metal (Ln^{3+}) ions exhibit ion radii r of approximately 0.1 nm ($r(Y^{3+})$= 0.09 nm) and the charge number z is 3, while z and r of Zn^{2+} are 2 and 0.07 nm, respectively. Thus the charge density ($ze/4\pi r^2$) of Ln^{+3} ions is approximately 25% lower than for Zn^{2+}, for example. Since the P_R values of Ln^{+3} are seven times smaller, the observed strong rejection cannot completely originate from electrostatic forces. Instead, an additional complex formation between the permeating Ln^{3+} ions and components of the membrane might occur.

Sequence of permeation measurements
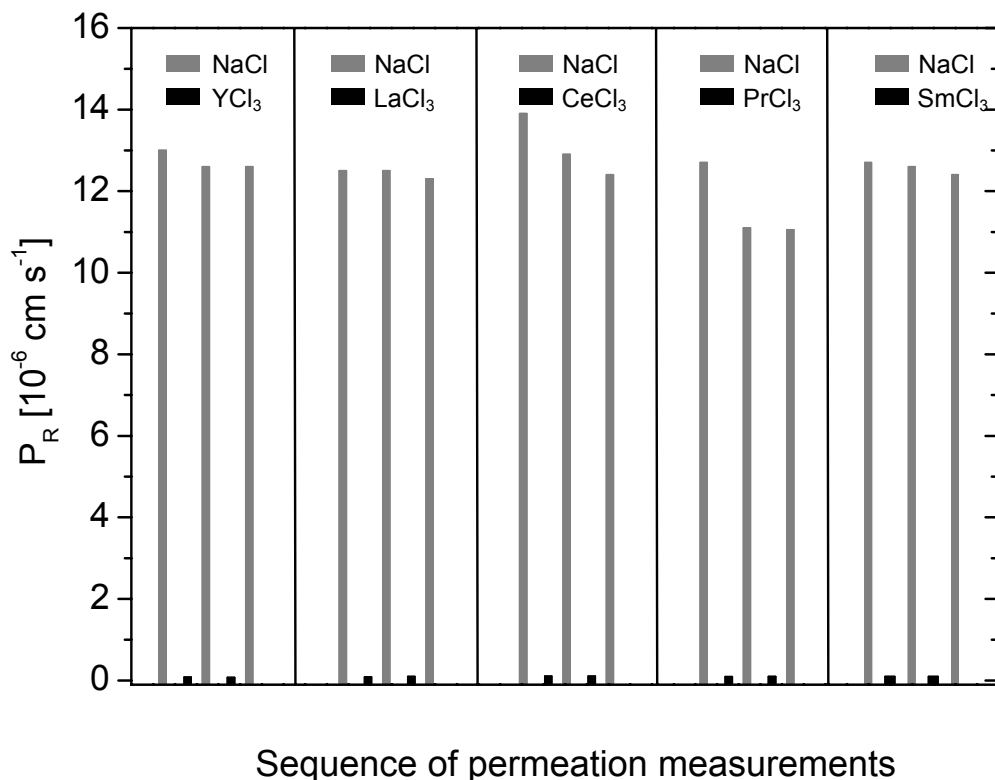
Fig. 3.33 Permeation rates of 0.1 molL^{-1} aqueous solutions of sodium chloride and various rare earth metal chlorides across **calix8**/PVA membranes.

In a number of recent papers [147,148,161], the formation of complexes between p- sulfonato-calix[n]arenes of different size n and rare earth metal ions or related ions (Y, Sc) was reported. The complexes were found in different stoichiometry, either in the presence or absence of co-ligands. Although there is no unique structure of these complexes and either layers, bilayers, tubular arrays or other aggregates were found, the complexes were always formed upon replacement of some of the aqua ligands of the trivalent rare earth metal ions by calixarene-bound sulfonate groups. Thus, it is likely that the rare earth metal ions become fixed in the membrane via complex formation, thereby introducing additional positive charges which act as barriers for other permeating cations. The barrier effect is so strong that the permeation of the sodium chloride is decreased after the membrane was exposed to rare earth metal ions as shown in Figure 3.33. Initially, the P_R value of sodium chloride was 13.9$^.$10^{-6} cm s^{-1}, while subsequent to permeation of cerium(III) chloride it only became 12.4$^.$10^{-6} cm s^{-1}. The same

experiment of successive permeation of two different electrolytes was also carried out with the other rare earth metal salts and yttrium chloride. As indicated in Figure 3.33, a decrease in the permeation rates was found in most experiments.

3.2.4.2 Transport of aromatic compounds through p-sulfonato-calix[n]arene/ PVA membranes

The skin layer of the composite membrane consists of a network structure with defined pore size in the nanometer range. In order to demonstrate a possible sieving of molecules, we now investigated the permeation of a variety of neutral and charged aromatic compounds across **calix8**/PVA and **calix6**/PVA membranes. The membranes were prepared from dipping solutions of pH 6.8 without any supporting electrolyte added.

Transport of uncharged aromatic compounds

Aromatic compounds were chosen because their concentration in the permeate could be easily detected upon UV-spectroscopy.
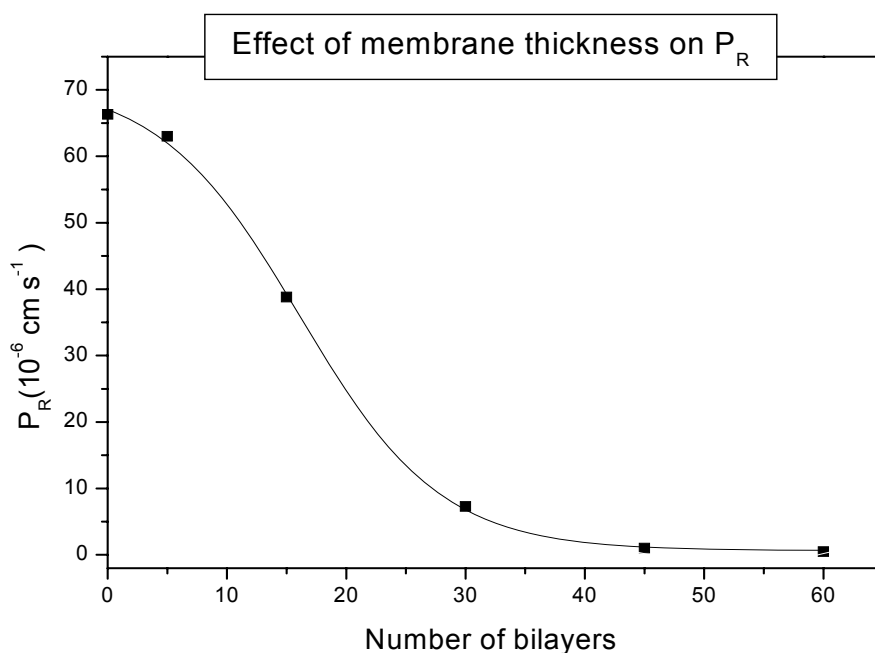
Fig. 3.34 Plot of the permeation rates P_R of 10 mmolL^{-1} solution of aniline in ethanol through **calix8**/PVA membrane as a function of the number of deposited bilayers.

First the permeation rates P_R of 10 mmolL^{-1} of aniline (An) in ethanol at different thickness of the membrane were studied as shown in Figure 3.34. The permeation rate through the bare substrate (PAN/PET with pore size 20 to 200 nm) was 66.3·10^{-6} cm s^{-1}. This permeation rate dropped sharply down to 7.18·10^{-6} cm s^{-1} when the substrate was coated with 30 bilayers of **calix8**/PVA. A further decrease to 0.50·10^{-6} cm s^{-1} was found after the number of bilayers was increased to 60. However, the experiment indicates that 30 bilayers are enough to reduce the permeation rate by about 90%, so that the transport is controlled by the pore size of the network structure of the membrane and not by the porous structure of the support. In order to obtain further information on transport mechanism and selectivity, the permeation of uncharged aromatic compounds with different size such as phenol (Ph) and naphthalene (Np) in ethanol was investigated (Table 3.4). Figure 3.35 shows low permeation rates of Ph and Np, while An exhibits a much higher value. From the P_R values, theoretical separation factors α(An/Ph) and α$'$(An/Np) of 6 and 14, respectively, could be calculated (see also Table 3.5).
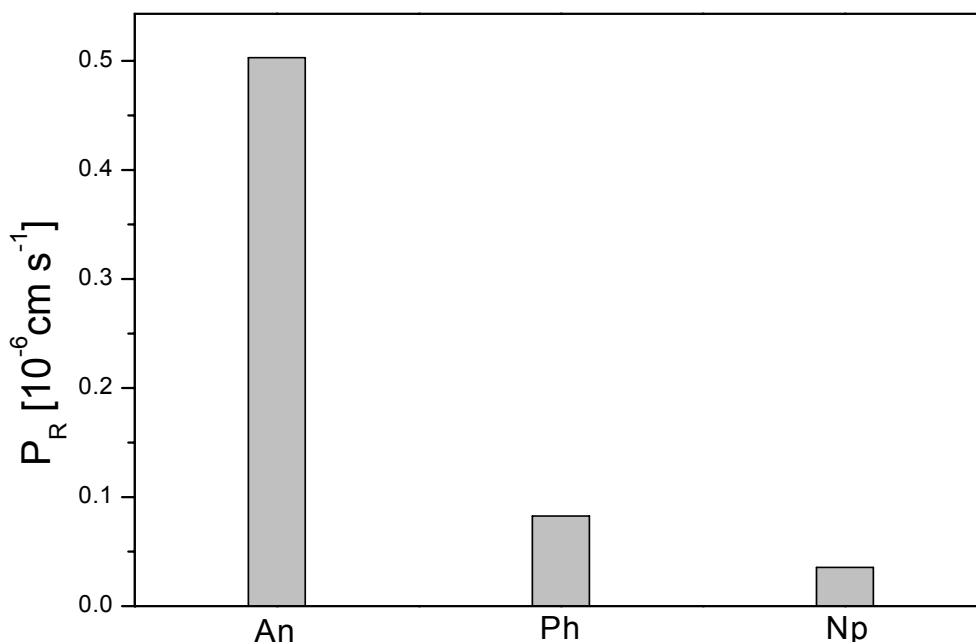
Fig. 3.35 Permeation rates of uncharged aromatic compounds (10 mmolL^{-1} in ethanol) across **calix8**/PVA membrane.

The permeation study demonstrates a selective transport of neutral aromatic compounds, which might be based on molecular sieving according to the different size of the molecules (Table 3.4). However, as indicated in the Table 3.4, the size of An and Ph molecules is comparable, only Np is clearly larger.

Table 3.4 Structures and sizes of organic compounds and abbreviations used in this study

Abbreviation	Compounds	Formula	Longest Molecular axies(nm)
An	Aniline		0.5886
Ph	Phenol		0.5573
Np	Naphthalene		0.7184
BS	Sodium benzene sulfonate		0.6291
NS	Sodium naphthalene-2-sulfonate		0.8584
1,3-BDS	Disodium benzene-1,3-disulfonate		0.7253
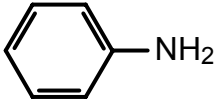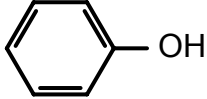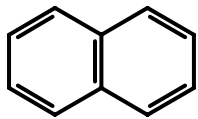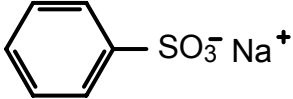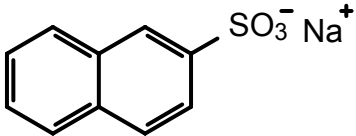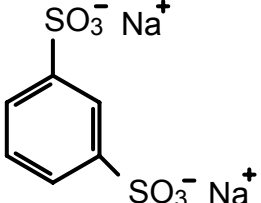
Therefore, the difference in permeation rates of An and Ph must have another reason. It can probably be attributed to the formation of phenol clusters occurring after dissolution in ethanol. Clearly, the size of the clusters will be an important factor determining the permeation rates through the membrane. When ethanol is used as solvent, a type of layered structure is favoured for Ph as shown in Figure 3.36 [163].
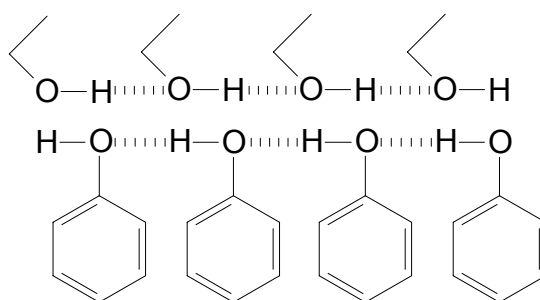
Fig. 3.36 Schematic diagram of the phenol clustering in ethanol [163]

The ethanol and phenol layers will interact via electrostatic and/or hydrogen-bonding interactions forming phenol clusters of different size. The same phenomenon will also occur in the solvation of aniline, but with lower stability and smaller size of the clusters, due to a lower charge density of aniline. Furthermore the H-bonds between phenol and solvent must be polarized; the electrostatic interaction among the polarized H-bond can support the stacking structure. The fact that aniline only functions as an acceptor for H-bonds also suggests that the stacking-type structure will be small. This means, the number of phenol molecules in the polarized cluster will be much larger than the number of aniline molecules in their clusters. Accordingly, the permeation rates of phenol and aniline will encounter with the size of the clusters. It is also possible that H-bonds are formed between the phenol molecules of the permeate and the phenolic sites of calixarene in the membrane. Furthermore, the interaction of phenol with ethanol might cause the formation of **phenolate** anions, which are electrostatically rejected by the sulfonate groups at the calixarene compound in the membrane, while aniline acts as a weak base when interacting with ethanol and forms an **anilinium** cation. The extremely low permeation rates of naphthalene ($0.0354 \cdot 10^{-6}$

cm s^{-1}) compared with aniline is attributed to the larger size of the molecules (Table 3.4) so that they are rejected.

Transport of charged aromatic compounds

For aromatic compounds with charged groups, a charge-selective transport exists in addition to the size-selective transport, which is based on electrostatic (Donnan) repulsion of the permeating ions by the equally charged parts of the membrane. A typical plot of the increase of the concentration C_p in the permeate versus the time t is shown in Figure 3.37 for uncharged phenol and a variety of charged aromatic compounds such as sodium benzene sulfonate (BS), sodium naphthalene-2-sulfonate (NS) and disodium benzene-1,3-disulfonate (1,3-BDS) in water.
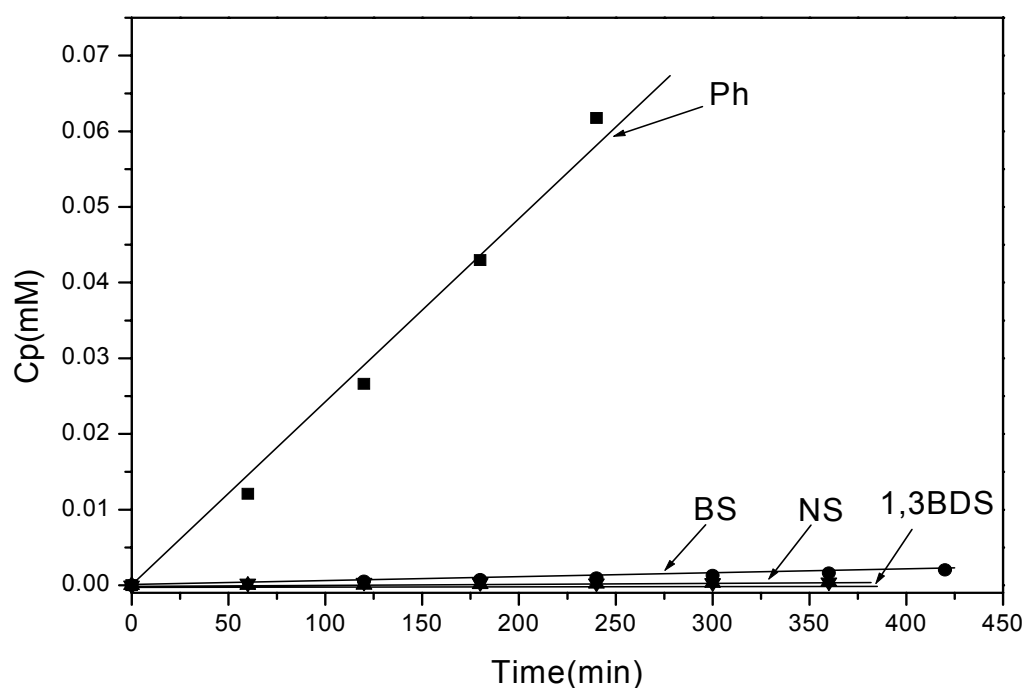
Fig. 3.37 Plot of concentration C_p of phenol and charged solutes in permeate vs. time t of the permeation measurement across **calix8**/PVA membrane.

Similar plots with a linear increase of C_p versus t were also obtained for the charged compounds with very low slopes compared with uncharged molecules such as phenol. From the slope $\Delta C_p/\Delta t$, the permeation rate P_R was calculated using the formula shown in the experimental part 4.2.4.2.
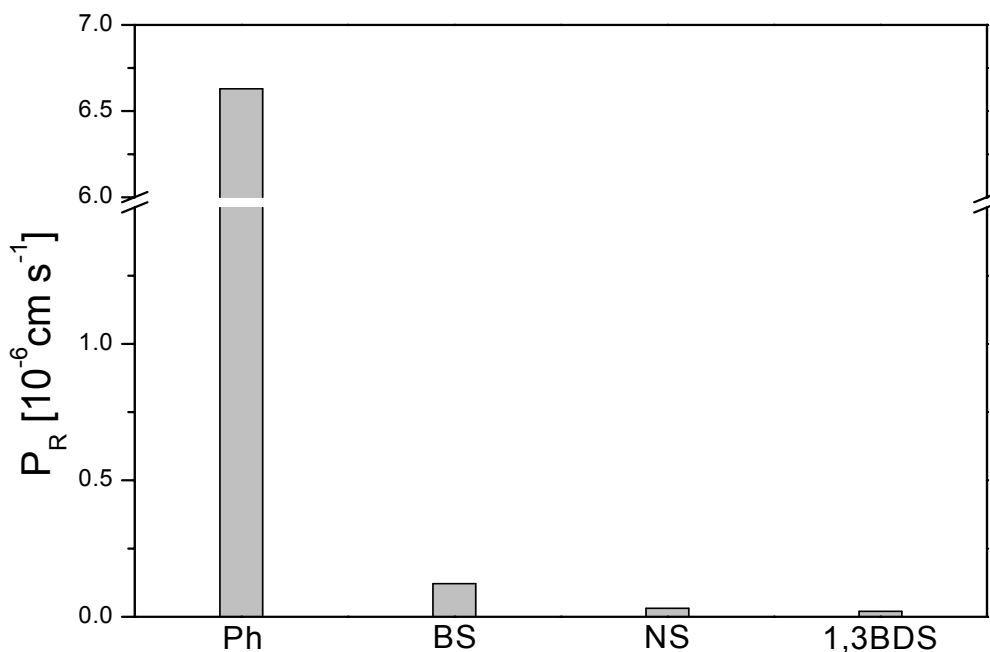
Fig. 3.38 Permeation rates of phenol and a variety of charged aromatic compounds (10 mmolL^{-1}) across **calix8**/PVA membrane.

In Figure 3.38, the P_R values of Ph, BS and 1,3-BDS in 10 mmolL^{-1} aqueous solution are represented. As can be derived from Table 3.5, the permeation rates of aqueous Ph, BS and 1,3-BDS across the **calix8**/PVA membrane are very different. The ratio of the P_R values of Ph: BS: 1,3-BDS is 6.63: 0.121: 0.0199. This means that the replacement of the phenolic OH group by a sulfonate group reduces the permeation rate to about 2 % of the P_R value for Ph, and the introduction of a second sulfonate group further decreases P_R to about 16.5 % of the value for BS. The data clearly show that the introduction of ionic groups strongly lowers the permeation rates of aromatic compounds and a selectivity in the transport of ions of different valency occurs. The selectivity in organic ion transport very much resembles the transport of inorganic ions, for which transport models have been derived in this work and previous work [63,162]. The model of Donnan rejection of highly charged ions [63] can be used to explain the transport of the aromatic ions. With increasing number of charged groups per molecule the

permeation rate progressively slows down due to increasing electrostatic rejection of the ions.

Table 3.5 The permeation rates and selectivity factors of different aromatic compounds and membranes.

Membranes	Permeation rates (10^{-6} cm s^{-1})						
	Water as solvent				Ethanol as solvent		
	Ph	BS	NS	1,3BDS	An	Ph	Np
PSS/PDADMA[*]	38.3	16.9 (2)	12.0 (3)	2.27 (16)	n.d	16.4	12.2
PSS/PAH[*]	16.6	4.07 (4)	1.0 (17)	0.063 (263)	n.d	6.17	0.22
Calix8/PVA	6.63	0.121 (55)	0.0312 (213)	0.0199 (333)	0.503	0.0827 [1.25 %]	0.0354
Calix6/PVA	22.4	3.79 (6)	3.13 (7)	1.55 (14)	32	20.6	12.5

   *   data adopted from reference [42]
( ) separation factor α ($P_{R(Ph)}/P_{R(BS,NS,1,3BD)}$)
n.d not determined
[ ] reduction of P_R of phenol by different solvent

From Figure 3.38 and Table 3.5 it can also be seen that the P_R values decrease in the series BS > NS, i.e. in the direction of increasing size of the anion. The separation factors α (Ph/BS) and $\alpha^{'}$ (Ph/NS) are 55 and 213, respectively. This indicates a size-selectivity in the transport of organic ions in addition to the charge selectivity mentioned above. Thus the permeation rates through the **calix8**/PVA membrane depend on both the size and the charge of the ions.

In a further set of experiments, the permeation rates of charged aromatic compounds dissolved in water and uncharged aromatic compounds dissolved in ethanol across membranes based on PVA and different calix[n]arenes with n=6 or

8 were studied (Figure 3.39). In general, the permeation rates of all compounds through **calix8**/PVA membrane are much lower than through **calix6**/PVA membranes (Table 3.5). The latter exhibit much higher permeation rates and lower selectivities. The permeation rates decrease with increasing size of the molecules and number of charged groups in the permeating molecules. This phenomenon can probably be related to thickness and density of the membrane. In the previous study [137] of the build-up of multilayered films on quartz substrates with different calix[n]arenes with n= 4, 6, and 8 and PVA it was shown that the three films strongly differ in the 208 nm absorbance, although the deposited number of layer pairs was identical.
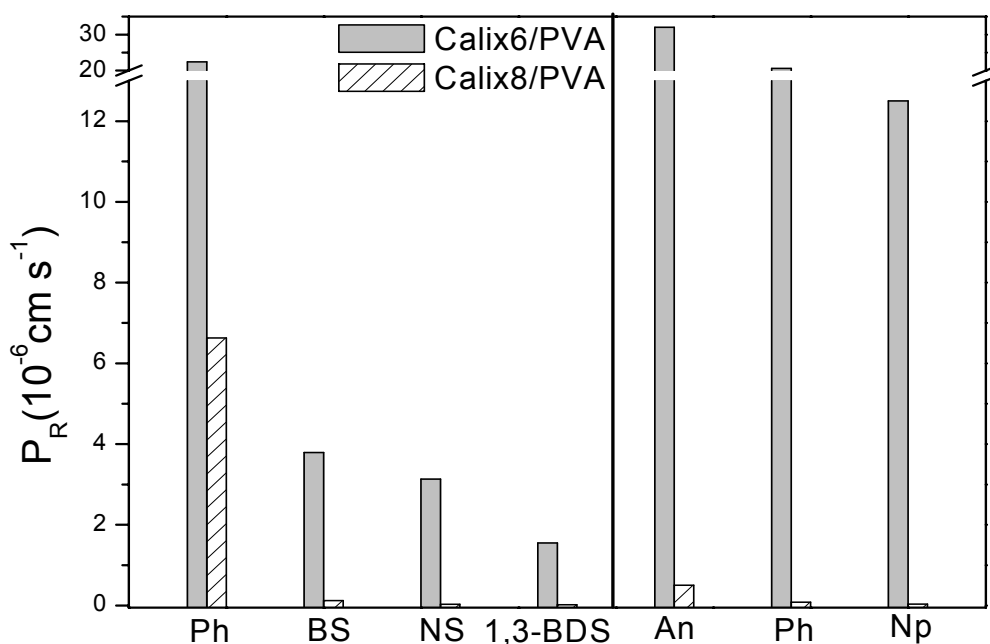
Fig. 3.39 Permeation rates of a variety of aromatic compounds in water (conc: 10 mmolL^{-1}) (left) and in ethanol (right) across **calix8**/PVA and **calix6**/PVA membranes.

For the three films, the absorbance increased in the ratio 1:2:3, although the size of calixarene rings and the number of benzene chromophores per ring only increased in the ratio 1:1.5:2. It was concluded that a larger amount of **calix8** is absorbed per dipping cycle than of the smaller **calix6** or **calix4** rings due to the presence of more ionic binding sites per ring and the fact that **calix8** attains a flat-plane conformation, which is better **calix8** being well suited for adsorption [164].

Furthermore, in the membranes based on **calix8** more polyelectrolyte will be deposited than in the membrane based on **calix6** or **calix4** in each layer pair. As a consequence, a denser and thicker membrane containing less defects will be formed and the transport rates of the permeating molecules are lower. This result also indicates that the aromatic compounds very likely to not permeate through the macrocyclic rings of the calixarenes, but rather permeate through the pores in the membranes formed between the macrocyclic compounds and the polyelectrolytes.

4 Experimental Details

All the results obtained in this work are based on several materials and measurements, which are described in detail in this chapter.

4.1 Materials

4.1.1 Chemicals used

Chemicals and polyelectrolytes used in this work are listed in Table 4.1(a and b). They were used without further purification. Milli-Q-water (18.2 MΩ) was used as the solvent. PVA was kindly supplied by BASF, Ludwigshafen.

Table 4.1 List of chemicals used in this work

 a) Polyelectrolytes and organic compounds

Substance	Symbol	Supplier	Mol. W.t. [g mol^{-1}]
Polyvinylamine	PVA	BASF	100,000
Polyvinylsulfate potassium salt	PVS	Acros	350,000
Polyallylamine hydrochloride	PAH	Aldrich	70,000
Sodium polystyrene sulfonate	PSS	Aldrich	70,000
Polyethylenimine branched	PEI	Polyscience	70,000
1,4,7,10,13,16-Hexaazacyclo-octadecane trisulfate	aza6	Fluka	552.65
Tetra-p-sulfonatocalix[4] arene	calix4	95%Acros	744.75
Hexa-p-sulfonatocalix[6] arene	calix6	95%Acros	1117
Octa-p-sulfonatocalix[8] arene	calix8	97% Acros	1489
3-Aminopropylmethyldiethoxysilane		>97%Fluka	191.35
Toluene		>99.5%Acros	92.14
Methanol		99.8%Acros	32.04

b) Other chemicals

Substances	Symbol	Supplier	Assay
Sodium chloride	NaCl	Fluka	99.5 %
Potassium chloride	KCl	Acros	99.0 %
Lithium chloride	LiCl	Fluka	>99.0 %
Sodium sulfite anhydrous	Na_2SO_3	Merck	98.0 %
Sodium sulfate decahydrate	$Na_2SO_4 \cdot 10H_2O$	Fluka	99.0 %
Zinc chloride	$ZnCl_2$	Fluka	98%
Magnesium chloride hexahydrate	$MgCl_2 \cdot 6H_2O$	Fluka	> 99.5 %
Magnesium sulfate heptahydrate	$MgSO_4 \cdot 7H_2O$	Acros	> 99.5 %
Lanthanium(III) chloride heptahydrate	$LaCl_3 \cdot 7H_2O$	Aldrich	99.9 %
Samarium(III) chloride hexahydrate	$SmCl_3 \cdot 6H_2O$	Aldrich	> 99.0 %
Praseodymium(III) chloride hexahydrate	$PrCl_3 \cdot 6H_2O$	Aldrich	99.9 %
Cerous(III) chloride heptahydrate	$CeCl_3 \cdot 7H_2O$	Fluka	> 98.5 %
Yttrium(III) chloride hexahydrate	$YCl_3 \cdot 6H_2O$	Fluka	> 98.5 %
Copper(II) acetate monohydrate	$(CH_3COO)_2Cu \cdot H_2O$	Aldrich	98%
Cobalt (II) acetate tetrahydrate	$(CH_3COO)_2Co \cdot 4H_2O$	Aldrich	> 99%
Nickel (II) acetate monohydrate	$(CH_3COO)_2Ni \cdot 4H_2O$	Aldrich	> 99%
Hydrochloric acid	HCl	Merck	
Sodium hydroxide	NaOH	Fluka	>98%
Barium chloride	$BaCl_2$	Merck	99.5%
Iron(III) chloride hexahydrate	$FeCl_3 \cdot 6H_2O$	Fluka	98%
Potasium hexacyanoferrate(II) trihydrate	$K_4Fe(CN)_6 \cdot 3H_2O$	Fluka	> 99.5%
Crown ether	18-Crown-6	Acros	99%
Aniline	An	Merck	99.5%
Phenol	Ph	Merck	99.5%
Naphthalene	Np	Merck	99.7%
Sodium benzene sulfonate	BS	Acros	98%
Sodium naphthalene-2-sulfonate	NS	Acros	> 99%
Disodium benzene-1,3-disulfonate	1,3-BDS	Acros	80%

4.1.2 Porous support

In our study, porous PAN/PET supporting membranes (100 μm of polyethylene terephthalate, PET, fleece coated with 80 μm of polyacrylonitrile, PAN, pore sizes 20-200 nm) were kindly provided by Sulzer Chemtech GmbH, Neunkirchen. The advantage of the porous support is that the transport of ions is little affected by the substructure so that the separation achieved can be exclusively ascribed to the ultrathin polyelectrolyte multilayer adsorbed at the surface. Prior to adsorption of the separation layer, the membrane surface was rendered hydrophilic upon treatment with oxygen plasma for 1 min, which was carried by Sulzer Chemtech.

4.2 Measurements

4.2.1 Preparation of polyelectrolyte solutions

Ultrathin multilayers were adsorbed from aqueous solutions containing different concentration of macrocycles and polyelectrolytes of 10^{-4}, 10^{-3}, and, 10^{-2} monomolL^{-1} (moles of monomer units per liter of Milli-Q-water). In this work, the pH of the aqueous dipping solution was varied from 0.9 to 7.0 and adjusted upon addition of aqueous HCl or NaOH (concentration: 0.1 molL^{-1}). The pH of aqueous dipping solutions was measured using a pH-Meter CG 825 from Schott Company in combination with a glass electrode. For calibration, buffer solutions of pH 4.0 and 7.0 were used.

4.2.1.1 Preparation of aza6 hexachloride solutions

To prepare highly soluble **aza6** hexachloride in aqueous solution, 0.582 g (10^{-3} molL^{-1}) of **aza6** trisulfate and 0.625 g ($3 \cdot 10^{-3}$ mol L^{-1}) of BaCl$_2$ were dissolved in 1.0 L pure water. A white precipitate of BaSO$_4$ formed, which was removed upon centrifugation at 2,000 r.p.m. for 1.0 h. The residual aqueous solution contained **aza6** as chloride. It was directly used as dipping solution.

4.2.2 Preparation of multilayer films on quartz support

For compounds carrying a UV-absorbing chromophor unit, the progress of building-up polyelectrolyte multilayer films was monitored using a double beam UV/VIS spectrometer, Lambda 14 from Perkin-Elmer Company. For UV spectroscopic studies, quartz substrates (Suprasil 30 x 12 x 1 mm^2, Hellma GmbH, Müllheim / Baden Germany) were used. Quartz substrates were first cleaned with piranha solution for 30 min (7:3 mixture of H_2SO_4: H_2O_2, caution: the mixture is strongly oxidizing and may detonate upon contact with organic material) and then carefully washed with water. After ultrasonication in water at 60 ^{o}C for 30 min the substrates were successively immersed in pure methanol, a methanol-toluene (1:1) mixture and in pure toluene for 30 min each, respectively. Then the substrates were transferred into a 5.0 % solution of 3-aminopropylmethyldiethoxysilane in toluene and kept there overnight (for at least 12 h). Subsequently the substrates were immersed in toluene, a methanol-toluene (1:1), methanol and finally water for 30 min, respectively. To obtain a better adsorption, the substrates were consecutively precoated with three bilayers of cationic (PVA or PAH) and anionic (PVS or PSS) polyelectrolytes in alternate sequence.

For preparation of organized polyelectrolyte multilayer assemblies, the pretreated quartz substrates were sequentially immersed in:

   a) a solution of the anionic compound,
   b) pure water,
   c) a solution of the cationic compound, and
   d) pure water again.

Immersion times for step a) and c) were 30 min each, for washing steps b) and d) only 5 min two times each. Steps a) to d) were repeated many times as required. All dipping experiments were done at room temperature.

4.2.3 Preparation of multilayer films on ZnSe support

In order to clearly prove the presence of certain compounds in the multilayer films, ATR-IR spectra of the multilayered films on zinc-selenide substrate were recorded using an FTIR spectrometer, Spectrum 1000 from Perkin-Elmer Company. The zinc-selenide crystal substrate (size 50 x 10 x 3 mm^3) was cleaned with ethanol before use. For organized multilayer deposition on ZnSe, the same steps (from a to d) described in the previous section 4.2.2 were used.

ATR (attenuated total reflectance spectroscopy) is a technique which is based on internal reflection (Figure 4.1). The incident radiation is directed first into the zinc-selenide substrate of high refractive index and after penetration beyond the surface is reflected from the sample which has a lower refractive index.
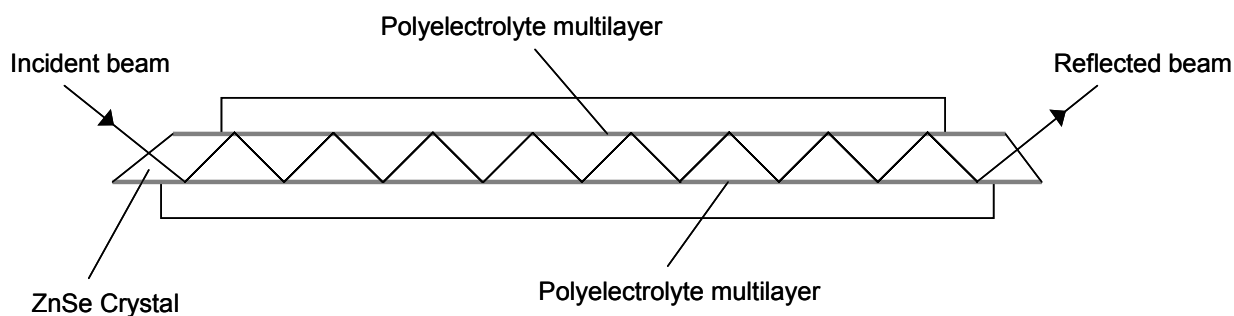
Fig. 4.1 Scheme of multiple internal reflections in ZnSe crystal [1].

If a polymer sample, which selectively absorbs radiation, is placed in contact with a reflecting surface, some frequencies of the incident beam will be absorbed while other frequencies are transmitted and reflected. By multiple reflection the radiation is measured and plotted as a function of the wavenumber resulting in an absorption spectrum of the sample.

4.2.4 Preparation of the multilayered separation membrane

The ultrathin separation layer was deposited on a PAN/PET porous support through alternating layer-by-layer assembly of cationic and anionic polyelectrolytes. By using a home-made computerized apparatus (Figure 4.2), the membrane (size of 12 x 12 cm^2) was mounted in the apparatus after careful washing with Milli-Q-water.
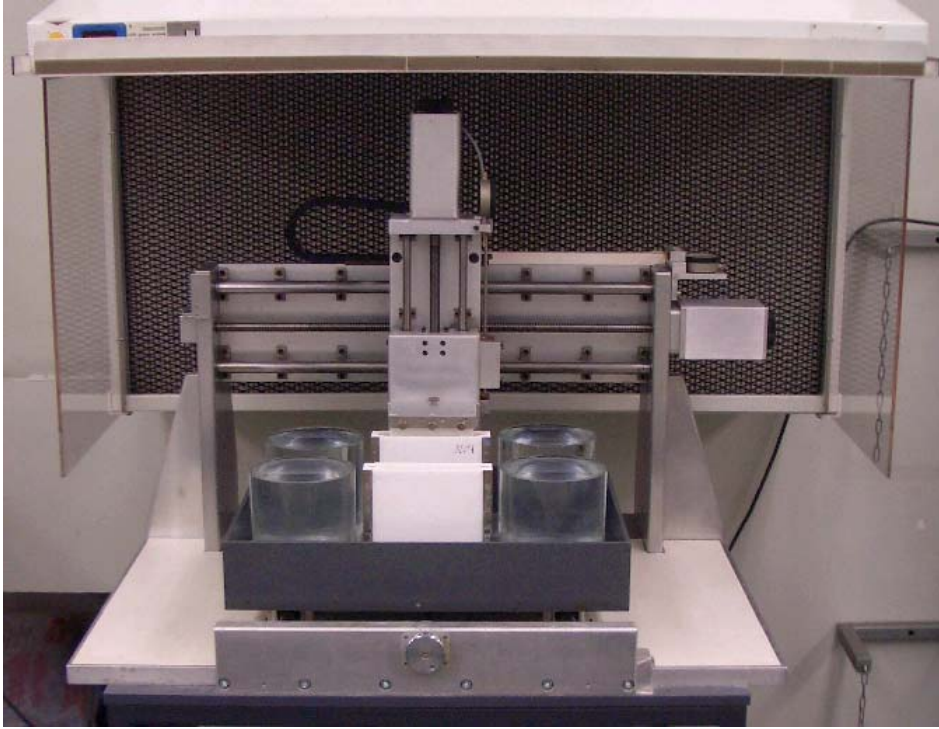
Fig. 4.2 Home-made automatic dipping machine for preparation of ultrathin separation membrane based on layer-by-layer adsorption.

First, the porous supporting membrane was dipped automatically into an aqueous solution of the cationic polyelectrolyte for 30 min and the polyelectrolyte was adsorbed at the surface. Surplus polyelectrolyte was removed by twice dipping the membrane into water for 5 min. Subsequently the membrane was dipped into a solution of the anionic polyelectrolyte which led to its rapid adsorption at the interface and then the membrane was washed again. By multiple repetition of the dipping cycle, the ultrathin separation layer was obtained. Up to 60 bilayers were deposited. The concentration and immersion times were the same as used for the quartz substrates (Sec. 4.2.2).

4.2.4.1 Ion permeation

In order to study the ion permeation across the polyelectrolyte multilayered membrane, the home-made U-shaped cell shown in Figure 4.3 was used. The cell consists of two chambers separated by the membrane with the cross section area A being 4.52 cm^2. One of the chambers contains a certain volume (V_0= 60 ml) of

the aqueous salt solution (conc. c_0 0.1 molL^{-1}) and the other one is filled with the same volume of pure Milli-Q-water.
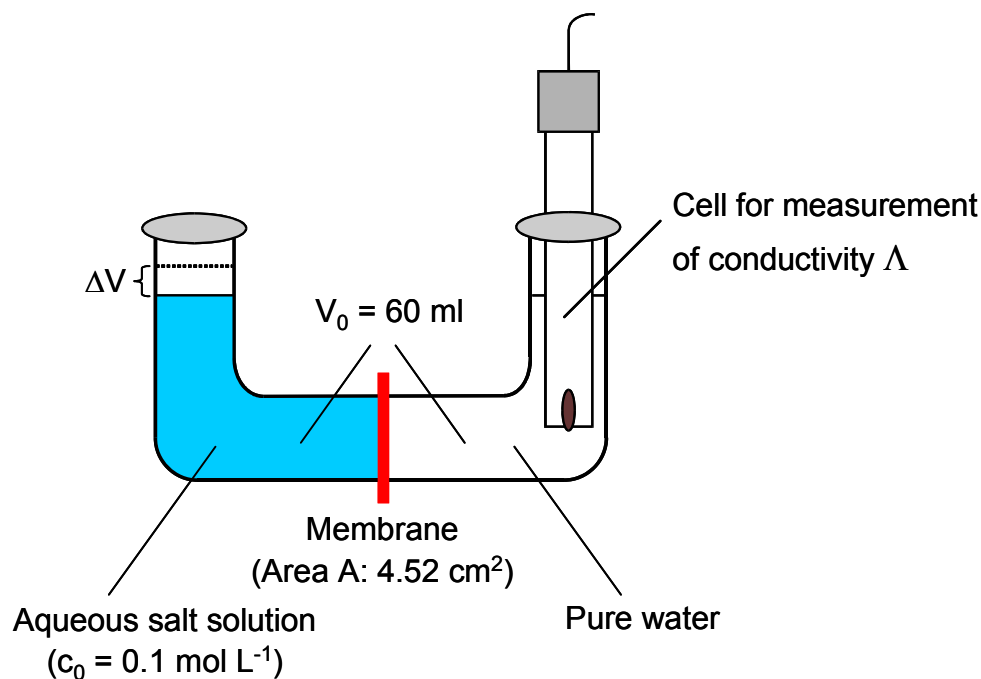
Fig. 4.3 Schematic representation of the cell used for measurement of ion permeation.

The initial increase in conductivity ($\Delta\Lambda/\Delta t$) in the water chamber was measured using a conductometer 703 from Knick company. The permeation rate P_R (cm s^{-1}) was calculated using equation (4.1) shown below:

$$P_R = \left(\frac{\Delta\Lambda}{\Delta t}\right)(V_0 - \Delta V)\Lambda_m^{-1}(Ac_0)^{-1},$$ (4.1)

with Λ_m being the molar conductivity, and ΔV being the change of the volume after permeation.

Permeation rates displayed in the Figures are always the average values of two permeation measurements across the same membrane, the error $2(P_{R,1} - P_{R,2})(P_{R,1} + P_{R,2})^{-1} \cdot 100\%$ being between 2 and 6 % ($P_{R1,2}$ are the permeation rates of the first and second measurement).

4.2.4.2 Permeation of aromatic compounds

Permeation measurements of charged and neutral organic compounds were carried out using a home-made apparatus as described in Figure 4.4. The concentration c_p of the aromatic compounds in the permeate chamber was detected UV spectroscopically. For the UV measurement, a small amount of the permeate solution (about 3 ml) was periodically collected and the concentration of the permeate was determined by measuring the peak absorbance in a UV/vis spectrometer. After measurement, each sample was immediately returned to the permeate solution chamber (which took about 2-3 min).
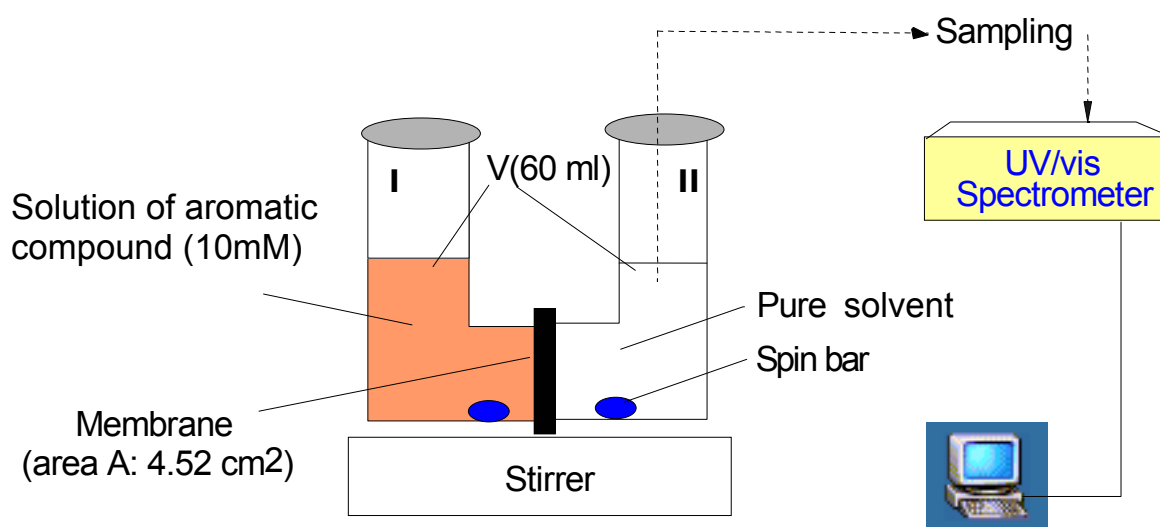
Fig. 4.4 Schematic representation of the cell used for measurement of the transport of aromatic compounds.

The permeation rate P_R of the aromatic compounds in the permeate chamber was calculated according to formula (4.2)

$$P_R = \left(\frac{\Delta c_p}{\Delta t}\right) V_0 (Ac_f)^{-1} \, , \tag{4.2}$$

with Δc_p being the change in solute concentration in the permeate chamber during the time period Δt of the permeation measurement. The value of $\Delta c_p/\Delta t$ was obtained from the plot of c_p against t. V_0, A and c_f represent the initial volume of the feed and permeate solution, the area of the membrane and the solute

concentration of the feed solution, respectively. The separation factor α is defined as the ratio of the P_R values of corresponding compounds.

4.2.4.3 Nanofiltration

Nanofiltration (NF) is a pressure-driven separation process. Measurements across **aza6**/PVS membranes were carried out using a home-made apparatus working under stirred dead end conditions. The apparatus consists of a temperature-controlled pressure chamber made of stainless steel (volume V=1.8 L; maximum pressure up to 40 bar adjusted with nitrogen gas from a pressurized bottle), and a stirrer (rotating speed = 700 r.p.m.). At the bottom, the cell is equipped with an outlet for the permeate solution (Figure 4.5).

a) Nanofiltration measurement

For nanofiltration experiments, **aza6**/PVS membranes were used, which were either treated with $Cu(OAc)_2$ or used without copper acetate treatment. In the first step, **aza6**/PVS membranes, which were either treated or non-treated with copper acetate (20 layer pairs), were conditioned with pure water at 5 bar for 3 h in order to remove residual salt, which was eventually left in the membrane from the preparation process. For this purpose the chamber was filled with 1.8 L of water and the applied pressure p was adjusted with nitrogen gas from a pressurized bottle.

As the second step, the pure water flux J_w (eq. 2) was determined at 5 bar by collecting the permeated water in a beaker over a time period of 2-3 h.

In the third step, the pure water was replaced by the mixed salt solution of low concentration (10 $mmolL^{-1}$ of NaCl and Na_2SO_4 each). After a 2 h prerunning was made at different applied pressures (5, 10, 15, bar) to reach a steady state, the permeate solutions were collected over a period of 2 to 3 h and the concentration was determined using HPLC, respectively.
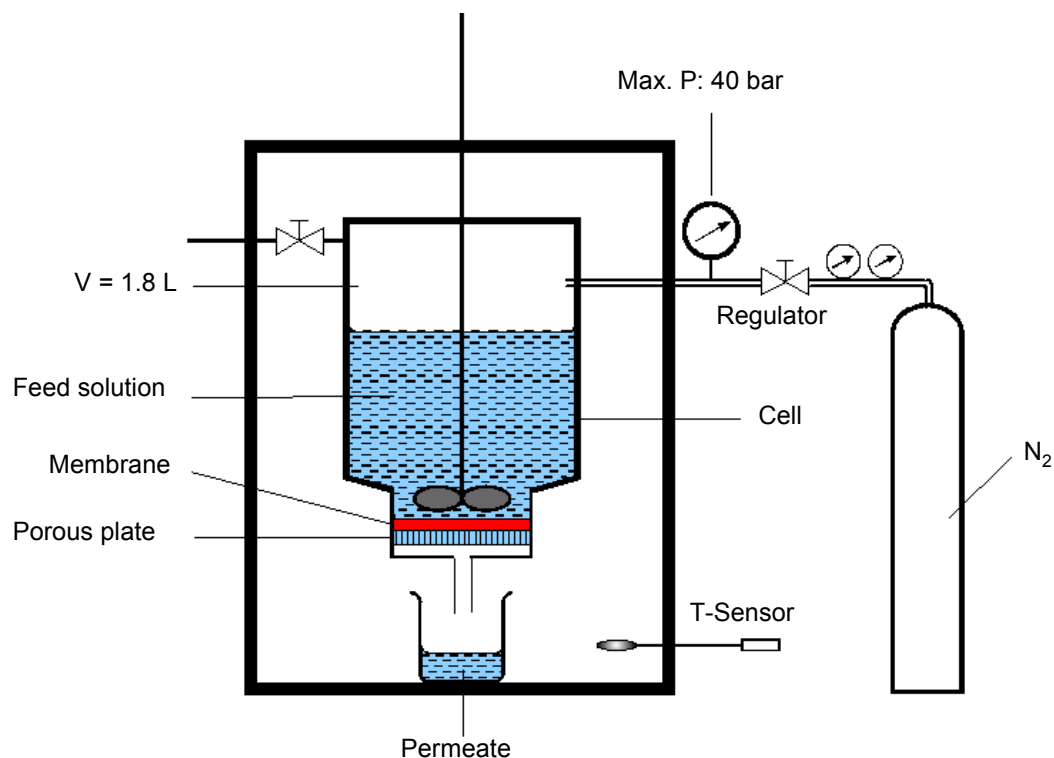
Fig. 4.5 Schematic representation of the apparatus used for measurement of ion permeation under nanofiltration conditions.

In the next step, the pressure was returned to the previous value, the permeate solution was again collected and the concentration was determined again to check the stability of the membrane. All experiments were carried out under stirring at room temperature.

b) Treatment of aza6/PVS membranes with copper acetate

For treatment with copper acetate, the **aza6**/PVS membrane was first mounted in the NF apparatus (Figure 4.5) and treated with 0.1 mol L^{-1} aqueous $Cu(OAc)_2$ solution at 10 bar for 60 min. Then the membrane was regenerated upon washing with pure water for 2 h at 10 bar to remove residual $Cu(OAc)_2$, which was eventually left in the membrane during the treatment process. The sequence of steps for rejection of salts after membrane treatment were the same as those for the non-treated membrane.

c) Determination of flux and ion content in feed and permeate

The permeation flux J was calculated from the measured volume V of the permeate solution, which was collected across the membrane of area A (36.8 cm^2) in the time period Δt,

$$J = \frac{V}{A\,\Delta t}. \qquad (4.3)$$

The percent rejection R of salt was calculated using the equation (4.4)

$$R = (1 - \frac{c_{perm}}{c_{feed}}) \times 100\%, \qquad (4.4)$$

with c_{perm} and c_{feed} being the salt concentrations in permeate and feed solution.

The quantitative analysis of feed and permeate salt concentrations was carried out using HPLC (high performance liquid chromatography), a computerized Knauer high-pressure liquid chromatograph consisting of a pump K1001, a thermostated column, a refractometer wellchrom K-2301, and a conductivity detector LFD 550101. The anionic salt concentrations were detected using a 150 mm x 4.6 mm anion column with an anion precolumn-kit. Degassed aqueous phthalic acid (4.0 mmol L^{-1}, pH=4.3 with LiOH) was used as mobile phase with flow rate 1.0 mL/min. The operating temperature was 35.0 ± 0.1 $^{\circ}$C. The ion concentration was determined from the corresponding peak area after equilibration with a set of standard electrolyte solutions of different concentration. c_{feed} and c_{perm} values represent average values of at least two chromatographic measurements from feed and permeate solutions. R and J values represent average values from three measurements under identical NF conditions.

The selectivity α of Cl$^-$ ions over SO$_4^{2-}$ is defined by equation (4.5) [76]:

$$\alpha = \frac{c_{Cl^-,perm}}{c_{Cl^-,feed}} \frac{c_{SO_4^{2-},feed}}{c_{SO_4^{2-},perm}} = \frac{100 - R_{Cl^-}}{100 - R_{SO_4^{2-}}}. \qquad (4.5)$$

5 Summary and Conclusions

Our studies indicate that cationic and anionic macrocyclic compounds are suitable for electrostatic layer-by-layer assembly on solid supports. The assemblies represent dense films of thickness in the nanometer range. A wide variety of compounds can be used as counterions ranging from inorganic ions to macrocyclic polyelectrolytes. If the conditions are properly chosen, a regular film growth takes place, i. e., the same amount of ions is adsorbed in each dipping cycle. The protonation of **aza6** occurs in a wide pH-range and therefore the multilayer formation is strongly pH-dependent. At medium pH-values, **aza6** is only partially protonated. The lbl assembly was therefore carried out in the linear growth regime using dipping solutions of pH 6.0, whereas an exponential layer growth was found at pH 0.9, 2.7, 3.7 and 5.0 and the number of rings adsorbed per layer becomes strongly dependent on the concentration of the macrocycles in solution. The high tendency of **aza6** to complex inorganic anions could be used to prepare stable **aza6**/hexacyanoferrate(II) multilayers. The multilayers are highly reactive towards iron(III) forming deeply coloured PB crystallites. With other metal ions, formation of PB analogous complex salts can be expected, which makes the multilayers attractive as colour-specific sensors for di- and trivalent transition metal ions. It was also possible to build up multilayers entirely consisting of cationic and anionic macrocyclic compounds on a solid support. The alternating lbl assembly of positively charged **aza6** and negatively charged **calix6** or **calix8** was studied.

The calixarenes of larger ring size are well suited for building up multilayered films. The high affinity to rare earth metal cations even allows to prepare lbl assemblies of La(III) and **calix8**. Surprisingly, the formation of films of La(III)/**calix8** assemblies could be further improved, if additional neutral crown ethers such as 18-crown-6 were present in the La(III) dipping solution. The reason is a complex formation between the three compounds (La(III), 18-crown-6, **calix8**), the structure of the complex still being unknown.

The latter experiment opens the possibility to combine different compounds known from supramolecular chemistry in order to form new complex architectures on solid substrates via electrostatic, hydrogen-bonding and charge transfer interactions.

Studying transport behaviour of macrocyclic membranes, a number of interesting and surprising results were obtained. Using **aza6** and **calix8**-containing multilayers, the ion transport across the membrane can be significantly influenced. Specific interaction between certain ring sizes and distinct ions are striking. As a consequence, very high selectivities in transport of certain ions are obtained.

For the first time the electrostatic layer-by-layer assembly of ultrathin membranes consisting of the cationic **aza6** and PVS as an anionic polyelectrolyte, and the ion permeation behaviour of the membranes were studied. Moreover, it was demonstrated that the **aza6** compound is able to form a stable complex with copper(II) acetate in the membrane. As a result of the complex formation, the selectivity in ion transport can be strongly enhanced. The reason is that the complex formation is accompanied by the formation of negative excess charges in the membrane causing an efficient Donnan-rejection of divalent anions such as sulfate, sulfite and thiosulfate, the theoretical separation factors $\alpha(Cl^-/SO_4^{2-})$ and $\alpha(Cl^-/SO_3^{2-})$ being 110 and 1420, for example, while divalent metal cations still can pass the membrane. Furthermore, the complex formation of **aza6** with cobalt(II) acetate and nickel(II) acetate and its impact on the separation behaviour of the membranes were studied. It was also shown that **aza6**/PVS membrane is capable of rejecting ions from aqueous electrolyte solutions, if a pressure is applied to the feed side of the membrane. The rejection of both Cl^- and SO_4^{2-} ions increased with increasing the number of deposited bilayers. However, it was unusual that the rejection decreases with increasing operating pressure. A possible origin is a pressure-induced structural rearrangement, which leads to an increase of the pore size in the separating layers. Based on 56.5% rejection of Cl^- ions and 98.6% rejection of SO_4^{2-} ions found for a membrane of 60 bilayers at 14 bar, a selectivity of 31 was reached. The permeation flux increased linearly with operating pressure and decreased with increasing the number of bilayers deposited.

Layer-by-layer assemblies of **calix8** and PVA could be easily prepared on porous supports, if suitable conditions (pH 6.5 of the dipping solution, no salt added) were applied. The membranes exhibited a highly selective transport of inorganic metal chloride salts. The transport of mono- and divalent-metal ions was mainly controlled by electrostatic forces comparable with all polyelectrolyte multilayer membranes, that means the permeation rates of monovalent ions were high and those of divalent ions low. Furthermore, the study shows that the transport rates of rare earth metal ions are extremely low. Since this effect cannot merely originate from electrostatic forces an additional complex formation with the calixarene units is postulated. It is likely that specific interaction of the lanthanide ions with the sulfonate groups of the calixarenes occur as they are know from various bulk complexes of these compounds. Due to the complex formation, the membrane is almost impermeable for rare earth metal ions. Very high separation factors $\alpha(NaCl/LnCl_3)$ up to 138 were observed. The strong rejection of the lanthanides renders the membranes useful for enrichment of rare earth metal ions and related ions such as Y(III) from aqueous solution.

Furthermore, the permeation of a variety of neutral and charge aromatic compounds was investigated. The transport of neutral compounds was controlled by the pore size of the membrane and the molecular size of the compounds. The membranes act as molecular sieves and reject compounds larger than the pore size of the membrane. Aromatic compounds with ionized groups exhibited a size-selectivity as well as a charge-selective transport. Charge-selectivity is based on the fact that compounds with two ionized groups receive a stronger Donnan rejection from equally charged parts of the membrane than compounds with single ionized group, similar to the different rejection of mono- and divalent inorganic ions reported previously.

In conclusion, it is demonstrated that incorporation of cationic **aza6** in lbl-assembled membranes is useful for achieving a highly selective rejection of divalent inorganic anion. Moreover, it could be demonstrated that anionic **calix8**-based membranes are well suited for rejection of cations.

6 References

[1]   L. M. Blinov, Usp. Khim. **155** (1988) 443.

[2]   Y. M. Lvov, L. A. Feirgin, Kristallografiya **32** (1987) 800.

[3]   G. Ozin, Adv. Mater. **4** (1992) 612.

[4]   R. Maoz, L. Netze, J. Gun, J. Sagiv, J. Chim. Phys. **85** (1988) 1059.

[5]   J. M. Lehn, Angew. Chem. **102** (1990) 1347.

[6]   H. Lee, L. Kepley, H. Hong, T. Mallouk, J. Am. Chem. Soc. **110** (1987) 618.

[7]   A. Kakkae, S. Yitzchaik, S. Roscoe, F. Kubota, D. Allan,T. Marks, W. Lin, G. Wong, Langmuir **9** (1993) 388.

[8]   J. Spinke, M. Liley, H. Guder, L. Angermair, W. Knoll, Langmuir **9** (1996) 1821.

[9]   G. Coulon, T. Russel, V. Deline, P. Green, Macromolecules **22** (1989) 2581.

[10]   G. Decher, J.-D. Hong, Ber. Bunsenges. Phys.Chem. **95** (1991) 1430.

[11]   G. Decher, J.-D. Hong, J. Schmitt*,* Thin Solid Films **210** (1992) 831.

[12]   G. Decher, J. Schmitt, Prog. Colloid Polym. Sci. **89** (1992) 160.

[13]   Y. Lvov, G. Decher, H. Möhwald, Langmuir **9** (1993) 481.

[14]   S. T. Dubas, J. B. Schlenoff, Macromolecules **32** (1999) 8153.

[15]   Y. Lvov, G. Decher, Crystal. Rep. **39** (1994) 628.

[16]   D. Q. Kurth, R. Osterhout, Langmuir **15** (1999) 4842.

[17]   M. Raposo, R. S. Pontes, L. H. C. Mattoso, O. N. Oliveira Jr., Macromolecules **30** (1997) 6095.

[18]   V. V. Tsukruk, V. N. Bliznyuk, D. Visser, A. L. Campbell, T. J. Bunning, W. W. Adam, Macromolecules **30** (1997) 6615.

[19]   T. Cooper, A. Campbell, R. Crane, Langmuir **11** (1995) 2713.

[20]   C. Tadeschi, F. Caruso, H. Möhwald, S. Kirstein, J. Am. Chem. Soc. **122** (2000) 5841.

[21]   I. Suzuki, T. Ishizaki, H. Inoue, Macromolecules **35** (2002) 6470.

[22]   Y. Lvov, K. Ariga, I. Ichinose, T. Kunitake, J. Am. Chem. Soc. **117** (1995) 6117.

[23]   G.B. Sukhorukov, H. Möhwald, G. Decher, Y. M. Lvov, Thin Solid Films, **284** (1996) 220.

[24]   A. Liu, J. Anzai, Langmuir **19** (2003) 4043.

[25]   P. Kohli, G. J. Blanchard, Langmuir **16** (2000) 4655.

[26]   J. S. Major, G. J. Blanchard, Langmuir **17** (2001) 1163.

[27]   S. Katsuhiko, S. Iwao, A. Jun-ichi, Langmuir **19** (2003) 7406.

[28]   X. Yang, S. Johnson, J. Shi, T. Holesinger, B. Swanson, Sensors and Actuators B., **45** (1997)87.

[29]   J. J. Cox, K. W. Kittredge, D. V. Ca, J. Solid State Electrochem. **8** (2004) 722.

[30]   J. Schmitt, G. Decher, Adv. Mater. **9** (1997) 61.

[31]   P. Schuetz, F. Caruso, Chem. Mater. **16** (2004) 3066.

[32]   J. Schmitt, T. Grünewald, G. Decher, P. S. Pershan, K. Kjaer, M. Lösche, Macromolecules **26** (1993) 7058.

[33]   W. Jin, A. Toutianoush, M. Pyrasch, J. Schnepf, H. Gottschalk, W. Rammensee, B. Tieke, J. Phys. Chem. B **107** (2003) 12062.

[34]   H. Hong, R. Steity, S. Kirstein, D. Davidov, Adv. Mater. **10** (1998) 1104.

[35]   K. Lowack, C. A. Helm, Macromolecules **31** (1998) 823.

[36]   D. Yoo, S. S. Shiratori, M. F. Rubner, Macromolecules **31** (1998) 4309.

[37]   M. Lösche, J. Schmitt, G. Decher, W. G. Bouwman, K. Kjaer, Macromolecules **31** (1998) 8893.

[38]   J. B. Schlenoff, H. Ly, M. Li, J. Am. Chem. Soc. **120** (1998) 7626

[39]   T. Farhat, G. Yassin, S. T. Dubas, J. B. Schlenoff, Langmuir **15** (1999) 6621.

[40]   M. Gao, B. Richter, S. Kirstien, H. Möhwald, J. Phys. Chem. B **102** (1998) 40969.

[41]   G. Ladam, P. Schaad, J. C. Voegel, P. Schaaf, G. Decher, F. Cuisinier, Langmuir **16** (2000) 1249.

[42]   S. S. Shiratori, M. F. Rubner, Macromolecules **33** (2000) 4213.

[43]   M. Castelnovo, J. F. Joanny, Langmuir **16** (2000) 7524.

[44]   J. B. Schlenoff, S. T. Dubas, Macromolecules **34** (2001) 592.

[45]   R. Steitz, W. Jaeger, R. von Klitzing, Langmuir **17** (2001) 4471.

[46]   R. A. McAloney, M. Sinyor, V. Dudnik, M. C. Goh, Langmuir **17** (2001) 6655.

[47]   B. Schoeler, G. Kumaraswamy, F. Carusi, Macromolecules **35** (2002) 889.

[48]   A. F. Xie, S. Granick, Macromolecules **35** (2002) 1805.

[49]   G. Decher, Science **277** (1997)1232.

[50]   M. Schönhoff, J. Phys.: Condens. Matter **15** (2003) 1781.

[51]   P. Bertrand, A. Jonas, A. Laschewsky, R. Legras, Macromol. Rapid Commun. **21** (2000) 319.

[52]   P. T. Hammond, Curr. Opin. Colloid Interface Sci. **4** (2000) 430.

[53]   P. T. Hammond, Adv. Mater. **16** (2004) 1271.

[54]   J. M. Levasalmi, T. J. McCarthy, Macromolecules **30** (1997) 1752.

[55]   F. van Ackern, L. Krasemann, B. Tieke, Thin Solid Films **329** (1998) 762.

[56]   D. M. Sullivan, M. L. Bruening, Chem. Mater. **15** (2003) 281.

[57]   L. Krasemann, B. Tieke, J. Membr. Sci. **150** (1998) 23.

[58]   L. Krasemann, B. Tieke, Mater. Sci. Eng. **8-9** (C1999) 513.

[59]   L. Krasemann, B. Tieke, Chem. Eng. Technol. **23** (2000) 211.

[60]   L. Krasemann, A. Toutianoush, B. Tieke, J. Membr. Sci. **181** (2001) 221.

[61]   A. Toutianoush, L. Krasemann, B. Tieke, Colloids Surf. **198-200** (A2002) 881.

[62]   A. Toutianoush, B. Tieke, Mater. Sci. Eng. **22** (C 2002) 459.

[63]   L. Krasemann, B. Tieke, Langmuir **16** (2000) 287.

[64]   J. J. Harris, J. L. Stair, M. L. Bruening, Chem. Mater. **12** (2000)1941.

[65]   J. L. Stair, J. J. Harris, M. L. Bruening, Chem. Mater. **13** (2001) 2641.

[66]   J. Dai, A. M. Balachandra, J. II Lee, M. L. Bruening, Macromolecules **35** (2002) 3164.

[67]   A. M. Balachandra, J. Dai, M. L. Bruening, Macromolecules **35** (2002) 3171

[68]   M. L. Bruening, D. M. Sullivan, Chem. Eur. J. **8** (2002) 3833.

[69]   A. Toutianoush, B. Tieke, in: Novel Methods to Study Interfacial Layers; Moebius, D., Miller, R., Eds.; Elsevier: Amsterdam, **11** (2001) 415.

[70]   A. Toutianoush, B. Tieke, Mater. Sci. Eng. **22** (C 2002) 135.

[71]   M. L. Bruening, J. J. Harris, D. M. Sullivan, Polym. Mater. Sci. Eng. **85** (2001) 525.

[72]   W. Jin, A. Toutianoush, B. Tieke, Langmuir **19** (2003) 2550.

[73]   B. W. Stanton, J. J. Harris, M. D. Miller, M. L. Bruening, Langmuir **19** (2003) 7038.

[74]   X. Liu, M. L. Bruening, Chem. Mater. **16** (2004) 351.

[75]   M. Miller, M. L. Bruening, Langmuir **20** (2004) 11545.

[76]   S. Uk Hong, R. Malaisamy, M. L. Bruening, Langmuir **23** (2007) 1716.

[77]   A. Toutianoush, W. Jin, H. Deligöz, B. Tieke, Appl. Surf. Sci. **246** (2005) 437.

[78]   R. von Klitzing, H. Möhwald, Thin Solid Films **284** (1996) 352.

[79]   W. Jin, A. Toutianoush, B. Tieke, Appl. Surf. Sci. **246** (2005) 444.

[80]   M. Mulder, "Basic Principles of Membrane Technology", Kluwer, Dordrecht, **1991**.

[81]   A. Toutianoush, Dissertation, Universität zu Köln, **2003.**

[82]   M. Urairi, T. Tsuru, S. Nakao, S. Kimura, J. Membr. Sci. **70** (1992) 153.

[83]   T. Tsuru, S. Nakao, S. Kimura, J. Membr. Sci. **108** (1995) 269.

[84]   B. Tieke, A. Toutianoush, in 'Encyclopedia of Nanoscience and Nanotechnology', Dekker, New York, **2004**, p. 1591.

[85]   B. Tieke, F. van Ackern, L. Krasemann, A. Toutianoush, Eur. Phys. J. E **5** (2001) 29.

[86]   B. Tieke, In 'Handbook of Polyelectrolytes and Their Applications' Eds.: S. k. Tripathy, J. Kumar H. S. Nalwa; Vol. **3**, Amer. Sci. Publ., 2002, p. 115.

[87]   A. C. Warden, M. Warren, M. T. W. Hearn, L. Spiccia, New J. Chem. **28** (2004) 1301.

[88]   B. Dietrich, Pure & Appl. Chem. **65** (1993) 1457.

[89]   J. Cullinane, R. I. Gelb, T. N. Margulis, L. J. Zompa, J. Am. Chem. Soc. **104** (1982) 3048.

[90]   A. Salimi, M. Shamsipur, J. Inclusion Phenomena and Macrocyclic Chemistry, **34** (1999) 455.

[91]   E. Kimura, M. Kodama, T. Yatsunami, J. Am. Chem. Soc., **104** (1982) 3182.

[92]   R. I. Gelb,B. T. Lee, L. J. Zompa, J. Am. Chem. Soc. **107** (1985) 909.

[93] E. Kimura, A. Sakonaka, J. Am. Chem. Soc., **104** (1982) 4984.

[94] E. Kimura, A. Sakonaka, T. Yatsunami, M. Kodama, J. Am. Chem. Soc., **103** (1981) 3041.

[95] V. N. Afanas'ev, A. G. Grechin, Russ. Chem. Rev. **71** (2002) 775.

[96] T. Yatsunami, A. Sakonaka, E. Kimura, Anal. Chem. **53** (1981) 477.

[97] C. Mertesdorf, T. Plesnivy, H. Ringsdorf, P. A. Suci, Langmuir **8** (1992) 2531.

[98] C. D. Gutsche, B. Dhawan, K. Hyun No, R. Muthukrishnan, J. Am. Chem. Soc. **103** (1981) 3782.

[99] V. Böhmer, Angew. Chem. Int. Ed. Engl. **34** (1995) 713.

[100] Z. Asfari, V. Böhmer, J. Harrowfield, J. Vicens, "Calixarenes", Kluwer, Dordrecht, **2001**.

[101] G. W. Gokel, "Crown Ethers and Cryptands: Monographs in Supramolecular Chemistry", Royal Society of Chemistry,**1991**.

[102] G. Wenz, Angew. Chem. Int. Ed. Engl. **33** (1994) 803.

[103] M. Sonoda, K. Hayashi, M. Nishida, D. Ishii, I. Yoshida, Analyt. Sci. **14** (1998) 493.

[104]   H. B. Li, Y. Y. Chen, S. L. Liu, J. Appl. Polym. Sci. **89** (2003) 1139.

[105] S. Memon, E. Akcevlan, B. Sap, M. Tabakei, D. M. Roundhill, M. Yilmaz, J. Polym. Environ. **11**(2003) 67.

[106] R. M. Izatt, J. D. Lamb, R. T. Hawkin, P. R. Brown, S. R. Izatt, J. J. Christensen, J. Am. Chem Soc. **105** (1983) 1782.

[107] L. Mutihac, H. J. Buschmann, E. Diacu, Desalination **148** (2002) 253.

[108] S. K. Chang, H. S. Hwang, H. Son, J. Youk, Y. S. Kang, Chem. Commun. (**1991**) 217.

[109]   N. J. van der Veen, E. Rozniecka, L. A. Woldering, M. Chudy, J. Huskens, F. C. J. van Veggel, D. N. Reinhoudt, Chem. Eur. J. **7** (2001) 94878.

[110] X.Yang, S. Johnson, J. Shi, T. Holesinger, B. Swanson, Sens. Actuators B **45** (1997) 87.

[111] S. Shinkai, S Mori, H. Koreishi, T. Tsubaki, O. Manabe, J. Am. Chem. Soc. **108** (1986) 2409.

[112]   S. Shinkai, K. Araki, T. Matsuda, N. Nishiyama, H. Ikeda, I. Takasu, M. Iwamoto, J. Am. Chem. Soc. **112** (1990) 9053.

[113]   C. D. Gutsche, I. Alam, Tetrahedron **44** (1988) 4689.

[114]   S. G. Bott, A. W. Coleman, J. L. Atwood, J. Am. Chem. Soc. **108** (1986) 1709

[115]   X. Yan, V. Janout, J. T. Hsu, S. L. Regen, J. Am. Chem. Soc. **124** (2002) 10962.

[116]   M. D. Conner, V. Janout, I. Kudelka, P. Dedek, J. Zhu, S. L. Regen, Langmuir **9** (1993) 2389.

[117]   P. Shahgaldian, A. W. Coleman, Langmuir **17** (2001) 6851.

[118]   Y. Ishikawa, T. Kunitake, T. Matsuda, T. Otsuka, S. Shinkai, Chem. Commun. (**1989**) 736.

[119]   Z. H. Yang, W. X. Cao, Chin. J. Polym. Sci. **21** (2003) 473.

[120]   B. Lonetti, P. Lo Nostro, B. Ninham, P. Baglioni, Langmuir **21** (2005) 2242.

[121]   J. L. Atwood, L. J. Barbour, M. J. Hardie, C. L. Raston, Coord. Chem. Rev. **222** (2001) 3.

[122]   T. Arimori, S. Shinkai, J. Chem. Soc., Perkin Trans. 1, **1** (1993) 887.

[123]   S. J. Dalgarno, C. L. Raston, Chem. Commun. (**2002**) 2216.

[124]   T. Ness, P. J. Nichols, C. L. Raston, Eur. J. Inorg. Chem. (**2001**) 1993.

[125]   T. Okubo, M. Suda, J. Colloid Interface Sci. **213** (1999) 565.

[126]   T. Okubo, M. Suda, J. Colloid Interface Sci. **277** (1999) 813.

[127]   K. Shinbo, K. Suzuki, K. Katto, F. Kaneko, S. Kobayashi, Thin Solid Films **327** (1998) 209.

[128]   M. R. Linford, M. Auch, H. Möhwald, J. Am. Chem. Soc. **120** (1998) 178.

[129]   S. L. Clark, M. F. Montague, P. T. Hammond, Macromolecules **30** (1997) 7237.

[130]   S. T. Dubas, J. B. Schlenoff, Macromolecules **34** (2001) 3736.

[131]   N. G. Hoogeveen, M. A. Cohen Stuart, G. J. Fleer, M. R. Böhmer, Langmuir **12** (1996) 3675.

[132]   J. Choi, M. F. Rubner, Macromolecules **38** (2005) 116.

[133]   T. Shutava, M. Prouty, D. Kommireddy, Y. Lvov, Macromolecules **38** (2005) 2850.

[134]   K. Ariga, Y. Lvov, T. Kunitake, J. Am. Chem. Soc. **119** (1997) 2224.

[135]   O. M. Tanchak, C. J. Barrett, Chem. Mater. **16** (2004) 2734.

[136]   C. Picart, Ph. Lavalle, P. Hubert, F. J. G. Cuisinier, G. Decher, P. Schaff, J. C. Voegel, Langmuir **17** (2001) 7414.

[137]   A. Toutianoush, J. Schnopf, A. EL-Hashani, B. Tieke, Adv. Funct. Mater. **15** (2005) 700.

[138]   A. Laschewsky, E. Wischerhoff, Macromolecules **30** (1997) 8304.

[139]   J. D. Mendelson, C. J. Barrett, V. V. Chan, A. J. Pal, Am. Mayes, M. F. Rubner, Langmuir **16** (2000) 5017.

[140]   R. Advincula, E. Aust, W. Meyer, W. Knoll, Langmuir **12** (1996) 3536.

[141]   Ph. Lavalle, C. Gergely, F. J. G. Cuisinier, G. Decher, P. Schaaf, J. C. Voegel, C. Picart, Macromolecules **35** (2002) 4458.

[142]   E. Kimura, T. Koike, Chem. Commun. **1998**, 1495.

[143]   R. I. Gelb, L. M. Schwartz, L. J. Zompa, Inorg. Chem. **25** (1986) 1527.

[144]   B. Dietrich, M. W. Hosseini, J. M. Lehn, R. B. Sessions, J. Am. Chem. Soc. **103** (1981) 1282.

[145]   A. C. Warden, M. Warren, M. T. W. Hearn, L. Spiccia, Inorg. Chem. **43** (2004) 6936.

[146]   M. Pyrasch, A. Toutianoush, W. Jin, J. Schnepf, B. Tieke, Chem. Mater. **15** (2003) 245.

[147]   Y. Israeli, G. P. A. Yap, Ch. Detellier, Supramol. Chem. **12** (2001) 457.

[148]   J. L. Atwood, L. J. Barbour, S. Dalgarno, C. L. Raston, H. R. Webb, J. Chem. Soc. Dalton Trans. **2002**, 4351.

[149]   A. Drljaca, M. J. Hardie, J. A. Johnson, C. L. Raston, H. R. Webb, Chem. Commun.(**1999**) 1135.

[150]   T. Ness, P. J. Nichols, C. L. Raston, Eur. J. Inorg. Chem. (**2001**) 1993.

[151]   C. Wartelle, P. M. Viruela, R. Viruela, E. Ortí, F. X. Sauvage, E. Levillain, F. Le Derf, M. Sallé, J. Phys. Chem. A **109** (2005) 1188.

[152]   A. K. Sharma, G. Singh, A. K. Yadav, L. Prakash, Molecules **2** (1997) 129.

[153]   R. von Klitzing, B. Tieke, Adv. Polym. Sci. **165** (2004) 177.

[154]   M. Kodama, E. Kimura, S. Yamaguchi, J. Chem. Soc., Dalton Trans. (**1980**) 2536.

[155]   D. J. Royer, G. J. Grant, D. G. van Derveer, M. J. Castillo, Inorg. Chem.
        21 (1982) 1902.

[156]   S. Chandrasekhar, D. G. Fortier, A. McAuley, Inorg. Chem. **32** (1993)
        1424.

[157]   J. E. Barker, Y. Lin, N. D. Martin, T. Ren, J. Am. Chem. Soc. **125** (2003)
        13332.

[158]   J. E. Barker, Y. Lin, G. T. Yee, W. Chen, G. Wang, V. M. Rivera, T. Ren,
        Inorg. Chem. **45** (2006) 7973.

[159]   B. K. Koo, Bull. Korean Chem. Soc. **22** (2001) 113.

[160]   P. W. Atkins, 'Physikalische Chemie', 2nd edition, VCH Weinheim,**1996**, p.
        299.

[161]   J. L. Atwood, L. S. J. Dalgarno, M. J. Hardie, C. L. Raston, New J. Chem.
        28 (2004) 326.

[162]   T. R. Farhat, J. B. Schlenoff, Langmuir **17** (2001) 1184.

[163]   A. Wakisaka, Y. Yamamoto, Y. Akiyama, H. Takeo, F.Mizukami, K.
        Sakaguchi, J. Chem. Soc. Faraday Trans. **92** (1996) 3339.

[164]   F. Perret, V. Bonnard, O. Danylyuk, K. Suwinska, A. W. Coleman,
        New J. Chem. **30** (2006) 987.

Ich versichere, dass ich die von mir vorgelegte Dissertation selbstständig angefertigt habe, die benutzten Quellen und Hilfsmittel vollständig angegeben und die Stellen der Arbeit – einschließlich Tabellen, Karten und Abbildungen -, die anderen Werken im Wortlaut oder dem Sinn nach entnommen sind, in jedem Einzelfall als Entlehnung kenntlich gemacht habe; dass diese Dissertation noch keiner anderen Fakultät oder Universität zur Prüfung vorgegelegen hat; dass sie abgesehen von unten angegebenen Teilpublikationen noch nicht veröffentlicht worden ist, sowie, dass ich eine solche Veröffentlichung vor Abschluss des Promotionsverfahrens nicht vornehmen werde.

Die Bestimmungen der geltenden Promotionsordnung sind mir bekannt. Die von mir vorgelegte Dissertation ist von Prof. Dr. B. Tieke betreut worden.

Köln, den 26.11.2007

Publications

[1] *Toutianoush, A; Schnepf, J; El-Hashani, A; Tieke, B*: Highly selective ion transport across layer-by-layer assemblies of p-sulfonato-calix[n]arenes and cationic polyelectrolytes, *Adv. Funct. Mater.* **15**, 700 (2005).

[2] *Toutianoush, A; El-Hashani, A; Schnepf, J; Tieke, B*: Multilayer membranes of p-sulfonato-calix[8]arene and polyvinylamine and their use for selective enrichment of rare earth metal ions, *Appl. Surf. Sci.* **246**, 437 (2005).

[3] *El-Hashani, A; Tieke, B*: Electrostatic layer-by-layer assembly of ultrathin films containing hexacyclen and p-sulfonato-calix[n]arene macrocycles, *J. Nanosci. Nanotech.* **6**, 1710 (2006).

[4] *El-Hashani, A; Toutianoush, A; Tieke, B*: Layer-by-layer assembled membranes of protonated 18-azacrown-6 and polyvinylsulfate and their application for highly efficient anion separation, *J. Phys. Chem.* **B 111**, 8582 (2007).

[5] *Tieke, B; El-Hashani, A; Toutianoush, A; Fendt, A*: Multilayered films and membranes based on macrocyclic polyamines, calixarenes and cyclodextrins, *Thin Solid Films* 2007, submitted.

Curriculum Vitae (CV)

Personal data

First name	Ashraf
Surname	EL-Hashani
Full name	Ashraf M. EL-Hashani
Date of birth	3rd septembre 1967
Place of birth	Benghazi-Libya
Nationality	Libyan
Sex	Male
Marital status	Married with four children (Marwa, Isra, Aya, and Malak)

Academic record

High school Diploma 1987	In Benghazi- Libya
B.Sc. 1991	Chemistry, University of Garyounis -Libya
M.Sc. 1999	Physical chemistry, University of Garyounis-Libya
Ph.D. student from11/2002	Institute of Physical Chemistry, University of Koeln

Experience

Demonstrator 1992-1998	Teaching assistant for undergraduate students, University of Garyounis -Libya
Assistant Lecturer 1999-2002	University of Garyounis -Libya